AD-A035 223 TRW DEFENSE AND SPACE SYSTEMS GROUP REDONDO BEACH CALIF F/G 20/3
CURRENT COMPUTATION BY THE FINITE ELEMENT METHOD.(U)
NOV 76 A SANKAR, T C TONG N00123-76-C-0729
UNCLASSIFIED NL

1 OF 2
ADA035223

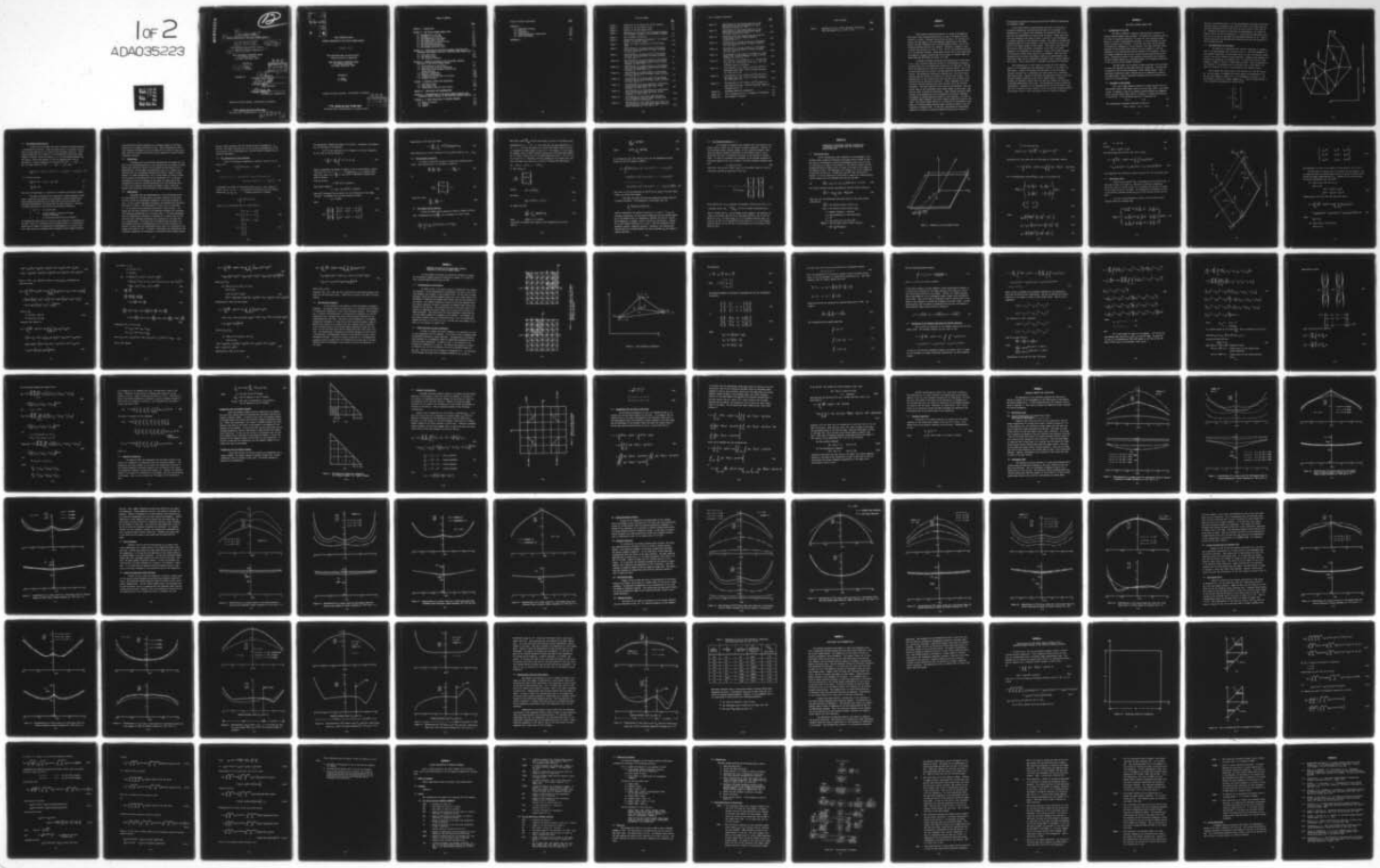

(12) B.S.

(9) FINAL TECHNICAL REPORT,

(6) CURRENT COMPUTATION BY THE FINITE ELEMENT METHOD.

(11) Nov 76 (12) 97p.

Work performed under the Navy Contract

(15) N00123-76-C-0729 for NELC/6240 New

NAVAL ELECTRONICS LABORATORY CENTER
271 Catalina Boulevard
San Diego, California 92152

Prepared by

(10) A. Sankar
T. C. Tong

APPROVED BY:

A. Sankar, Project Manager

R. M. Webb, Manager
EMH&T Department

R. M. Webb for
D. Jortner, Manager
Vulnerability & Hardness Lab.

TRW DEFENSE AND SPACE SYSTEMS GROUP
ONE SPACE PARK · REDONDO BEACH · CALIFORNIA 90278

409637 LB

FINAL TECHNICAL REPORT

"CURRENT COMPUTATION BY THE FINITE ELEMENT METHOD"

Nov 76

Work performed under the Navy Contract
N00123-76-C-0729 for NELC/6240

NAVAL ELECTRONICS LABORATORY CENTER
271 Catalina Boulevard
San Diego, California 92152

Prepared by

A. Sankar
T. C. Tong

TRW DEFENSE AND SPACE SYSTEMS GROUP
ONE SPACE PARK · REDONDO BEACH · CALIFORNIA 90278

TABLE OF CONTENTS

Table of Contents (continued)

LIST OF FIGURES

List of Figures (Continued)

LIST OF TABLES

CHAPTER I

INTRODUCTION

The problem concerning scattering of a plane electromagnetic wave from a thin conducting square plate is easy to formulate but very difficult to solve. The major difficulties are due to (1) the edge condition, (2) the highly if not nonintegrable singularity of the dyadic Green's function associated with a two-dimensional surface, and (3) the stability problem caused by its thinness. Obviously, attempts to seek a closed form solution are bound to fail, and the only promising approach is to use numerical methods. Among those who did work in this area using the numerical integral equation solution by method of moments (MOM) are Ramat-Samii and Mittra[1], and Wang, et al [2].

Although the moment method has been demonstrated in many cases to be a very successful numerical method for electromagnetic problems, its application to a two-dimensional problem has not been good. The MOM offers two approaches to solve the surface current problems. One is the wire grid modeling which suffers from many numerical and physical difficulties. The geometrical structure is modeled into a wire grid representation and the results are sensitive to selected wire radius. Grid representation of the structure has loops and thus loop currents can be excited which are manifestly unphysical. Again, depending on the grid structure, internal resonance may occur and thus, alter the external resonances. The other approach is the surface patch modeling. Here the results seem to vary drastically with slight changes in patch size. The matrices tend to become ill-conditioned. Edges present particular difficulties in the manipulation of the integrand in the patch H modeling. Convergence is another important problem in this approach. In order to circumvent these drawbacks, the finite element method [3] is used in this study. The finite element method is a relatively old approximation technique for solving boundary-value problems formulated either in the differential or integral form. In the past, this method had been mainly applied to the field of structural mechanics [4] and only recently to

electromagnetic problems concerning electrostatics [5][6] and propagation in waveguides [7][8].

In the finite element method approach used here, the solution is obtained by minimizing a variational functional for the problem. An approximation to a function that minimizes the variational form is constructed from combinations of certain trial functions. These trial functions are defined on the region in which a solution to the differential or integral equation of the problem is sought. The region is divided into subregions which are called elements. Each trial function is zero on all parts of the region except for one element. The various trial functions which may be linear functions, polynomials or the like, are joined together at the boundaries of the element. Values of the trial functions are defined at certain points (nodes) of the elements. When the trial functions which are also called shape functions are substituted in the variational form, and the optimization procedure taken, a matrix equation will result. This is then solved to determine the quantity of interest.

The remaining part of this report is divided into five chapters. Chapter II is concerned with the fundamental concepts of the finite element method. Chapter III presents the derivation of the variational integral equations for a conducting flat-square plate and a conducting bent-square plate. Chapter IV discusses the numerical solution of the variational integral equations by the finite element method. Chapter V presents the numerical results while the last one, Chapter VI, gives the concluding remarks about this study. Two appendices are also included for completeness. Appendix A is on transformation of the entire surface integral into a repeated surface integral for the variational integral equation, and Appendix B gives a brief description about the computer programs.

CHAPTER II

THE FINITE ELEMENT METHOD (FEM)

2.1 Fundamentals of the FEM

The FEM is primarily a numerical discretization procedure for solving complex boundary value problems. The method was originally used in the field of structural mechanics; but since its roots belong in mathematics as a class of approximation procedure, it can be applied to a wide range of nonstructural problems. In the FEM, the region of the problem is divided into subdomains or finite elements, with some functional representation of the solution being adopted over the elements so that the parameters of the representation become unknowns of the problem. Usually the element parameters are the nodal values and their derivatives at the nodes. Although the region of the problem is discretized into elements, the whole domain remains as a continuum because of the imposed restriction on the continuity across element interfaces.

The FEM itself can be further divided according to the procedure by which the equations in the nodal values are formulated. The most popular method is the so-called variational finite element method. Here, a stationary principle is used to derive the set of equations in terms of the nodal values — often a functional obtained from the variational principle is the starting point.

2.2 Statement of the Problem

Let L be a linear operator defined on a dense set M of the complex Hilbert space H with inner product (u,v) and norm $\|u\|^2 = (u,u)$ where $u,v \in H$. In general, L has to be neither positive definite nor symmetric and it could be either differential or integral or integral-differential in nature [9]. If the governing equation is represented by

$$Lu = f \quad , \quad f \in H \tag{1}$$

the corresponding stationary functional is given by

$$F(u) = (Lu,u) - (u,f) - (f,u). \tag{2}$$

Since it is stationary about u, if the approximation solutions differ from the exact ones by an amount in the order of ε where ε is a small quantity, then the calculation of F(u) from (2) will give an error of the order of ε^2. Therefore the better the solutions are approximated, the closer the results will be to the true values of u. In practice the stationary property of (2) is used to determine the approximate solution to (1). This is called classically the Rayleigh-Ritz procedure which will be discussed in the following sections.

2.3 The Subdivision of the Region

The region R is subdivided into discrete subregions or elements, each of the same general form, as shown in Fig. 1., with the boundaries of each element being plane or curvilinear faces, and with the adjacent boundaries of any pair of elements being coincident. Commonly used elements for surfaces are triangular or polygonal form. At similar positions in each element, a number of points are identified as nodes. They are generally at the vertices of the elements, and at positions such as the center of an edge, the centroid of a face or the centroid of the element volume.

Let us denote the nodal values of the solution ϕ at the p^{th} node as ϕ_p. Let the number of elements into which region R is subdivided be N^t, and the total number of nodes in R = D + B (Boundary) be n_d and n_b. The total number of nodes in a single element be n_s. Then the nodal values of ϕ can be generally expressed as a column vector

$$\{\phi\} = \begin{bmatrix} \phi_1 \\ \phi_2 \\ \vdots \\ \phi_{n_d} \\ \vdots \\ \phi_{n_d+n_b} \end{bmatrix} \tag{3}$$

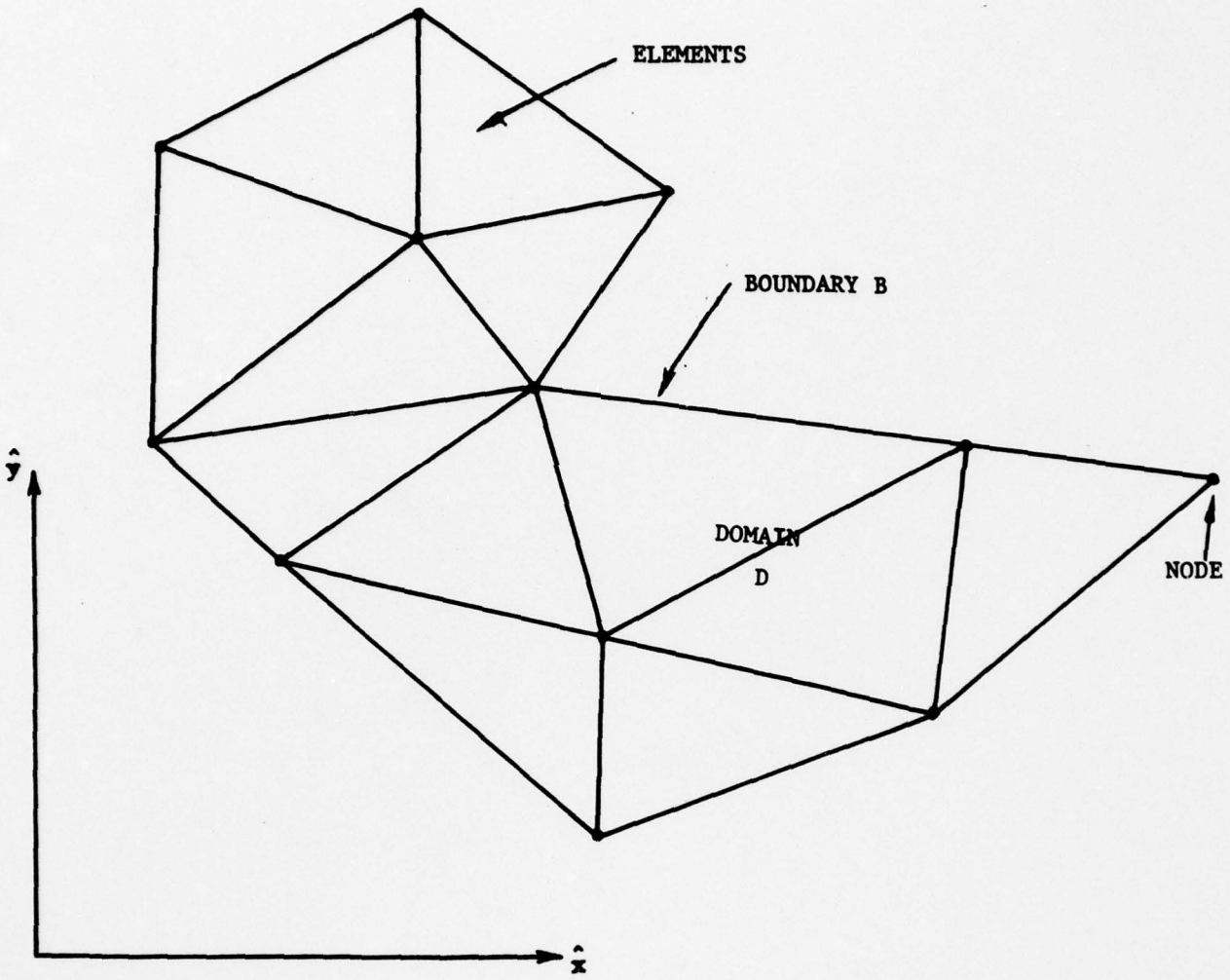

Figure 1. Subdivision of the Region into Finite Elements

2.4 The Element Shape Function

To solve (2) by the FEM, one needs to define some shape functions or interpolation functions. These functions allow us to express the solution ϕ at any position of R in terms of only the nodal values $\{\phi\}$. Therefore,we assume that the solution ϕ can be prescribed in functional forms, element by element, across the region, i.e., can be defined piecewise over the region. Within each element, it will be supposed that ϕ can be described by a linear combination of functions N_1^e, N_2^e, ... N_k^e, ... N_s^e, and nodal values ϕ_1^e, ϕ_2^e, ... , ϕ_k^e ..... ϕ_s^e, thus

$$\phi = \sum_e N_1^e \phi_1^e + N_2^e \phi_2^e + N_3^e \phi_3^e + \ldots N_k^e \phi_k^e + \ldots + N_s^e \phi_s^e \qquad (4)$$

or, in matrix notation

$$\phi = \sum_e (N_1^e \; N_2^e \; \ldots \; N_k^e \; \ldots \; N_s^e) \; \{\underline{\phi}^e\} \qquad (5)$$

$$= \sum_e (\underline{N}^e) \; \{\underline{\phi}^e\} \qquad (6)$$

Note that the superscript e is used here to identify a particular element.

The shape functions $\underline{N}^e$ are restricted to being functions of positions. Since the true solution ϕ is prescribed as being continuous and with continuous derivatives (up to some order) across the region, the piecewise representation (6) should have the same properties. Therefore the shape functions are restricted by the following conditions:

1. $N_j^e = 1$ at the j^{th} node
2. $= 0$ outside element e, with the j^{th} node as one of its nodes
3. $=$ a position function within the elements.

In choosing the shape function, one has to pay attention to convergence in the FEM. Since it is recognized that the FEM solution to a problem with a given size of element is necessarily an approximation to the exact solution, there must be an assurance that successive finite element solutions

using smaller and smaller elements will converge smoothly to the exact solution as the element size tends to zero. While comprehensive conditions ensuring convergence are not yet known for all types of linear problems, there are certain criteria that must be observed in order to obtain convergent solutions:

(1) Completeness

This means that the piecewise representation (6) within the element of the variable/derivative in a key integral must be capable of representing any continuous function as the element size decreases to zero. Mathematically, the piecewise representation calls for a complete set of functions such as a polynomial function with infinite number of terms. However, in a FEM representation, only a finite number of terms is taken. But as pointed out by Melosh [10] and by Zienkiewicz [11], a monotonic convergence can still be obtained if the number of terms used in the representation allow the variable/derivative up to and including order t to take up any constant value within the element, where t being the highest-order derivative of the variable in the variational functional.

(2) Compatibility

This means that the representation of the variable/derivative in a key integral of (2) must tend to the same continuity as the exact solution, across the interelement boundaries, as the size decreases to zero. If for a given variational functional, the highest-order derivative involved is of order t, the derivatives of order up to and including (t - 1) are known as the principal derivatives of that variable. Presuming that the exact solutions of the dependent variables are continuous with continuous derivatives up to at least order t. One weak requirement that the compatibility criterion is satisfied is to require that the variable and their principal derivatives are continuous in the shape function representation. This means that the highest-order derivative in a key integral will have a representation that is at worst piecewise continuous, in which case the representation will tend to be continuous as the element size tends to zero. In general, completeness and compatibility are sufficient conditions for convergence in variational finite element method.

However, these conditions are very strong and can be relaxed [12]. In practice, the shape functions will not be an exact representation of the true solution, but an approximate one, and the solution obtained will be similarly approximate.

2.5 The Subdivision of the Functional

Since (1) represents essentially a quadratic function, we can write it as

$$\Phi = \int_D F(u_1, u_2, u_3 \ \ldots \ , u_d)\, dD \tag{7}$$

where

$$F(u_1 \ , u_2 \ , u_3 \ \ldots \ , u_d) = a_{11}\, u_1^2 + a_{12}\, u_1\, u_2 + a_{13}\, u_1\, u_3 + a_{21}\, u_2\, u_1 + a_{22}\, u_2^2 + \ldots . + a_{dd}\, u_d^2 \tag{8}$$

D represents the domain of integration which can be a line, surface or volume, and u_1, u_2, u_3 ... , u_d represent the solution ϕ and its various derivatives, ϕ_x, ϕ_{xy}, ϕ_y ... . In matrix notation (7) becomes

$$\Phi = \int_D \{u\}^T [A]\ \{u\}\, dD \tag{9}$$

where [A] is a dxd matrix and {u} a dxl vector, or

$$[A] = \begin{bmatrix} a_{11} & a_{12} & \ldots . & a_{1d} \\ a_{21} & a_{22} & \ldots . & a_{2d} \\ \vdots & & & \\ a_{d1} & a_{d2} & \ldots . & a_{dd} \end{bmatrix} \tag{10}$$

$$\{u\} = \begin{bmatrix} u_1 \\ u_2 \\ \vdots \\ u_d \end{bmatrix} \tag{11}$$

and superscript T denotes the adjoint of a matrix. In general, the elements a_{ij} are functions of the position.

If Φ^e is the contribution of an element to the total integration in (9), then (9) can be written as

$$\Phi = \sum_{e=1}^{\ell} \Phi^e = \sum_{e=1}^{\ell} \int_{D_e} \{u\}^T [A] \{u\} \, dD_e \tag{12}$$

where D_e represents the domain of element e, let us now consider a typical term u_r in $\{u\}$ r = 0, 1, 2, ... By definition, u_r is a spatial derivative of ϕ, that is $u_r = \frac{\partial^r}{\partial \S^r} \phi = D_r \phi$, where § represents a spatial variable of concern.

From (6) we have

$$u = (N^e) \{\phi^e\} \text{ in element e.}$$

Thus within element e

$$u_r = D_r \phi = (D_r N^e)\{\phi^e\} = (U_r{}^e)\{\phi^e\} \tag{13}$$

when $(U_r{}^e)$ represents the row vector for the r-derivative of the shape function. So applying (13) for every element we obtain

$$\{u\} = (U) \{\phi^e\} \tag{14}$$

where

$$[U] = \begin{Bmatrix} U_1{}^e \\ U_2{}^e \\ \vdots \\ U_d{}^e \end{Bmatrix} = \begin{bmatrix} D_1 N_1{}^e & D_1 N_2{}^e & \cdots & D_1 N_s{}^e \\ D_2 N_1{}^e & D_2 N_2{}^e & \cdots & D_2 N_s{}^e \\ \vdots & \vdots & & \vdots \\ D_d N_1{}^e & Dd N_2{}^e & \cdots & D_d N_s{}^e \end{bmatrix} \tag{15}$$

Substitution of (14) into (9) yields

$$\Phi = \sum_{e=1}^{\ell} \int_{D_e} \{\phi^e\}^T [U]^T [A] [U] \{\phi^e\} \, dD_e \tag{16}$$

which shows that Φ is now a function of the n_d nodal values $\phi_1, \phi_2, \cdots \phi_{n_d}$.

2.6 The Stationary Condition

In order to solve (16) we have to invoke the variational principle. The condition that Φ is stationary is given by

$$\frac{\partial \Phi}{\partial \phi_1} = \frac{\partial \Phi}{\partial \phi_2} = \frac{\partial \Phi}{\partial \phi_3} = \cdots\cdots = \frac{\partial \Phi}{\partial \phi_{n_d}} = 0 \tag{17}$$

or

$$\frac{\partial \Phi}{\partial \{\phi\}} = \begin{Bmatrix} \partial \Phi / \partial \phi_1 \\ \partial \Phi / \partial \phi_2 \\ \vdots \\ \partial \Phi / \partial \phi_{n_d} \end{Bmatrix} = \{0\} \tag{18}$$

From (12) we get

$$\sum_{e=1}^{\ell} \frac{\partial \Phi^e}{\partial \{\phi\}} = 0 \tag{19}$$

2.7 The Element Matrix Equation

To get the element matrix equation we have to combine (19) and (16). Considering the term $\frac{\partial \Phi^e}{\partial \{\phi\}}$ for an element e in (16), we get

$$\frac{\partial \Phi^e}{\partial \{\phi^e\}} = \int_{D_e} \frac{\partial}{\partial \{\phi^e\}} \left[\{\phi^e\}^T [U]^T [A] \, [U] \, \{\phi^e\} \right] dD_e \tag{20}$$

Note that a term $\partial\Phi^e/\partial\phi_p$ will be zero unless p is one of the element nodes identified by 1, 2, .. k, ..s. Also note that the node identifiers 1, 2, 3, .. k, .. s are not the same as the system node numbers which are used to represent the total number of nodes in D. For example, if the triangular element e has its three vertices identified in the system node numbers as 7, 9, and 5, then we can let its node identifiers (now s = 3) as $1 \leftrightarrow 7$, $2 \leftrightarrow 9$ and $3 \leftrightarrow 5$. Therefore, the only elements in the column vector (18) that are nonzero are those that, in terms of element node identifiers, are $\partial\Phi^e/\partial\phi_1$, $\partial\Phi^e/\partial\phi_2$, ... $\partial\Phi^e/\partial\phi_s$.

So (18) reduces to

$$\frac{\partial \Phi^e}{\partial \{\phi^e\}} = \begin{Bmatrix} \partial\Phi/\partial\phi_1 \\ \partial\Phi/\partial\phi_2 \\ \vdots \\ \partial\Phi/\partial\phi_s \end{Bmatrix}^e \tag{21}$$

Letting

$$[B] = [U]^T[A][U] \tag{22}$$

and using

$$\frac{\partial}{\partial\{Y\}} \{Y\}^T[Q]\{Y\} = 2[Q]\{Y\} \tag{23}$$

we obtain from (20)

$$\frac{\partial \Phi^e}{\partial\{\phi^e\}} = \int_{D_e} 2[A^1]\{\phi^e\}\, dD_e \tag{24}$$

where $[A^1]$ is a s X s matrix

Since $\{\phi^e\}$ is constant with respect to the integration we can write (24) as

$$\frac{\partial \phi^e}{\partial \{\phi^e\}} = [A^{1e}]\{\phi^e\} \tag{25}$$

where
$$[A^{1e}] = \int_{D_e} 2[A^{1e}]dD_e \tag{26}$$

If we substitute (15) into (20) and carry out the mathematics we will obtain for the ij^{th} element of $[B^e]$ as

$$\begin{aligned} b_{ij} = \int_{D_e} 2\Big[& D_1 N_i^e (a_{11} D_1 N_j^e + a_{12} D_2 N_j^e + ... + a_{1d} D_d N_j^e) \\ & + D_2 N_i^e (a_{21} D_1 N_j^e + a_{22} D_2 N_j^e + ... + a_{2d} D_d N_j^e) \\ & + ... + \\ & + D_d N_i^e (a_{d1} D_1 N_j^e + a_{d2} D_2 N_j^e + ... + a_{dd} D_d N_j^e)\Big] dD_e \end{aligned} \tag{27}$$

Note that in (27) the subscripts on the N^e are in terms of the node identifiers, not system node numbers.

Note that the shape functions are explicitly defined functions of spatial variables. The integrand of a particular term, say

$$\int_{D_e} 2(D_2 N_i^e) a_{21} (D_1 N_j^e)\, dD_e$$

could be evaluated as an explicit function of x, y and z. If a_{ij} are constant coefficients, the prescribed integration over the defined domain D_e of the element would, in consequence, evaluate the term as a scalar. The integration, if simple, could be carried out analytically. However, if a_{ij} are complex functions of x, y and z, then the integration would generally require a numerical solution. Therefore, the computational time involved in a problem depends very much on whether a_{ij} are simple or complex functions.

2.8 The Boundary Condition (B.C.)

It is known in boundary-value problems that the solution is not unique unless it meets all the required boundary conditions. However, in the variational finite element methods, if the specified boundary conditions are natural boundary conditions for the problem, then it can be shown that the class of admissible functions is not required to satisfy these. In order to illustrate the treatment of the boundary condition in the matrix equation (25) let us assume a Dirichlet boundary condition such that

$$\phi = g(x,y,z) \text{ on } B. \tag{28}$$

Using (28), the n_b nodal values $(\phi_p)_B$ for the boundary nodes on B can be calculated yielding n_b equations of the form

$$\underset{\substack{\uparrow \\ p^{th} \text{ Position}}}{(0\ ,\ 0\ ,\ 0\ ,\ \ldots\ 0\ ,\ 1\ ,\ 0\ ,\ \ldots\ 0)} \begin{Bmatrix} \phi_1 \\ \phi_2 \\ \phi_p \\ \vdots \\ \phi_{n_b} \end{Bmatrix} = \begin{Bmatrix} g \\ g \\ g \\ \\ g \end{Bmatrix} \tag{29}$$

which implies that if ϕ_p satisfies the boundary condition and hence it is a constant value, then $\partial\phi^e / \partial\phi_p = 0$ for an element containing node p.

Thus to include the B.C. in the element matrix equation, the simplest procedure is to replace the p^{th} row of the matrix $[A^{1e}]$ in (25) by the row matrix of (29). In other words, if p is a boundary-condition node, put zeros in the p^{th} row of the $[A^{1e}]$ in (25) except for a 1 in the diagonal position and put in the p^{th} row of the driving vector the boundary value given by (28).

CHAPTER III

DERIVATION OF VARIATIONAL INTEGRAL EQUATIONS FOR A CONDUCTING FLAT-SQUARE PLATE AND A CONDUCTING BENT-SQUARE PLATE

3.1 Flat-Square Plate

We are considering a thin (compared to the wavelength of the incident wave), perfectly conducting flat-square plate as shown in Fig. 2. The plate is illuminated by a plane electromagnetic wave with its E vector polarized at an angle θ with respect to the positive x-axis, and its propagation vector $\underline{k}$ lying on the y-z plane at an angle ϕ with respect to the negative y-axis. The thickness of the plate is 2t and the dimensions of the plate are 2a x 2b. The MKS units and $e^{j\omega t}$ time variation are adopted. It is the objective of this study to compute the induced surface current density due to an incident plane wave by the FEM.

Let
$$\underline{E}^{in}(\underline{r}) = (\cos\theta\,\hat{x} + \sin\theta\,\hat{y})\, e^{-jk(y\cos\phi - z\sin\phi)} \tag{30}$$

The E-field integral equation governing the induced surface current is

$$\underline{E}^{in}(\underline{r}) = -j\omega\mu_o \int_{S'} \underline{J}(\underline{r}') \cdot \bar{\bar{G}}(\underline{r}|\underline{r}')dS' \tag{31}$$

where $\underline{r},\underline{r}'$ are the observation and source points on the plate surface respectively,

$\underline{E}^{in}(\underline{r})$ = the incident electric field $(v/_m)$

$\underline{J}(\underline{r}')$ = the surface current density $(a/_{m^2})$

ω = angular frequency (rad/sec)

μ_o = the permeability of free space $(h/_m)$

$j = \sqrt{-1}$

S' = the surface area of plate (m^2)

$\bar{\bar{G}}(\underline{r}|\underline{r}')$ = the free space dyadic Green's function

$$= \left(\bar{\bar{I}} + \frac{1}{k^2}\bar{\bar{\nabla}}\bar{\bar{\nabla}}\right) g(\underline{r}|\underline{r}') \tag{32}$$

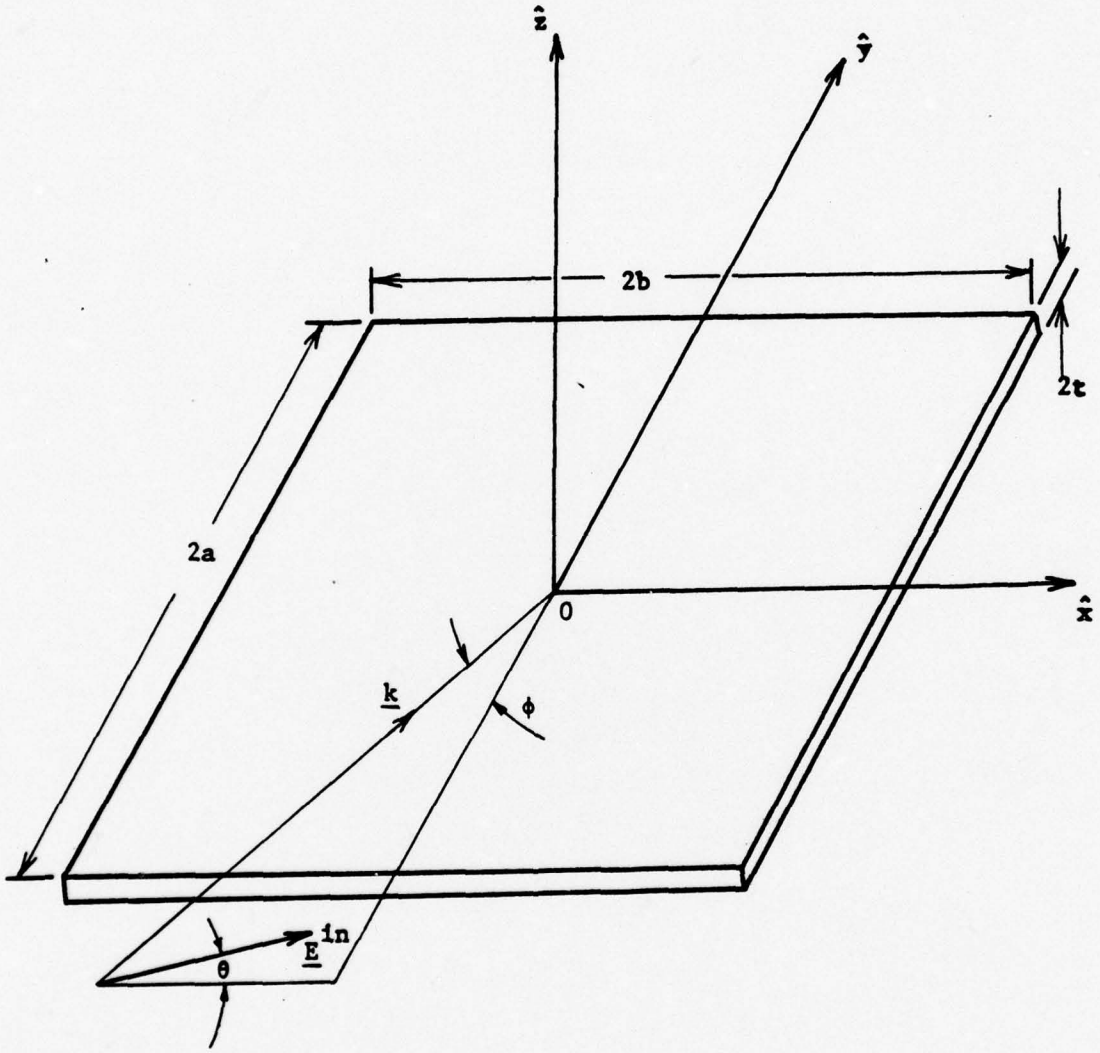

Figure 2. Geometry of the Flat-Square Plate

with $\bar{\bar{I}}$ = the unit dyad and

$$g(\underline{r}|\underline{r}') = g_o = -\frac{1}{4\pi}\frac{e^{-jkR}}{R}\ ,\ R = \left[|\underline{r}-\underline{r}'|^2 + t^2\right]^{1/2} \tag{33}$$

Kouyoumjian [13] has shown that the following is a stationary quantity

$$\Phi = -2\int_S \underline{E}^{in}(\underline{r}) \cdot \underline{J}(\underline{r})dS + j\omega\mu_o \int_S\int_{S'} \underline{J}(\underline{r}) \cdot \bar{\bar{G}}(\underline{r}|\underline{r}') \cdot \underline{J}(\underline{r}')dS'dS. \tag{34}$$

For a two-dimensional problem $\bar{\bar{G}}(\underline{r}|\underline{r}')$ takes the following form

$$\bar{\bar{G}}(\underline{r}|\underline{r}') = \begin{pmatrix} 1 + \frac{1}{k^2}\frac{\partial^2}{\partial x^2}\hat{x} & \frac{1}{k^2}\frac{\partial^2}{\partial x\partial y}\hat{y} \\ \frac{1}{k^2}\frac{\partial^2}{\partial x\partial y}\hat{x} & 1 + \frac{1}{k^2}\frac{\partial^2}{\partial y^2}\hat{y} \end{pmatrix} g(\underline{r}|r') \tag{35}$$

$$= \begin{pmatrix} \lambda_{xx}\hat{x} & \lambda_{xy}\hat{y} \\ \lambda_{yx}\hat{x} & \lambda_{yy}\hat{y} \end{pmatrix} \tag{36}$$

where

$$\lambda_{xx} = \frac{g_o}{R}\left\{\frac{(x-x')^2}{R}\left[\left(\Omega + \frac{1}{R}\right)^2 - \Omega/_R\right] - \Omega\right\} \tag{37}$$

$$\lambda_{xy} = \lambda_{yx} = \frac{g_o}{R^2}(x-x')(y-y')\left[\left(\Omega + \frac{1}{R}\right)^2 - \frac{\Omega}{R}\right] \tag{38}$$

$$\lambda_{yy} = \frac{g_o}{R}\left\{\frac{(y-y')^2}{R}\left[\left(\Omega + \frac{1}{R}\right)^2 - \frac{\Omega}{R}\right] - \Omega\right\} \tag{39}$$

with $$\Omega = jk + \frac{1}{R} \tag{40}$$

Letting

$$\underline{J}(\underline{r}) = J_x(\underline{r})\hat{x} + J_y(\underline{r})\hat{y} \tag{41}$$

and substituting (36) and (41) into (34) we obtain

$$\Phi = -2\int_S \underline{E}^{in}(\underline{r}) \cdot \underline{J}(\underline{r})dS + j\omega\mu_o \int_S \int_{S'} \Big[\lambda_{xx} J_x(\underline{r}) J_x(\underline{r}') + \lambda_{xy} J_x(\underline{r}) J_y(\underline{r}') + \lambda_{xy} J_x(\underline{r}') J_y(\underline{r}) + \lambda_{yy} J_y(\underline{r}) J_y(\underline{r}') \Big] dS'dS \tag{42}$$

(42) represents the variational integral equation for the flat-square plate.

3.2 Bent-Square Plate

Here we are concerned with a bent-square plate as shown in Fig. 3. The plate is bent at an angle ϕ_b. Because the problem is symmetrical about the y axis we can set up the x-y-z coordinate system with its origin on the y-axis and one of the edges. For mathematical convenience, we also set up another coordinate system x_b-y_b-z_b on the inclined surface and the bent.

Now for a three-dimensional problem, the free space Green's function takes the following form

$$\overline{\overline{G}}(\underline{r}|\underline{r}') = \begin{Bmatrix} 1 + \frac{1}{k^2}\frac{\partial^2}{\partial x^2}\hat{x}\hat{x} & \frac{1}{k^2}\frac{\partial^2}{\partial x \partial y}\hat{x}\hat{y} & \frac{1}{k^2}\frac{\partial^2}{\partial x \partial y}\hat{x}\hat{z} \\ \frac{1}{k^2}\frac{\partial^2}{\partial y \partial x}\hat{y}\hat{x} & 1 + \frac{1}{k^2}\frac{\partial^2}{\partial y^2}\hat{y}\hat{y} & \frac{1}{k^2}\frac{\partial^2}{\partial y \partial z}\hat{y}\hat{z} \\ \frac{1}{k^2}\frac{\partial^2}{\partial z \partial x}\hat{z}\hat{x} & \frac{1}{k^2}\frac{\partial^2}{\partial z \partial y}\hat{z}\hat{y} & 1 + \frac{1}{k^2}\frac{\partial^2}{\partial z^2}\hat{z}\hat{z} \end{Bmatrix} g(\underline{r}|\underline{r}') \tag{43}$$

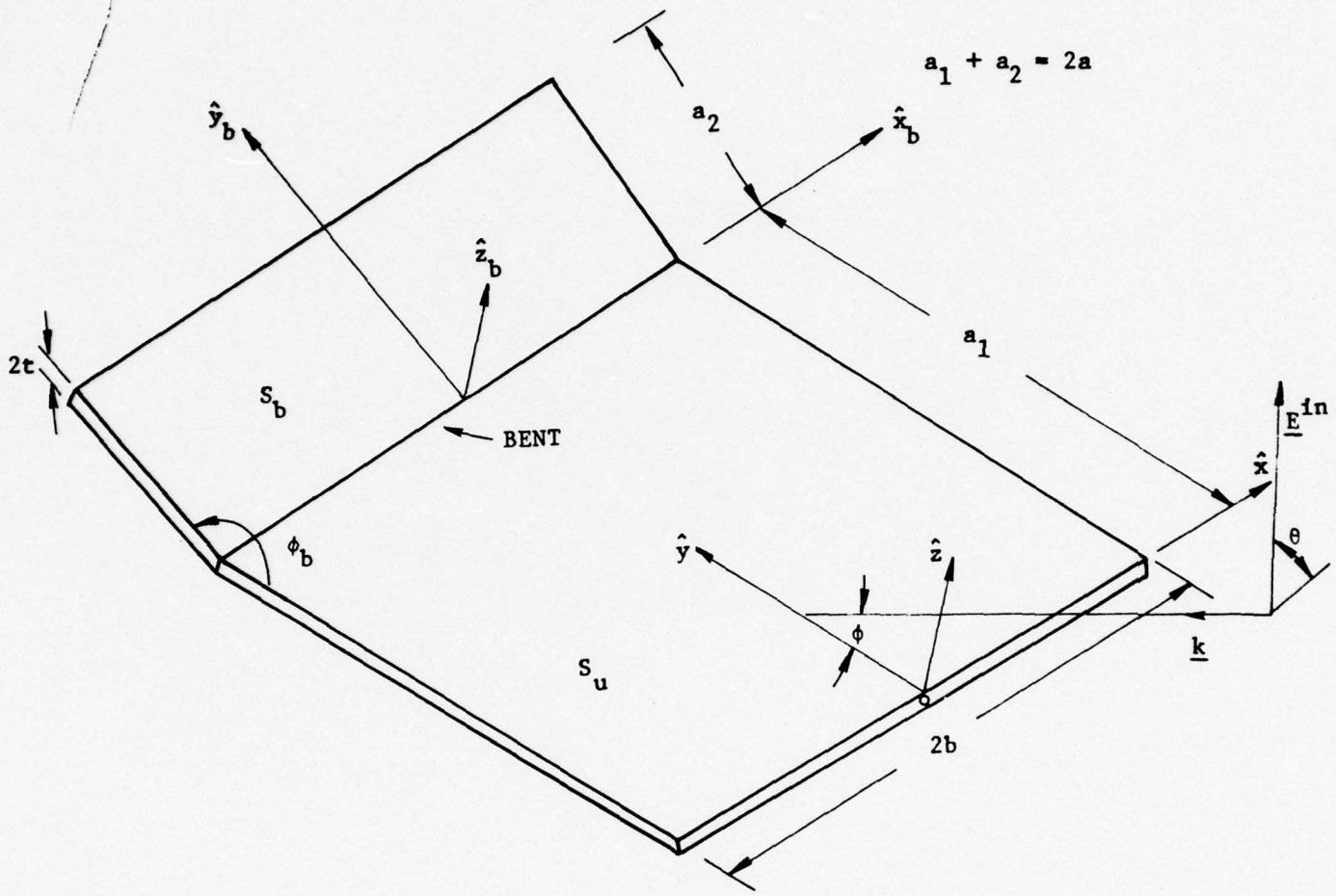

Figure 3. Geometry of the Bent-Square Plate

$$= \begin{Bmatrix} \lambda_{xx}\,\hat{x}\hat{x} & \lambda_{xy}\,\hat{x}\hat{y} & \lambda_{xz}\,\hat{x}\hat{z} \\ \lambda_{yx}\,\hat{y}\hat{x} & \lambda_{yy}\,\hat{y}\hat{y} & \lambda_{yz}\,\hat{y}\hat{z} \\ \lambda_{zx}\,\hat{z}\hat{x} & \lambda_{zy}\,\hat{z}\hat{y} & \lambda_{zz}\,\hat{z}\hat{z} \end{Bmatrix} \tag{44}$$

The computation of the λ's are similar to those given in (37) to (40).

We now divide the surface area of the plate into two regions: one is called the bent or inclined region denoted by S_b and the other one is called the unbent region denoted by S_u. Because of this we can divide the area of integration into four parts:

(1) when $\underline{r}$ and $\underline{r}'$ are both in S_u :

Here we let

$$\underline{J}(\underline{r}) = J_x(\underline{r})\hat{x} + J_y(\underline{r})\hat{y}$$
$$\underline{J}(\underline{r}') = J_x(\underline{r}')\hat{x} + J_y(\underline{r}')\hat{y} \tag{45}$$

Substituting of (45) into (34) and using (44) we get

$$\Phi_1 = -2\int_{S_u} \overset{in}{\underline{E}}(\underline{r}) \cdot \underline{J}(\underline{r})dS + j\omega\mu_o \int_{S_u}\int_{S_u'} \Big[\lambda_{xx}J_x(\underline{r})J_x(\underline{r}')$$
$$+ \lambda_{xy}J_x(\underline{r})J_y(\underline{r}') + \lambda_{yx}J_y(\underline{r})J_x(\underline{r}') + \lambda_{yy}J_y(\underline{r})J_y(\underline{r}')\Big]\, dS'\, dS \tag{46}$$

where

$$(\underline{r},\underline{r}') \in S_u$$

(2) when $\underline{r}$ and $\underline{r}'$ are both in S_b

Here we let

$$\underline{J}(\underline{r}) = J_{x_b}(\underline{r})\hat{x}_b + J_{y_b}(\underline{r})\hat{y}_b = J_{x_b}(\underline{r})\hat{x} + \cos\rho\, J_{y_b}(\underline{r})\hat{y} + \sin\rho\, J_{y_b}(\underline{r})\hat{z}$$

$$\underline{J}(\underline{r}') = J_{x_b}(\underline{r}')\hat{x}_b + J_{y_b}(\underline{r}')\hat{y}_b = J_{x_b}(\underline{r}')\hat{x} + \cos\rho\, J_{y_b}(\underline{r}')\hat{y} + \sin\rho\, J_{y_b}(\underline{r}')\hat{z} \tag{47}$$

where $\rho = 180° - \phi_b$, subscript b refers to the x_b-y_b-z_b coordinates and from (34) we get

$$\Phi_2 = -2\int_{S_b} E_x^{in}(\underline{r})\, J_{x_b}(\underline{r})dS + j\omega\mu_o \int_{S_b}\int_{S_b'} \left[J_{x_b}(\underline{r})\hat{x}\cos\rho\, J_{y_b}\,\hat{y} + \sin\rho\, J_{y_b}(\underline{r})\hat{z}\right]$$

$$x \left\{ J_{x_b}(\underline{r}')\left[\lambda_{xx}\hat{x} + \lambda_{xy}\hat{y} + \lambda_{xz}\hat{z}\right] + \cos\rho\, J_{y_b}(\underline{r}')\left[\lambda_{yx}\hat{x} + \lambda_{yy}\hat{y} + \lambda_{yz}\hat{z}\right]\right.$$

$$\left. + \sin\rho\, J_{y_b}(\underline{r}')\left[\lambda_{zx}\hat{x} + \lambda_{zy}\hat{y} + \lambda_{zz}\hat{z}\right]\right\} dS'dS \tag{48}$$

Since $\hat{x} = \hat{x}_b$

$$\hat{y} = \cos\rho\,\hat{y}_b - \sin\rho\,\hat{z}_b \tag{49}$$

$$\hat{z} = \sin\rho\,\hat{y}_b + \cos\rho\hat{z}_b$$

therefore (48) reduces to

$$\Phi_2 = -2\int_{S_b} \underline{E}^{in}(\underline{r}) \cdot \underline{J}(\underline{r})\, dS + j\omega\mu_o \int_{S_b}\int_{S_b'} \left\{\lambda_{xx}\, J_{x_b}(\underline{r})\, J_{x_b}(\underline{r}')\right.$$

$$+ \left[\cos\rho\,\lambda_{yx} + \sin\rho\,\lambda_{zx}\right] J_{x_b}(\underline{r})\, J_{y_b}(\underline{r}') + (\lambda_{xy}\cos\rho + \lambda_{xz}\sin\rho)$$

$$J_{y_b}(\underline{r})\, J_{x_b}(\underline{r}') + \left[\cos\rho\,(\lambda_{yy}\cos\rho + \lambda_{yz}\sin\rho) + \sin\rho\,(\lambda_{zy}\cos\rho\right.$$

$$\left.\left. + \lambda_{zz}\sin\rho)\right] J_{y_b}(\underline{r})\, J_{y_b}(\underline{r}')\right\} dS'dS. \tag{50}$$

Also since $x = x_b$

$$y = y_b \cos \rho + a_1 \tag{51}$$

$$z = y_b \sin \rho$$

and $$R = \left[(x-x')^2 + (y-y')^2 + (z-z')^2 + t^2\right]^{1/2}$$

$$= \left[(x_b-x_b')^2+(y_b \cos \rho-y_b' \cos \rho)^2+(y_b \sin \rho -y_b' \sin \rho)^2+t^2\right]^{1/2}$$

$$= \left[(x_b - x_b')^2 + (y_b - y_b')^2 + t^2\right]^{1/2} \tag{52}$$

So $$\frac{\partial R}{\partial x_b} = \frac{\partial R}{\partial x} \tag{53}$$

$$\frac{\partial R}{\partial y_b} = \frac{\partial R}{\partial y}\frac{\partial y}{\partial y_b} + \frac{\partial R}{\partial z}\frac{\partial z}{\partial y_b}$$

$$= \cos \rho \frac{\partial R}{\partial y} + \sin \rho \frac{\partial R}{\partial z} \tag{54}$$

$$\frac{\partial^2 R}{\partial y_b^2} = \left(\cos \rho \frac{\partial}{\partial y} + \sin \rho \frac{\partial}{\partial z}\right)\left(\cos \rho \frac{\partial R}{\partial y} + \sin \rho \frac{\partial R}{\partial z}\right)$$

$$= \cos^2 \rho \frac{\partial^2 R}{\partial y^2} + \sin \rho \cos \rho \frac{\partial^2 R}{\partial z \partial y} + \sin \rho \cos \rho \frac{\partial^2 R}{\partial y \partial z} + \sin^2 \rho \frac{\partial^2 R}{\partial z^2} \tag{55}$$

Combining (53) to (55) we have

$$\cos \rho \, \lambda_{yx} + \sin \rho \, \lambda_{zx} = \lambda_{y_b x_b}$$

$$\cos \rho \, \lambda_{xy} + \sin \rho \, \lambda_{xz} = \lambda_{x_b y_b}$$

$$\cos \rho \, (\lambda_{yy} \cos \rho + \lambda_{yz} \sin \rho) + \sin \rho \, (\lambda_{zy} \cos \rho + \lambda_{yz} \sin \rho) = \lambda_{y_b y_b} \tag{56}$$

and so (50) becomes

$$\Phi_2 = -2\int_{S_b} \underline{E}^{in}(\underline{r}) \cdot \underline{J}(\underline{r})dS + j\omega\mu_o \int_{S_b}\int_{S_b'} \Big\{\lambda_{x_bx_b}\, J_{x_b}(\underline{r})\, J_{x_b}(\underline{r}') \tag{57}$$

$$+ \lambda_{y_bx_b}\, J_{x_b}(\underline{r})\, J_{y_b}(\underline{r}') + \lambda_{x_by_b}\, J_{x_b}(\underline{r}')\, J_{y_b}(\underline{r}) + \lambda_{y_by_b}\, J_{y_b}(\underline{r})\, J_{y_b}(\underline{r}')\Big\} dS'dS$$

where $(\underline{r},\underline{r}') \in S_b$

(3) when $\underline{r}$ is in S_u and $\underline{r}'$ is in S_b

Here we have

$$\underline{J}(\underline{r}) = J_x(\underline{r})\hat{x} + J_y(\underline{r})\hat{y} \tag{58}$$

$$\underline{J}(\underline{r}') = J_{x_b}(\underline{r}')\hat{x}_b + J_{y_b}(\underline{r}')\hat{y}_b = J_{x_b}(\underline{r}')\hat{x} + \cos\rho\, J_{y_b}(\underline{r}')\hat{y} + \sin\rho\, J_{y_b}(\underline{r}')\hat{z}$$

Substitution of (58) into (34) yields

$$\Phi_3 = -2\int_{S_u} \underline{E}^{in}(\underline{r}) \cdot \underline{J}(\underline{r})\, dS + j\omega\mu_o \int_{S_b'}\int_{S_u} \Big\{\lambda_{xx} J_x(\underline{r})\, J_{x_b}(\underline{r}')$$

$$+ (\cos\rho\,\lambda_{yx} + \sin\rho\,\lambda_{zx})\, J_x(\underline{r})\, J_{y_b}(\underline{r}') + (\cos\rho\,\lambda_{yy} + \sin\rho\,\lambda_{zy})\, J_y(\underline{r})\, J_{y_b}(\underline{r}')$$

$$+ \lambda_{xy}\, J_{x_b}(\underline{r}')\, J_y(\underline{r})\Big\} dS'dS \tag{59}$$

where $\underline{r} \in S_u$; $\underline{r}' \in S_b$

(4) when $\underline{r}$ is in S_b and $\underline{r}'$ is in S_u

Here we have

$$\underline{J}(\underline{r}) = J_{x_b}(\underline{r})\,\hat{x}_b + J_{y_b}(\underline{r})\hat{y}_b = J_{x_b}(\underline{r})\hat{x} + \cos\rho\, J_{y_b}(\underline{r})\hat{y} + \sin\rho\, J_{y_b}(\underline{r})\hat{z}$$

$$\underline{J}(\underline{r}') = J_x(\underline{r}')\hat{x} + J_y(\underline{r}')\hat{y} \tag{60}$$

Substitution of (60) in (34) gives

$$\Phi_4 = -2\int_{S_b} \underset{\text{in}}{\underline{E}}(\underline{r}) \cdot \underline{J}(\underline{r})dS + j\omega\mu_o \int_{S_b}\int_{S_u'} \Big\{\lambda_{xx} J_{x_b}(\underline{r})\, J_x(\underline{r}')$$

$$+ \lambda_{yx}\, J_{x_b}(\underline{r})\, J_y(\underline{r}') + (\cos\rho\, \lambda_{xy} + \sin\rho\, \lambda_{xz})\, J_x(\underline{r}')\, J_{y_b}(\underline{r}) \tag{61}$$

$$+ (\lambda_{yy} \cos\rho\, \lambda_{y_z} \sin\rho)\, J_{y_b}(\underline{r})\, J_y(\underline{r}')\Big\}\, dS'dS$$

where $\underline{r} \in S_b$; $\underline{r}' \in S_u$

Equations (46), (57), (59) and (61) constitute the variational integral equations for the bent-square plate. These will be solved by the FEM in the next chapter.

3.3 The Thickness Parameter

In our solution of the problem, we have introduced a thickness parameter. The primary reason for doing this is to circumvent the difficulty of treating the singularity of the E-field integral equation. This singularity, if without any modification, is considered not integrable for the two-dimensional case, although there exists some analytical approach for the three-dimensional case [14]. Physically, this introduction of a thickness parameter is equivalent to using the so-called extended boundary condition method [15] in which it is required that the incident field be cancelled by the scattered field in an arbitrary region completely within the scatterer, so that the field point and the observation point would never coincide. One disadvantage of employing a thickness parameter is that instead of considering a two-dimensional problem, we are actually solving a three-dimensional problem. In order to restrict ourselves to a two-dimensional problem, we have to assume that the thickness of the plate has to be small compared with the wavelength of the incident field and the dimensions of the plate.

CHAPTER IV

NUMERICAL SOLUTION OF THE VARIATIONAL INTEGRAL EQUATIONS BY THE FINITE ELEMENT METHOD

In this chapter we discuss the numerical procedure of solving the variational integral equations developed in Chapter 3 for both the flat- and bent-square plates using the FEM.

4.1 Discretization of the Surface

As shown in Fig. 4 the square surface is subdivided into triangular elements. In the discretization, consideration is given to the structural symmetry with respect to the incident field. For the case of normal incidence, there are two-fold symmetry about the x and y axes, hence it is sufficient to represent the unknown nodal values over only one quadrant of the surface. For oblique incidence, we have just one-fold symmetry about the y-axis; therefore, we have to represent the unknown nodal values over one-half of the surface. The contributions due to the other parts of the surface in computing the matrix elements can be taken care of using the image techniques. Once the surface has been subdivided, system node numbers and element numbers are assigned to each element. For example, for the normal incidence case, as illustrated in Fig. 4 (a), the system node numbers are from 1 to 16 $\left(N^n = n_d + n_b = 16 \right)$ and the total number of elements for one quadrant is 18 $\left(N^t = 18 \right)$.

4.2 Shape Functions and Area Coordinates

In order to compute the matrix elements, it is necessary to carry out the integration over the elements. To do this we have to generate some interpolation functions or shape functions. The generation of interpolation functions for a triangular element is simplified considerably if one works with area coordinates. As shown in Fig. 5, the vertices of the triangle are numbered by ℓ, m and n. The partial area opposite to node ℓ is denoted by A_ℓ, and its coordinates in the x-y coordinate system are $\left(x_\ell, y_\ell \right)$. The total area of the element is designated by A. For any point in the triangle we assign three coordinates denoted by L_ℓ, L_m and L_n.

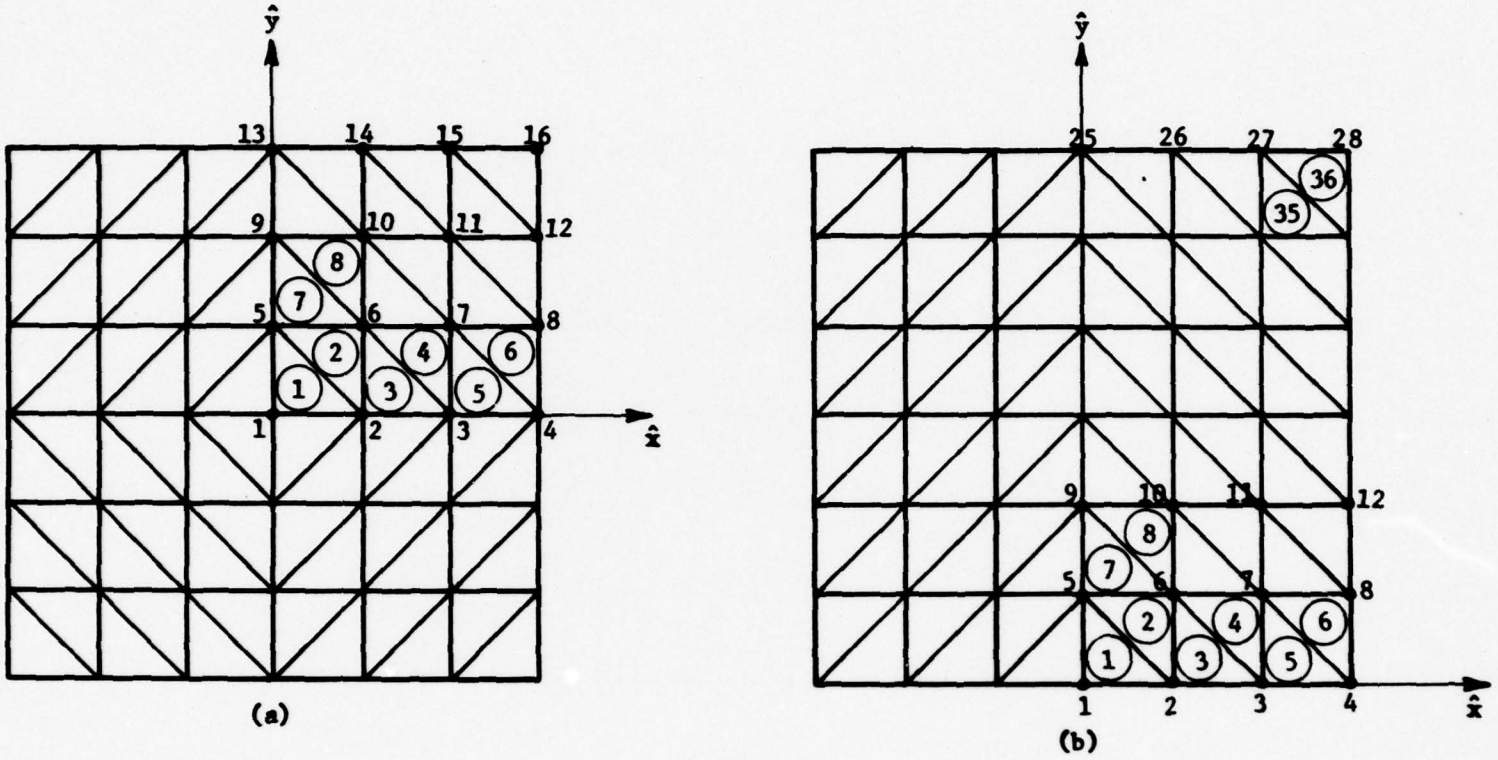

Figure 4. Subdivision of the Surface into Triangular Elements. (a) for Normal Incidence (b) for Oblique Incidence.

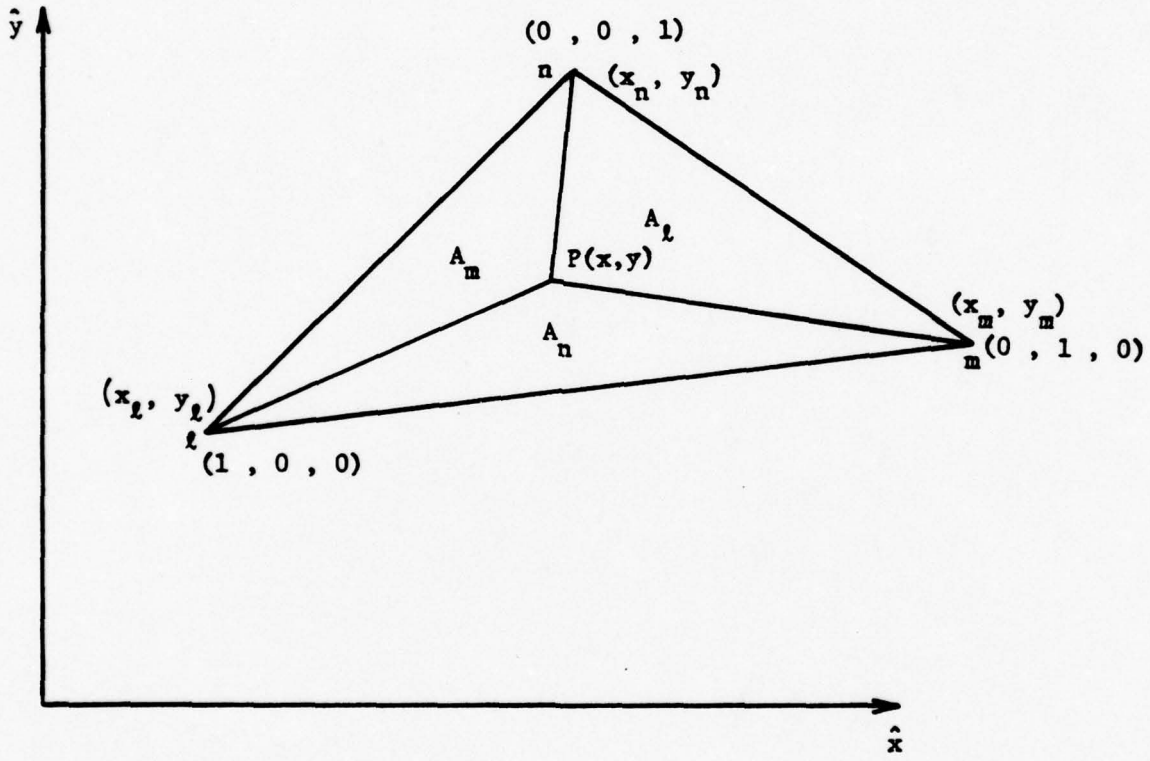

Figure 5. Area Triangular Coordinates

By definition

$$L_\ell = \frac{A_\ell}{A}\ ,\ L_m = \frac{A_m}{A} \text{ and } L_n = \frac{A_n}{A} \tag{62}$$

where
$$A = \frac{1}{2}\begin{vmatrix} 1 & x_\ell & y_\ell \\ 1 & x_m & y_m \\ 1 & x_n & y_n \end{vmatrix} \tag{63}$$

The relation between the Cartesian coordinates and the area coordinates is given by

$$\begin{Bmatrix} 1 \\ x \\ y \end{Bmatrix} = \begin{pmatrix} 1 & 1 & 1 \\ x_\ell & x_m & x_n \\ y_\ell & y_m & y_n \end{pmatrix} \begin{Bmatrix} L_\ell \\ L_m \\ L_n \end{Bmatrix} \tag{64}$$

or

$$\begin{Bmatrix} L_\ell \\ L_m \\ L_n \end{Bmatrix} = \begin{pmatrix} P_{mn} & Y_{mn} & X_{mn} \\ P_{\ell n} & Y_{\ell n} & X_{\ell n} \\ P_{\ell m} & Y_{\ell m} & X_{\ell m} \end{pmatrix} \begin{Bmatrix} 1 \\ x \\ y \end{Bmatrix} \tag{65}$$

where

$$\begin{aligned} P_{mn} &= P_\ell = \frac{1}{2A}\left(x_m y_n - x_n y_m\right) \\ Y_{mn} &= Y_\ell = \frac{1}{2A}\left(y_m - Y_n\right) \\ X_{mn} &= X_\ell = \frac{1}{2A}\left(x_n - x_m\right) \end{aligned} \tag{66}$$

Note that only two of the area coordinates are independent because

$$L_\ell + L_m + L_n = 1 \tag{67}$$

Since the expressions for the matrix elements involve Cartesian derivatives, it will be necessary to transform the derivatives too. The transformation laws are readily deduced from (65)

$$\begin{aligned} \frac{\partial}{\partial x}\left[f(L_\ell, L_m, L_n)\right] &= \sum_{i=1}^{3} \frac{\partial f}{\partial L_i}\frac{\partial L_i}{\partial x} = \sum_{i=1}^{3} Y_i \frac{\partial f}{\partial L_i} \\ \frac{\partial}{\partial y}\left[f(L_\ell, L_m, L_n)\right] &= \sum_{i=1}^{3} X_i \frac{\partial f}{\partial L_i} \end{aligned} \tag{68}$$

Higher derivatives are generated by repeated application of (68). For example,

$$\frac{\partial^2 f}{\partial x \partial y} = \sum_{i=1}^{3}\sum_{j=1}^{3} X_i Y_j \frac{\partial^2 f}{\partial L_i \partial L_j} \tag{69}$$

For integration we can easily show that

$$\int_A L_\ell dS = \frac{A}{3} \tag{70}$$

$$\int_A L_\ell L_m dS = \frac{A}{12} \qquad \ell \neq m \tag{71}$$

$$\int_A (L_\ell)^2 dS = \frac{A}{6} \tag{72}$$

and the following general formula:

$$\int_A L_\ell^{\,i}\, L_m^{\,j}\, L_n^{\,k}\, dS = \frac{(i!)(j!)(k!)}{(i+j+k+2)!}\, 2A \tag{73}$$

where i, j and k are positive integers.

In the above analysis, we have assumed a linear interpolation function or a first-order polynomial for the shape function since there are totally only three nodes available in an element. However, for higher accuracy, better approximation or for convergence reason, higher order polynomials may be used. This can be done by using more nodes by placing them on the sides of the triangles or inside the triangles as interior nodes. Another shape function that can easily be generated from the area coordinates is the sinusoidal shape function which is defined as

$$L_\ell^{\,S} = \sin\left(\frac{L_\ell \pi}{2}\right),\ L_m^{\,S} = \sin\left(\frac{L_m \pi}{2}\right) \text{ and } L_n^{\,S} = \sin\left(\frac{L_n \pi}{2}\right) \tag{74}$$

4.3 Conversion of the Integral Equations into Matrix Equations

Let us focus our attention on the integral equation for the flat-square plate. The integral equation for this case is (42).

$$\Phi = -2\int_S \underline{E}^{in}(\underline{r}) \cdot \underline{J}(\underline{r})dS + j\omega\mu_o \int_S \int_{S'} [\lambda_{xx} J_x(\underline{r}) J_x(\underline{r}')$$

$$+ \lambda_{xy} J_x(\underline{r}) J_y(\underline{r}') + \lambda_{xy} J_x(\underline{r}') J_y(\underline{r}) + \lambda_{yy} J_y(\underline{r}') J_y(\underline{r})]dS'dS$$

In terms of the discrete triangular elements, and using i and j to identify the unprimed and primed coordinates respectively, the above equation becomes

$$\Phi = -2 \sum_{i=1}^{N^t} \int_{\Delta_i} \underline{E}^{in}(\underline{r}) \cdot \underline{J}(\underline{r}) dS + j\omega\mu_o \sum_{i=1}^{N^t} \sum_{j=1}^{N^t} \int_{\Delta_i} \int_{\Delta_j} [\lambda_{xx} J_x(\underline{r}) J_x(\underline{r}')$$

$$+ \lambda_{xy} J_x(\underline{r}) J_y(\underline{r}') + \lambda_{xy} J_x(\underline{r}') J_y(\underline{r}) + \lambda_{xy} J_y(\underline{r}') J_y(\underline{r})] dS' dS$$

$$\underline{r} \in \Delta_i \, , \, \underline{r}' \in \Delta_j \tag{75}$$

where Δ_i and Δ_j represent the triangular elements for the observation point and the source point respectively. Now we can express the current density $\underline{J}$ in an element in terms of their nodal values. Thus for the x components

$$J_x(\underline{r}) = L_{\ell_i} J_x^{\ell_i} + L_{m_i} J_x^{m_i} + L_{n_i} J_x^{n_i}$$

$$J_x(\underline{r}') = L_{\ell_j} J_x^{\ell_j} + L_{m_j} J_x^{m_j} + L_{n_j} J_x^{n_j} \tag{76}$$

and similarly for the y components

$$J_y(\underline{r}) = L_{\ell_i} J_y^{\ell_i} + L_{m_i} J_y^{m_i} + L_{n_i} J_y^{n_i}$$

$$J_y(\underline{r}') = L_{\ell_j} J_y^{\ell_j} + L_{m_j} J_y^{m_j} + L_{n_j} J_y^{n_j} \tag{77}$$

Now let us write (30) as

$$\underline{E}^{in}(\underline{r}) = E_x^{in}(\underline{r}) \, \hat{x} + E_y^{in}(\underline{r}) \, \hat{y}$$

where

$$E_x^{in}(\underline{r}) = \cos\theta \, e^{-jk(y \cos\phi - z \sin\phi)}$$

$$E_y^{in}(\underline{r}) = \sin\theta \, e^{-jk(y \cos\phi - z \sin\phi)}$$

Substitution of (76) and (77) into (75) gives

$$\Phi = -2 \sum_{i=1}^{4N^t} \int_{\Delta_i} \left\{ E_x^{in} \left(L_{\ell_i} J_x^{\ell_i} + L_{m_i} J_x^{m_i} + L_{n_i} J_x^{n_i} \right) + E_y^{in} \left(L_{\ell_i} J_y^{\ell_i} + L_{m_i} J_y^{m_i} \right.\right.$$

$$\left.\left. + L_{n_i} J_y^{n_i} \right)\right\} dS + j\omega\mu_o \sum_{i=1}^{4N^t} \sum_{j=1}^{4N^t} \int_{\Delta_i} \int_{\Delta_j} \left\{ \lambda_{xx} \left(L_{\ell_i} J_x^{\ell_i} + L_{m_i} J_x^{m_i} + L_{n_i} J_x^{n_i} \right) \right.$$

$$\left(L_{\ell_j} J_x^{\ell_j} + L_{m_j} J_x^{m_j} + L_{n_j} J_x^{n_j} \right) \qquad (78)$$

$$+ \lambda_{xy} \left(L_{\ell_j} J_x^{\ell_j} + L_{m_j} J_x^{m_j} + L_{n_j} J_x^{n_j} \right) \left(L_{\ell_i} J_y^{\ell_i} + L_{m_i} J_y^{m_i} + L_{n_i} J_y^{n_i} \right)$$

$$+ \lambda_{xy} \left(L_{\ell_i} J_x^{\ell_i} + L_{m_i} J_x^{m_i} + L_{n_i} J_x^{n_i} \right) \left(L_{\ell_j} J_y^{\ell_j} + L_{m_j} J_y^{m_j} + L_{n_j} J_y^{n_j} \right)$$

$$\left. + \lambda_{yy} \left(L_{\ell_i} J_y^{\ell_i} + L_{m_i} J_y^{m_i} + L_{n_i} J_y^{n_i} \right) \left(L_{\ell_j} J_y^{\ell_j} + L_{m_j} J_y^{m_j} + L_{n_j} J_y^{n_j} \right) \right\} dS' dS$$

where

$$\ell_i , \ell_j = 1 , 2 , \ldots . N^n$$

$$i , j = 1 , 2 , \ldots . . N^t$$

and

N^n = total number of nodes for one quadrant. J_x^k and J_y^k are the unknown nodal values for J_x and J_y at the k^{th} node. To solve for J_x^k and J_y^k we differentiate (78) with respect to J_x^k and J_y^k and set equal to zero since Φ is stationary; thus, we get

$$\frac{\partial \Phi}{\partial J_x^k} = 2 \sum_{i=1}^{4N^t} \int_{\Delta_i} E_x^{in}\left(L_{\ell_i}\,\delta_{\ell_{ik}} + L_{m_i}\,\delta_{m_{ik}} + L_{n_i}\,\delta_{n_{ik}}\right)dS$$

$$+ j\omega\mu_o \sum_{i=1}^{4N^t}\sum_{j=1}^{4N^t} \iint_{\Delta_i\,\Delta_j} \Big\{\lambda_{xx}\Big[\Big(L_{\ell_i}\,\delta_{\ell_{ik}} + L_{m_i}\,\delta_{m_{ik}} + L_{n_i}\,\delta_{n_{ik}}\Big)$$

$$\left(L_{\ell_j} J_x^{\ell_j} + L_{m_j} J_x^{m_j} + L_{n_j} J_x^{n_j}\right) + \left(L_{\ell_j}\,\delta_{\ell_{jk}} + L_{m_j}\,\delta_{m_{jk}} + L_{n_j}\,\delta_{n_{jk}}\right) \qquad (79)$$

$$\left(L_{\ell_i} J_x^{\ell_i} + L_{m_i} J_x^{m_i} + L_{n_i} J_x^{n_i}\right)\Big] + \lambda_{xy}\left(L_{\ell_j}\,\delta_{\ell_{jk}} + L_{m_j}\,\delta_{m_{jk}} + L_{n_j}\,\delta_{n_{jk}}\right)$$

$$\left(L_{\ell_i} J_y^{\ell_i} + L_{m_i} J_y^{m_i} + L_{n_i} J_y^{n_i}\right) + \lambda_{xy}\left(L_{\ell_i}\,\delta_{\ell_{ik}} + L_{m_i}\,\delta_{m_{ik}} + L_{n_i}\,\delta_{n_{ik}}\right)$$

$$\left(L_{\ell_j} J_y^{\ell_j} + L_{m_j} J_y^{m_j} + L_{n_j} J_y^{n_j}\right)\Big\} dS'dS = 0$$

where $\delta_{\ell_{ik}} = 1$ if $\ell_i = k$

$\delta_{\ell_{ik}} = 0$ otherwise.

In a similar manner we can obtain $\frac{\partial \Phi}{\partial J_y^k}$ which is deducible from (79) by replacing λ_{xx} by λ_{yy}, E_x^{in} by E_y^{in} and J_x by J_y.

In matrix notation we have

$$[S]\{J\} = \{E\} \qquad (80)$$

where $[S]$ is a $(2N^n \times 2N^n)$ "Impedance" matrix

$\{J\}$ is a $(2N^n \times 1)$ column vector for the unknown nodal current densities.

$\{E\}$ is a $(2N^n \times 1)$ column vector for the driving incident field.

Specifically we have

$$\{J\} = \begin{Bmatrix} J_x^1 \\ J_x^2 \\ \vdots \\ J_x^{N^n} \\ J_y^1 \\ J_y^2 \\ \vdots \\ J_y^{N^n} \end{Bmatrix} \quad \{E\} = \begin{Bmatrix} E_x^1 \\ E_x^2 \\ \vdots \\ E_x^{N^n} \\ E_y^1 \\ E_y^2 \\ \vdots \\ E_y^{N^n} \end{Bmatrix} \tag{81}$$

$$[S] = \begin{bmatrix} S_{11} & S_{12} & S_{13} & \cdots & S_{1M} \\ S_{21} & S_{22} & S_{23} & \cdots & S_{2M} \\ \vdots & \vdots & & & \vdots \\ S_{M1} & S_{M2} & \cdots & & S_{MM} \end{bmatrix} \quad M = 2N^n$$

where the source term is given by

$$E_x^k = -2 \sum_{i=1}^{4N^t} \int_{\Delta_i} E_x^{in} \, \delta_{\ell_{mn}}^{ik} \, dS \tag{82}$$

$$E_y^k = -2 \sum_{i=1}^{4N^t} \int_{\Delta_i} E_y^{in} \, \delta_{\ell_{mn}}^{ik} \, dS \tag{83}$$

and the matrix elements are computed from

$$S_{kq} = j\omega\mu_o \sum_{i=1}^{4N^t} \sum_{j=1}^{4N^t} \iint_{\Delta_i \Delta_j} \lambda_{xx} \left[\delta^{ik}_{\ell mn} \left(L_{\ell_j} \delta_{\ell_{jq}} + L_{m_j} \delta_{m_{jq}} + L_{n_j} \delta_{n_{jq}} \right) \right.$$

$$\left. + \delta^{jk}_{\ell mn} \left(L_{\ell_i} \delta_{\ell_{iq}} + L_{m_i} \delta_{m_{iq}} + L_{n_i} \delta_{n_{iq}} \right) \right] dS' dS \qquad (84)$$

for $\quad 1 \leq k \, , \, q \leq N^n$

$$S_{kq} = j\omega\mu_o \sum_{i=1}^{4N^t} \sum_{j=1}^{4N^t} \iint_{\Delta_i \Delta_j} \lambda_{xy} \left[\delta^{ik}_{\ell mn} \left(L_{\ell_j} \delta_{\ell_{jq}} + L_{m_j} \delta_{m_{jq}} + L_{n_j} \delta_{n_{jq}} \right) \right.$$

$$\left. + \delta^{jk}_{\ell mn} \left(L_{\ell_i} \delta_{\ell_{iq}} + L_{m_i} \delta_{m_{iq}} + L_{n_i} \delta_{n_{iq}} \right) \right] dS' dS \qquad (85)$$

for

$$1 \leq k \leq N^n \text{ and } N^n \leq q + N^n \leq M$$

$$N^n \leq k + N^n \leq M \text{ and } 1 \leq q \leq N^n$$

$$S_{k+N^n, q+N^n} = j\omega\mu_o \sum_{i=1}^{4N^t} \sum_{i=1}^{4N^t} \iint_{\Delta_i \Delta_j} \lambda_{yy} \left[\delta^{ik}_{\ell mn} \left(L_{\ell_j} \delta_{\ell_{jq}} + L_{m_j} \delta_{m_{jq}} + L_{n_j} \delta_{n_{jq}} \right) \right.$$

$$\left. + \delta^{jk}_{\ell mn} \left(L_{\ell_i} \delta_{\ell_{iq}} + L_{m_i} \delta_{m_{iq}} + L_{n_i} \delta_{n_{iq}} \right) \right] dS' dS \qquad (86)$$

for

$$N^n \leq k + N^n \, , \, q + N^n \leq M$$

where

$$\delta^{ik}_{\ell mn} = L_{\ell_i} \delta_{\ell_{ik}} + L_{m_i} \delta_{m_{ik}} + L_{n_i} \delta_{n_{ik}}$$

$$\delta^{jk}_{\ell mn} = L_{\ell_j} \delta_{\ell_{jk}} + L_{m_j} \delta_{m_{jk}} + L_{n_j} \delta_{n_{jk}} \qquad (87)$$

As an example, let us consider Fig. 4(a). We have here a total of 16 nodes. Therefore, we should have 16 unknown nodal values for J_x and another 16 for J_y. Hence, the matrix size will be 32 x 32. The first 16 rows of the matrix represent J_x coupling to J_x and J_y whereas the next 16 rows are for J_y coupling to J_x and J_y. For a typical node, say node 2, we get from (84) to (86)

$$S_{22} = 4\, j\omega\mu_o \left\{ \int_{\Delta_1}\int_{\Delta_1'} + \int_{\Delta_2}\int_{\Delta_2'} + \int_{\Delta_3}\int_{\Delta_3'} \right\} \lambda_{xx}\, L_2\, L_2\, dS'\, dS \tag{88}$$

The factor 4 accounts for four quadrants

$$\begin{aligned} S_{25} = j\omega\mu_o \Bigg\{ & \int_{\Delta_1}\int_{\Delta_1'} + \int_{\Delta_1}\int_{\Delta_2'} + \int_{\Delta_1}\int_{\Delta_7'} + \int_{\Delta_2}\int_{\Delta_1'} + \int_{\Delta_2}\int_{\Delta_2'} \\ & + \int_{\Delta_2}\int_{\Delta_7'} + \int_{\Delta_3}\int_{\Delta_1'} + \int_{\Delta_3}\int_{\Delta_2'} + \int_{\Delta_3}\int_{\Delta_7'} \Bigg\} \lambda_{xx}\, L_2\, L_5\, dS'\, dS \\ & + \text{Images Contributions} \end{aligned} \tag{89}$$

$$S_{18\ 18} = 4\, j\omega\mu_o \left\{ \int_{\Delta_1}\int_{\Delta_1'} + \int_{\Delta_2}\int_{\Delta_2'} + \int_{\Delta_3}\int_{\Delta_3'} \right\} \lambda_{yy}\, L_2\, L_2\, dS'\, dS \tag{90}$$

and so on.

4.4 Numerical Integration

By using the FEM, the integration over the whole surface is now reduced to a summation of integrations over the individual elements. The integration over each element can be carried out numerically using one of the existing numerical quadrature formulas such as Simpson's rule, Gaussian quadrature, Romberg's extrapolation method, etc. However, the simplest method is to replace the integration by its Riemann sum with unit-weighting coefficients. That is, if we divide the i^{th} element into N subareas we have

$$\int_{\Delta_i} f(x,y)\, dxdy = \sum_{j=1}^{N} f(x_{ij},y_{ij})\, \Delta S_{ij} \qquad (91)$$

where Δ_i = the area of the i^{th} element

ΔS_{ij} = the j^{th} subarea of the i^{th} element

x_{ij},y_{ij} = the x and y coordinates of the centers of the j^{th} subarea of the i^{th} element.

Integration over the Singular Element

Since the singular element involves singularity, the integration over this element should be performed more accurately than the non-singular (regular) element. As shown in Fig. 6(a), the singular element is divided equally into square and isosceles triangle subdivisions (size δ_s). Within each subdivision, the current is assumed constant and represented by the value at the center of the square or the midpoint of the diagonal of the triangle. If the field point and the source point are in the same subdivision, then the subdivision is again divided into smaller cells (size δ_{ss}). In this way the accuracy of integration over the singular element can be controlled by specifying two numbers — one for the division of the singular element and the other for the subdivision. It should be noted that the integration over the singular element is performed only once in the program.

Integration over the Regular Element

Since less accuracy is usually required for integration over a regular element, the regular element is normally divided into a larger subdivision (size δ) as shown in Fig. 6(b). No further dividing is needed for the subdivision.

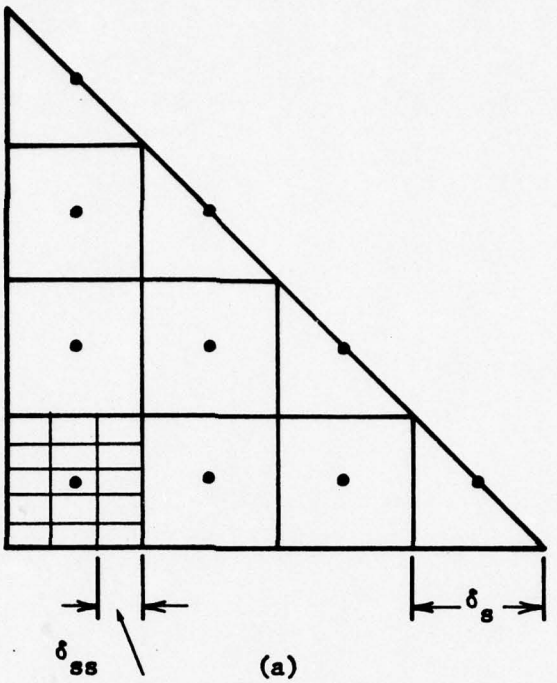

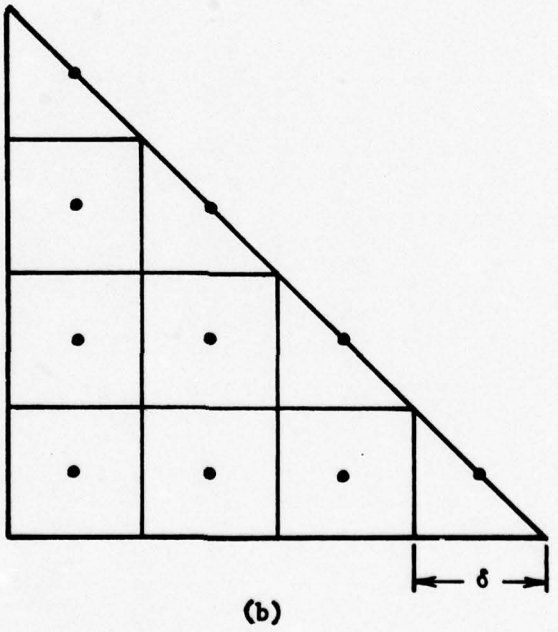

Figure 6. Subdivision for Numerical Integration
(a) Singular Element (b) Regular Element

4.5 Symmetry Consideration

Although structural symmetry allows us to reduce the total nodal unknowns of the problem to those for either one quadrant or one-half of the surface, in computing the matrix elements we still have to carry out the integration over the whole surface. However, by using the image technique, we can restrict our integration to only either one quadrant or one-half of the surface. This is feasible because of the following consideration:

Without loss of generality let us use (84) to calculate S_{kq}. It is seen that every term in the integrand is constant except λ_{xx} which is a function of positions for the observation point and the source point. Moreover, for each element in the first quadrant, there will be a similar element (image) in the other quadrants or other half. Therefore, assuming normal incidence, we have three images (Fig. 7) and if we place the observation point in the first quadrant we can write (85) as

$$S_{kq} = j4\omega\mu_o \sum_{i=1}^{N^t} \sum_{j=1}^{N^t} \iint_{\Delta_i} \iint_{\Delta_j} \left(\lambda_{xx}^1 + \lambda_{xx}^2 + \lambda_{xx}^3 + \lambda_{xx}^4 \right) \Big[\delta_{\ell mn}^{ik} \Big(L_{\ell_j} \delta_{\ell jq} + L_{m_j} \delta_{m jq} + L_{n_j} \delta_{n jq} \Big) + \delta_{\ell mn}^{jk} \Big(L_{\ell iq} \delta_{\ell iq} + L_{m_i} \delta_{m iq} + L_{n_i} \delta_{n iq} \Big) \Big] dS' dS \tag{92}$$

$$\begin{aligned} \lambda_{xx}^1 &= \S(x^- , y^-) \quad \text{(first quadrant)} \\ \lambda_{xx}^2 &= \S(x^+ , y^-) \quad \text{(second quadrant)} \\ \lambda_{xx}^3 &= \S(x^+ , y^+) \quad \text{(third quadrant)} \\ \lambda_{xx}^4 &= \S(x^- , y^+) \quad \text{(fourth quadrant)} \end{aligned} \tag{93}$$

with

$$\S(u , v) = \frac{g_o}{R} \left\{ \frac{u^2}{R} \left[\left(\Omega + \frac{1}{R}\right)^2 - \frac{\Omega}{R} \right] - \Omega \right\} \tag{94}$$

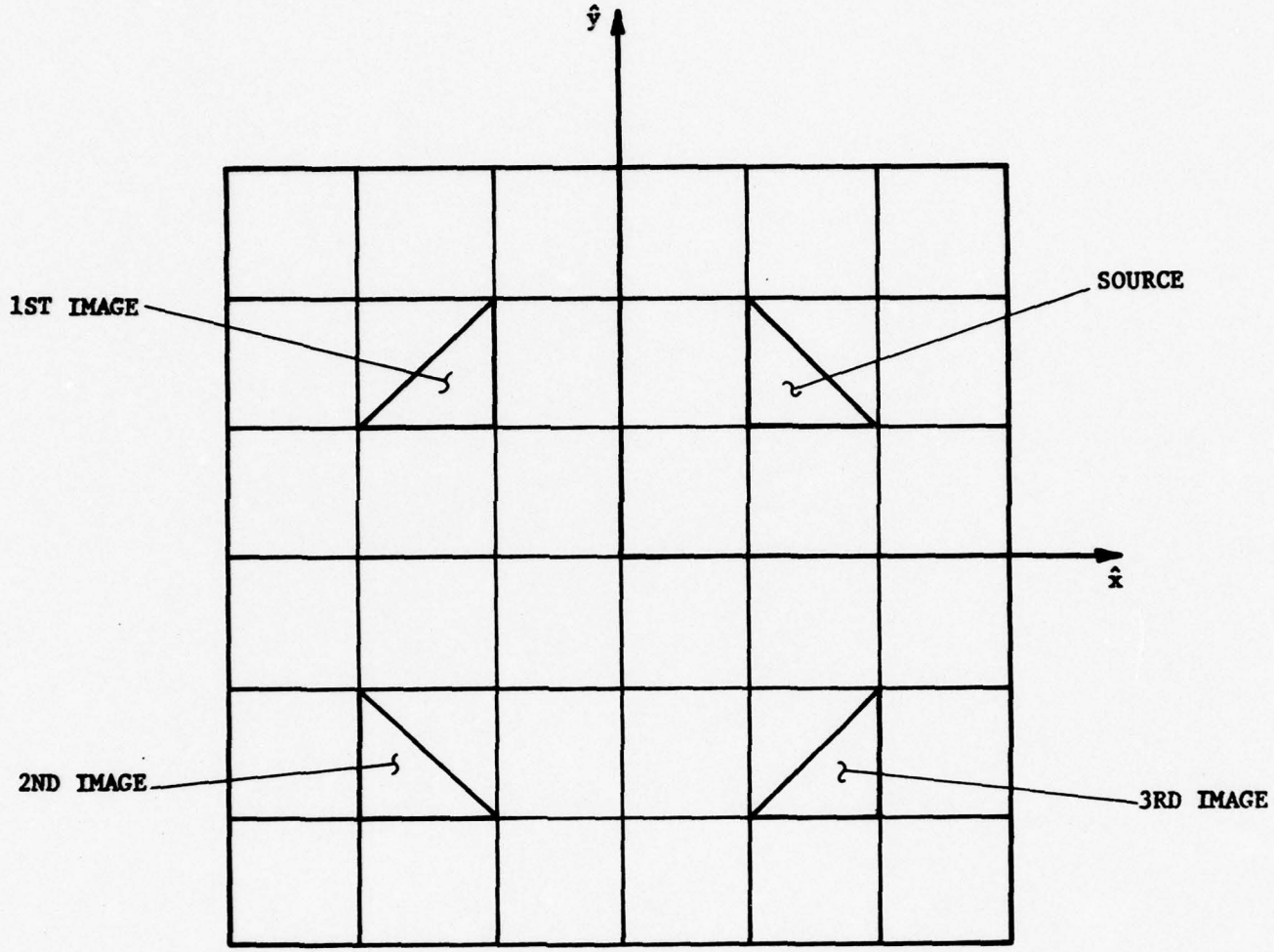

Figure 7. Images for Normal Incidence for the Flat-Square Plate

$$R = \sqrt{u^2 + v^2 + t^2} \tag{95}$$

$$x^- = x - x' \ , \ y^- = y - y'$$
$$x^+ = x + x' \ , \ y^+ = y + y' \tag{96}$$

4.6 Integration over One Side of the Plate

In the surface integration of (34), the integration has to be carried out over the entire surface of the plate. If we neglect the contribution due to the sides corresponding to the thickness (this is not a bad approximation since the thickness is small compared to the other sides and the wavelength of the incident field) and represent surface areas of the top side and the bottom side by S_+ and S_-, we can write (34) as

$$\Phi = -2 \int_{S_+} \underline{E}^{in}(\underline{r}) \cdot \underline{J}(\underline{r}) dS - 2 \int_{S_-} \underline{E}^{in}(\underline{r}) \cdot \underline{J}(\underline{r}) dS$$

$$+ j\omega\mu_o \Bigg\{ \int_{S_+} \int_{S'_+} \underline{J}(\underline{r}) \cdot \bar{\bar{G}}(\underline{r}'\underline{r}') \cdot \underline{J}(\underline{r}') dS' dS \tag{97}$$

$$+ \int_{S_+} \int_{S'_-} \underline{J}(\underline{r}) \cdot \bar{\bar{G}}(\underline{r}'\underline{r}') \cdot \underline{J}(\underline{r}') dS' dS + \int_{S_-} \int_{S'_+} \underline{J}(\underline{r}) \cdot \bar{\bar{G}}(\underline{r}'\underline{r}') \cdot \underline{J}(\underline{r}') dS' dS$$

$$+ \int_{S_-} \int_{S_-} \underline{J}(\underline{r}) \cdot \bar{\bar{G}}(\underline{r}'\underline{r}') \cdot \underline{J}(\underline{r}') dS' dS \Bigg\}$$

It is known that for sufficiently large plate sizes the current on the bottom side S_-, which is not facing the incident field, is relatively small compared to that of the top side S_+ except near the edges where the current exhibits singular behavior (for straight edges, the current component parallel to the edge behaves like $\frac{1}{\sqrt{s}}$ while the component perpendicular to the edge behaves like $\sqrt{s}$, where s is a small distance from the edge). Therefore we can neglect the integration over S_- except the small region close to the edges. Let us denote that small region by δS_-, and so (94) reduces to

$$\Phi = -2\int_{S_+ + \delta S_-} \underline{E}^{in}(\underline{r}) \cdot \underline{J}(\underline{r})dS + j\omega\mu_o \left\{ \int_{S_+}\int_{S'_+} \underline{J}(\underline{r}) \cdot \bar{\bar{G}}(\underline{r}'\underline{r}') \cdot \underline{J}(\underline{r}')dS'dS \right.$$

$$+\int_{S_+}\int_{\delta S'_-} \underline{J}(\underline{r}) \cdot \bar{\bar{G}}(\underline{r}'\underline{r}') \cdot \underline{J}(\underline{r}')dS'dS + \int_{\delta S_-}\int_{S'_+} \underline{J}(\underline{r}) \cdot \bar{\bar{G}}(\underline{r}'\underline{r}') \cdot \underline{J}(\underline{r}')dS'dS \quad (98)$$

$$\left. +\int_{\delta S_-}\int_{\delta S'_-} \underline{J}(\underline{r}) \cdot \bar{\bar{G}}(\underline{r}'\underline{r}') \cdot \underline{J}((\underline{r}')dS'dS \right\}$$

which can be combined into the following form

$$\Phi = -2\int_{S_+ + \delta S_-} \underline{E}^{in}(\underline{r}) \cdot \underline{J}(\underline{r})dS + j\omega\mu_o \left\{ \int_{S_+ + \delta S_-}\int_{S'_+} \underline{J}(\underline{r}) \cdot \bar{\bar{G}}(\underline{r}'\underline{r}') \cdot \underline{J}(\underline{r}')dS'dS \right.$$

$$\left. +\int_{S_+ + \delta S_-}\int_{\delta S'_-} \underline{J}(\underline{r}) \cdot \bar{\bar{G}}(\underline{r}'\underline{r}) \cdot \underline{J}(\underline{r}')dS'dS \right\} \quad (99)$$

or

$$\Phi = -2\int_{S_+ + \delta S_-} \underline{E}^{in}(\underline{r}) \cdot \underline{J}(\underline{r})\, dS + j\omega\mu_o \int_{S_+ + \delta S_-}\int_{S_+' + \delta S'_-} \underline{J}(\underline{r}) \cdot \bar{\bar{G}}(\underline{r}|\underline{r}') \cdot \underline{J}(\underline{r})\, dS'\, dS$$

If we let $\delta(S - \delta S_-)$ denote the current density on δS_-, where

$$\delta(S - \delta S_-) = \text{a value if } \underline{r} \in \delta S_-$$
$$= 0 \quad \text{otherwise} \tag{100}$$

and note that the current on δS_- has a reverse direction, then we can write (96) as

$$\Phi = -2 \int_{S_+} \overset{in}{\underline{E}}(\underline{r}) \cdot \underline{J}(\underline{r}) [\, 1 - \delta(S - \delta S_-)] \, dS$$

$$+ j\omega\mu_o \int_{S^+} \int_{S^+} [\, 1 - \delta(S - \delta S_-)] \, \underline{J}(\underline{r}) \cdot \overline{\overline{G}}(\underline{r}|\underline{r}') \cdot \underline{J}(\underline{r}') [\, 1 - \delta(S' - \delta S_-')] \, dS \, dS' \tag{101}$$

Equation (101) now shows that the integration is restricted only to the top side of the plate. Note that the factor $\delta(S - \delta S_-)$ is equal to zero when the observation point is far from the edge. When the field point is close to the edge, $\delta(S - \delta S_-)$ can take on any values larger or smaller than zero. From study of canonical problems concerning currents near edges of thin objects, we can approximate $\delta(S - \delta S_-)$ by the following:

For the parallel component

$$\delta(S - \delta S_-) = 1/2 \qquad \text{when } \underline{r} \in \delta S_- \tag{102}$$

For the perpendicular component

$$\delta(S - \delta S_-) = 0 \qquad \text{when } \underline{r} \in \delta S_- \tag{103}$$

Physically this means that very close to the edges, the current component parallel to the edge on the bottom side is equal to half that on the top side whereas the current component perpendicular to the edge on the bottom side is equal to zero.

Without introducing the factor $\delta(S - \delta S_{-})$ which is known as edge modification, we cannot interpret the unknown $\underline{J}(\underline{r})$ as the current density on the top side, because as pointed out by Jones [16], the integral over both sides of the plate can be replaced by an integral over one side provided that the current is replaced by the difference between its value on the two sides. Therefore, by using the $[1 - \delta(S - \delta S_{-})]$ factor in our equation, we have included (although not rigorously) the contribution due to the bottom side in our computation.

4.7 Boundary Conditions

On account of the edge condition, we require that the normal component of the current must vanish on the rim of the plate. So we impose this as the boundary condition in our solution. Mathematically, we have

$$\hat{n}_e \cdot \underline{J}(\underline{r}) = 0 \tag{104}$$

where $\hat{n}_e$ is a unit normal to the edge of concern.

CHAPTER V

NUMERICAL RESULTS AND DISCUSSIONS

The expressions of all pertinent equations and functions as derived in Chapter IV are programmed on a CDC 6500 system at TRW Defense and Space Systems Group. A brief description about the computer codes is given in Appendix B. This chapter presents the numerical results obtained for various parameters.

5.1 Flat-Square Plate

(a) Current Distributions for Various Plate Sizes (Less than One Wavelength)

Figures 8 and 9 show the plots for $|J_x|$ along the x- and the y-axes respectively for various plate sizes at normal incidence ($\phi = 0$). In each computer run, the thickness to plate length ratio was kept constant $\left(1/20\right)$ and no edge conditions were imposed. The number of nodal points used is 16 with four nodes in each x and y direction. It is seen that in general the shapes of $|J_x|$ are consistent with physical intuition — that is for small plate sizes, $|J_x|$ should decrease from the center in the x direction and increase in the y direction. Since the same number of nodes was used in each case, it is logical that the results for small plates should be more accurate than those for larger plates. The plots for the phase part show a fairly constant behavior. Since only 16 nodes were used in each direction, the current does not show a very strong edge behavior. However, improvement can be obtained if more nodes were used as shown in the next section.

(b) Convergence Test

The numerical solution obtained for a well posed boundary-value problem using the FEM should converge to the exact solution as the element size decreases. This is illustrated in Figures 10 and 11 for a square plate of 0.6λ in size. The numerical results presented here were obtained using three different numbers of total nodes 16, 25 and 36 (with equal number nodes in the x and the y directions) and linear shape

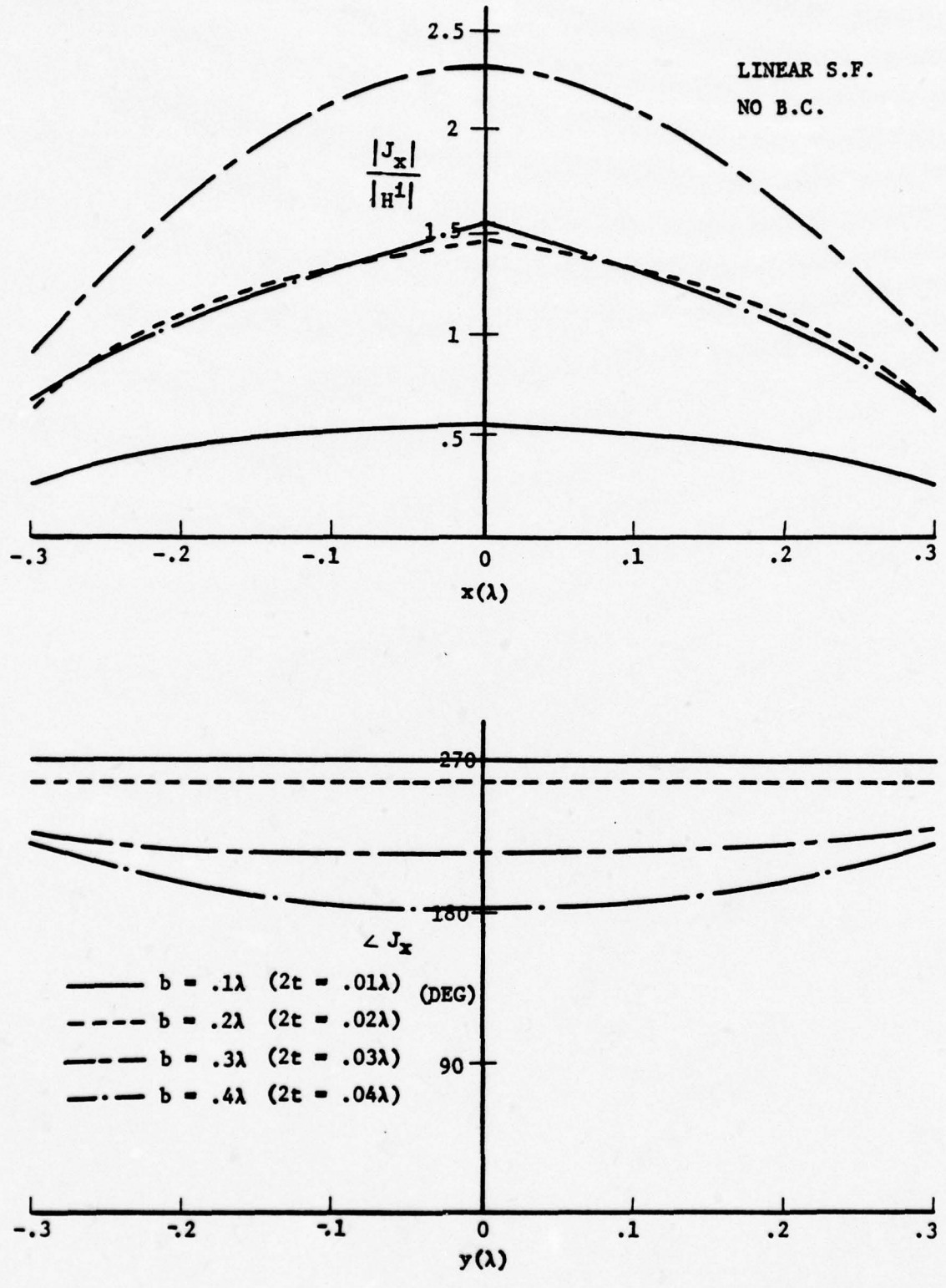

Figure 8. Distributions of J_x Along x-Axis for Flat-Square Plates of Various Dimensions at Normal Incidence ($\phi = 90°$) and $\theta = 0$.

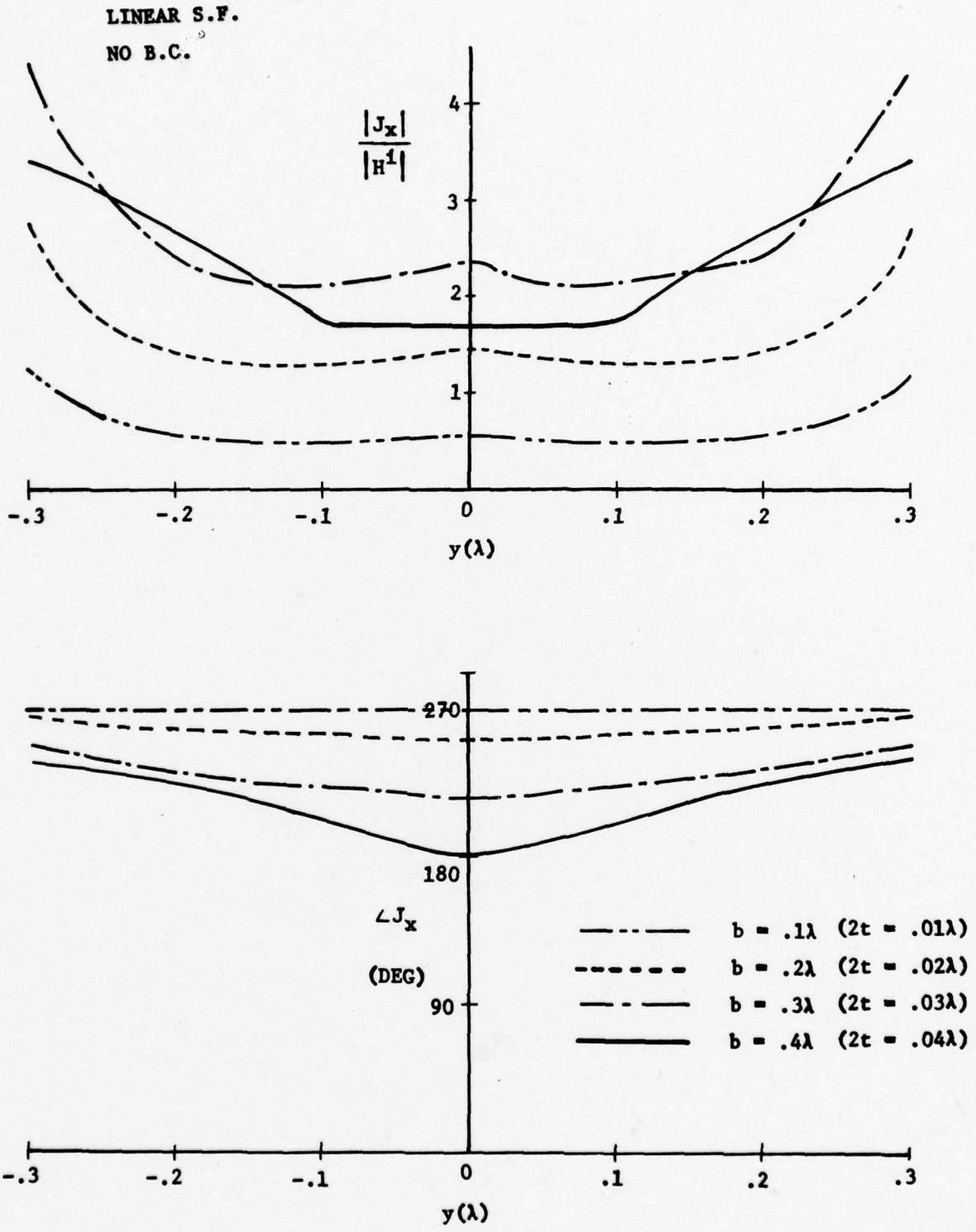

Figure 9. Distributions of J_x Along y-Axis for Flat-Square Plates of Various Dimensions at Normal Incidence ($\phi = 90°$) and $\theta = 0$.

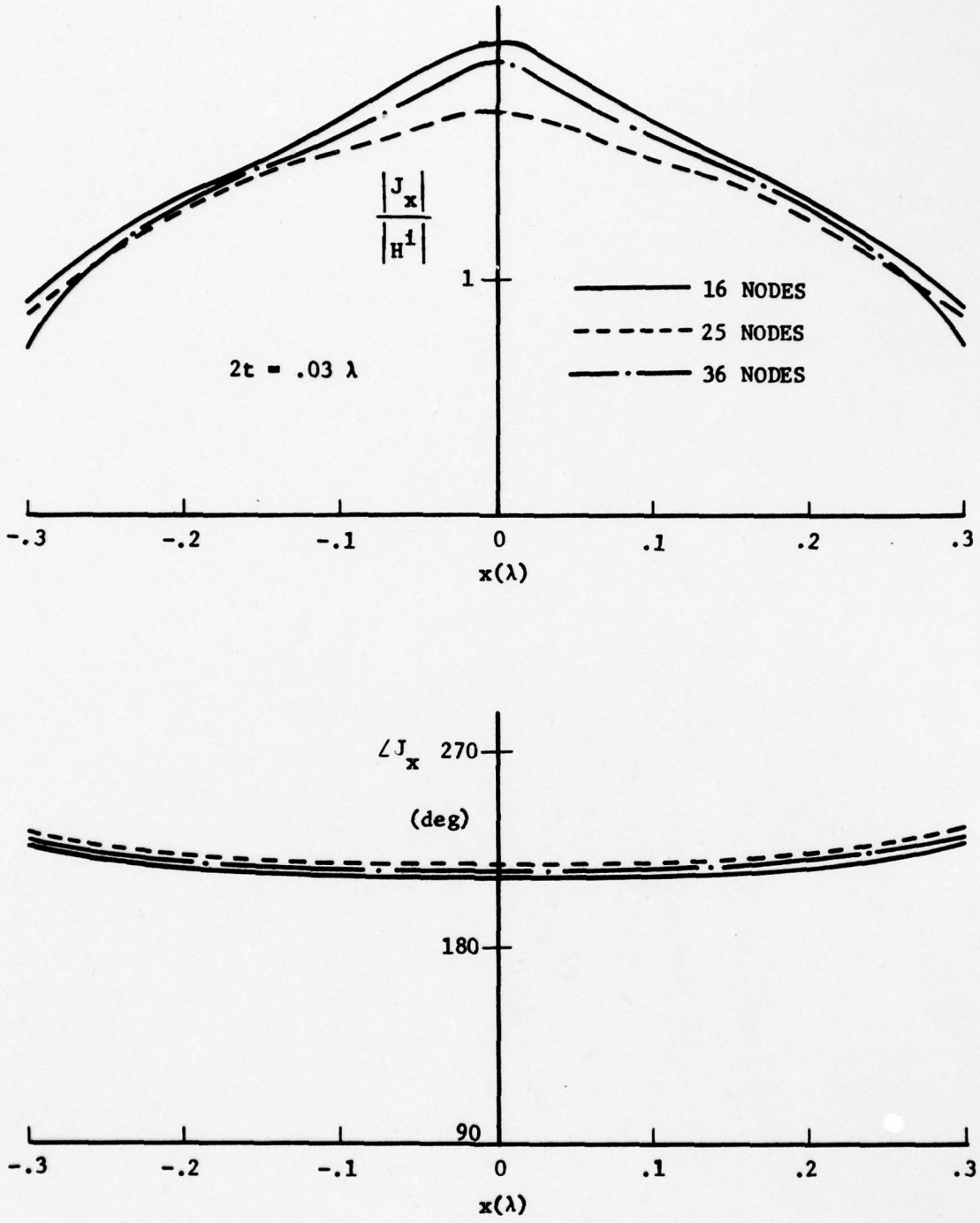

Figure 10. Distributions of J_x Along x-Axis for a Flat-Square Plate for Various Numbers of Nodal Points, Normal Points, Normal Incidence ($\phi = 90°$) and $\theta = 0$.

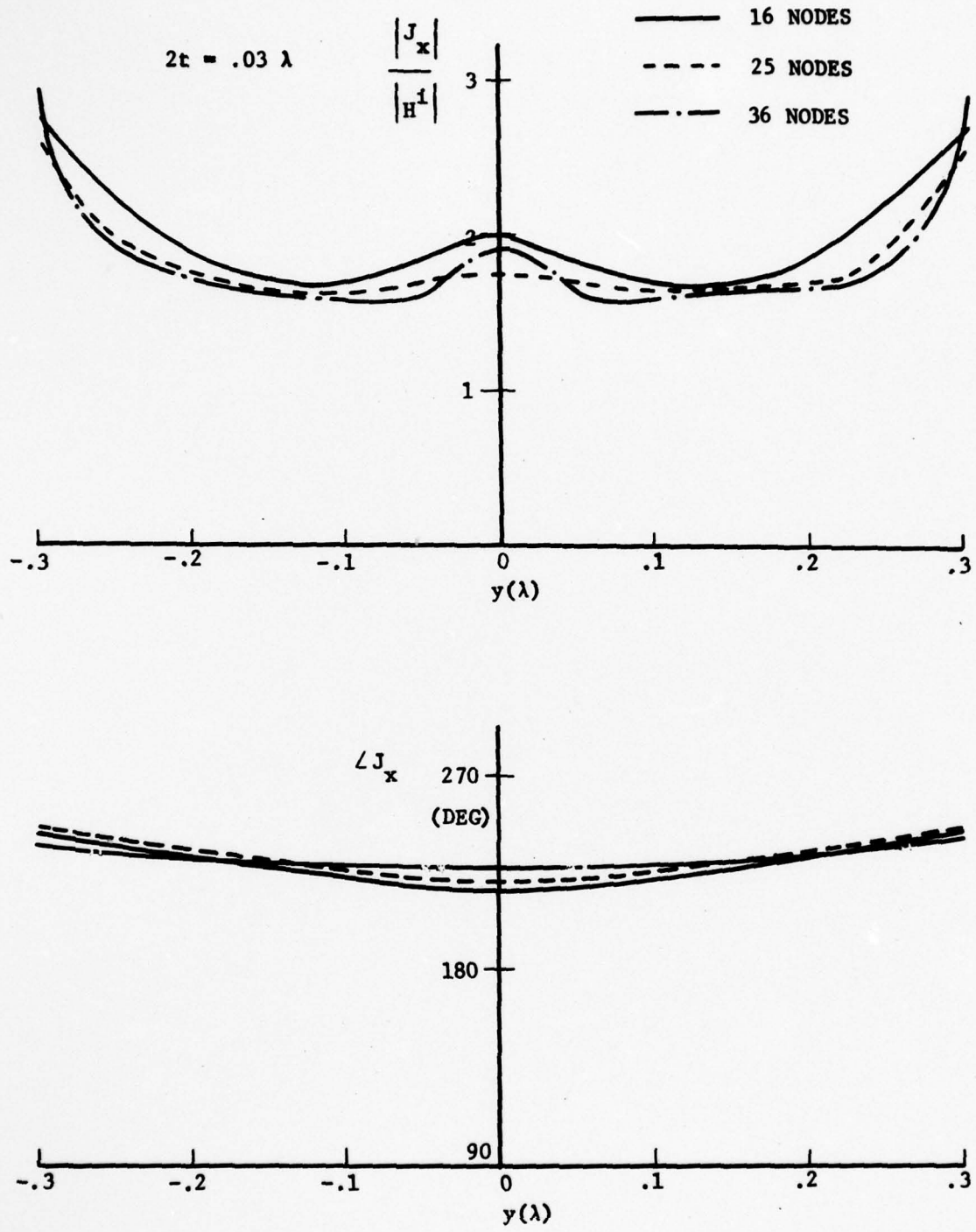

Figure 11. Distributions of J_x Along y-Axis for a Flat-Square Plate for Various Numbers of Nodal Points, Normal Incidence ($\phi = 90°$) and $\theta = 0$.

function. Here, higher integration accuracy was enforced in the numerical integration. Within numerical accuracy, the results do indicate convergence. However, convergence is not very uniform, since the plots for $|J_x|$ show more disagreement near the plate center than elsewhere. Careful examination of many numerical results reveals that the points near the plate center are more sensitive to integration accuracy, plate thickness, and the number of nodes used. One reason for this sensitivity is due to the way in which the numerical integration is performed. In a typical computer run, for economical reasons, the integration is performed over only a specified region around a given node. Therefore the nodes close to the center may be coupled to more nodes than the nodes near the edges.

(c) Plate Thickness

Figures 12 and 13 show the distributions of J_x along x- and y-axes respectively for a square plate of 0.4λ length and various thickness (2t). Sixteen node points and linear shape functions were used for the computation. It is seen that the amplitude of the current varies in an inverse manner to the plate thickness. As the plate thickness becomes larger than $.02\lambda$, some small ripples and a dip occur on the plots. However, the phase remains relatively constant. As will be discussed in a later section, the plate thickness is a relative — not absolute — parameter. It is found that the numerical solution depends actually on the ratio of the plate thickness to the subdivision size in the integration.

(d) Linear and Sinusoidal Shape Functions

Figures 14 and 15 show the comparison of $|J_x|$ for a square plate of 0.6λ long at normal incidence using linear and sinusoidal shape functions. The difference between these two results is small for the size of plate considered here. But for larger element sizes, the difference will be more noticeable, and it is expected that the sinusoidal shape function produce better results. However, there is an advantage of using the linear shape function in the computation, since it consumes less time.

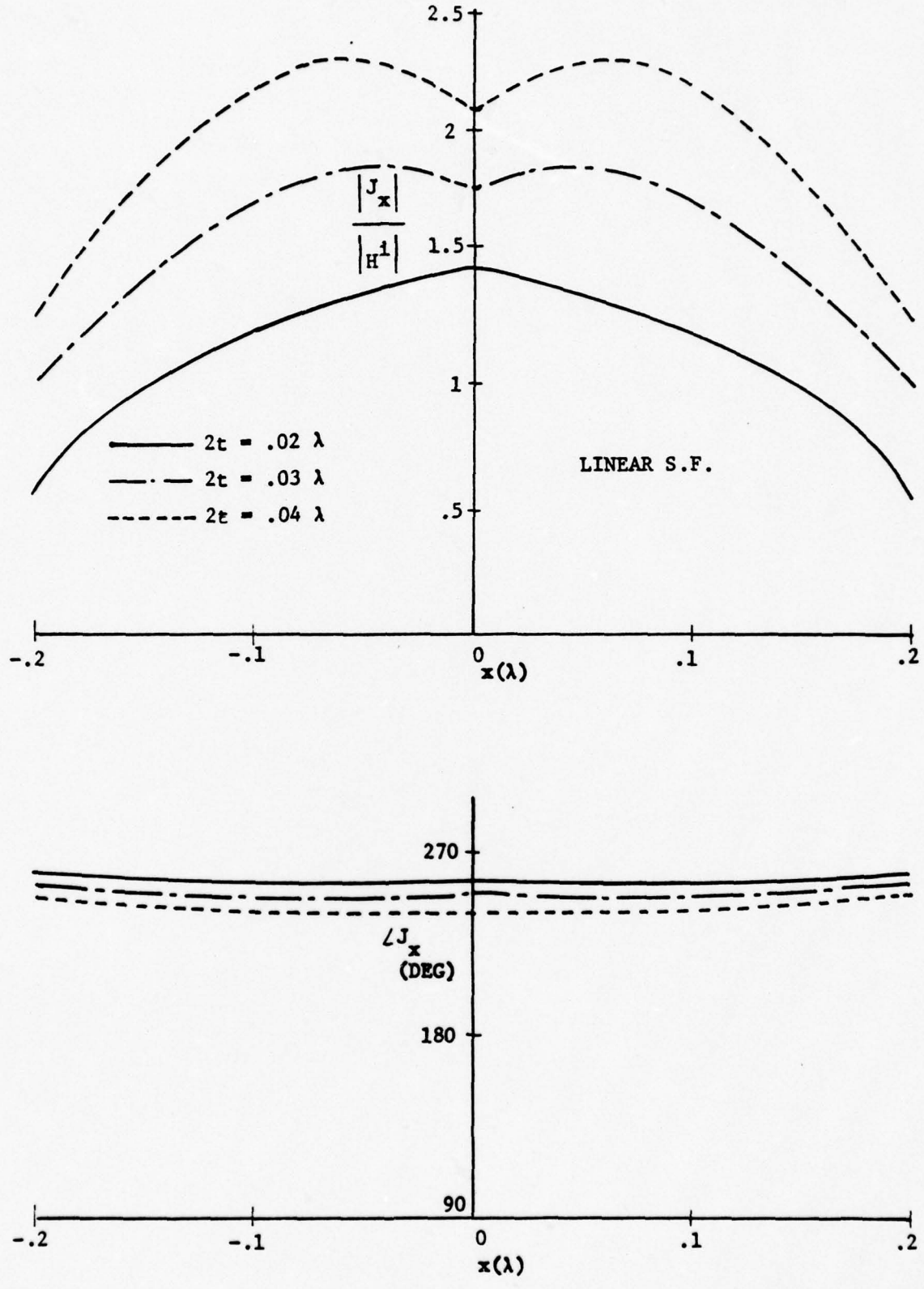

Figure 12. Distributions of J_x Along x-Axis for Flat-Square Plates of Various Plate Thickness, Normal Incidence ($\phi = 90°$) and $\theta = 0$.

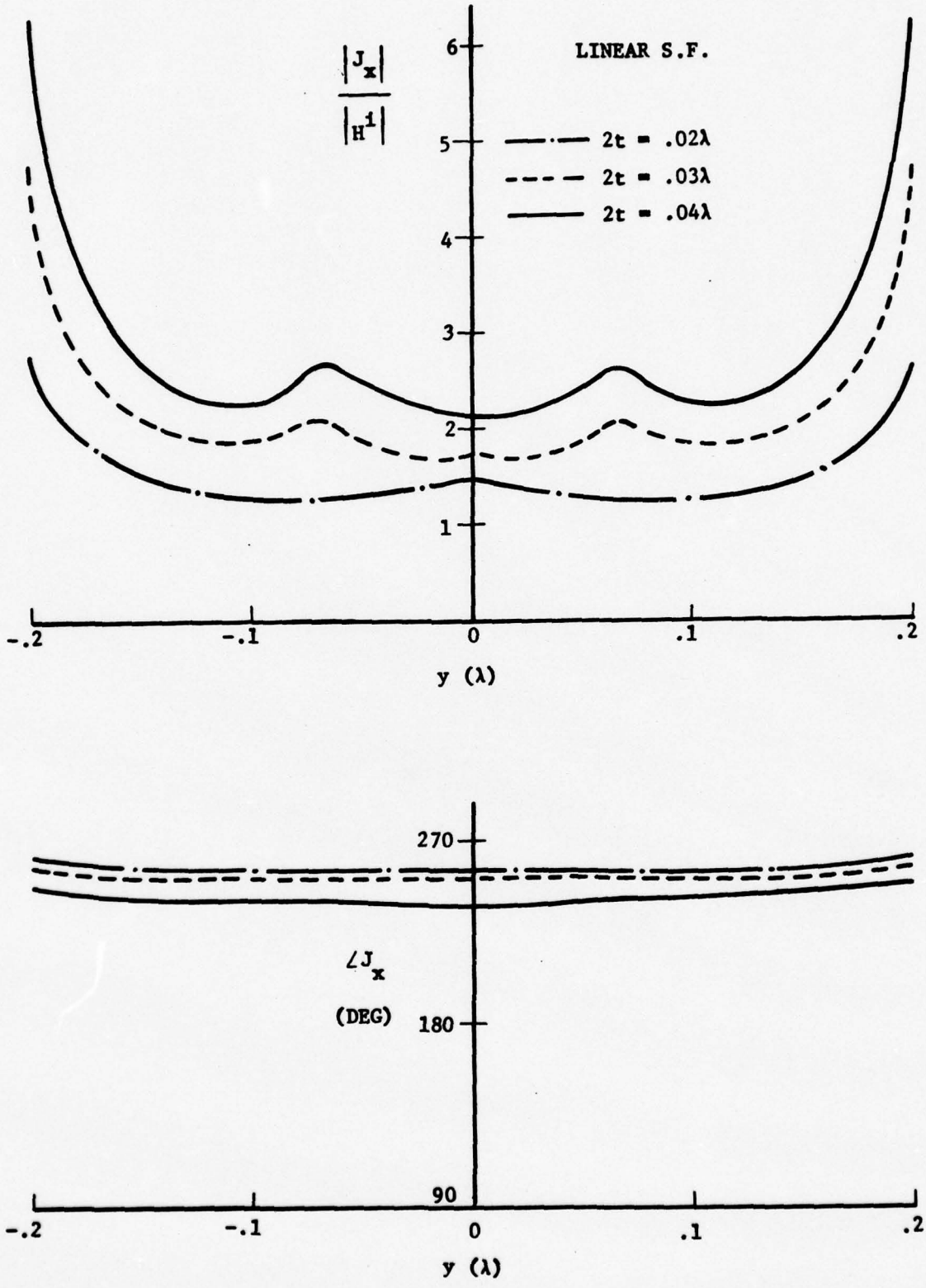

Figure 13. Distributions of J_x Along y-Axis for Flat-Square Plates of Various Plate Thickness, Normal Incidence ($\phi = 90°$) and $\theta = 0$.

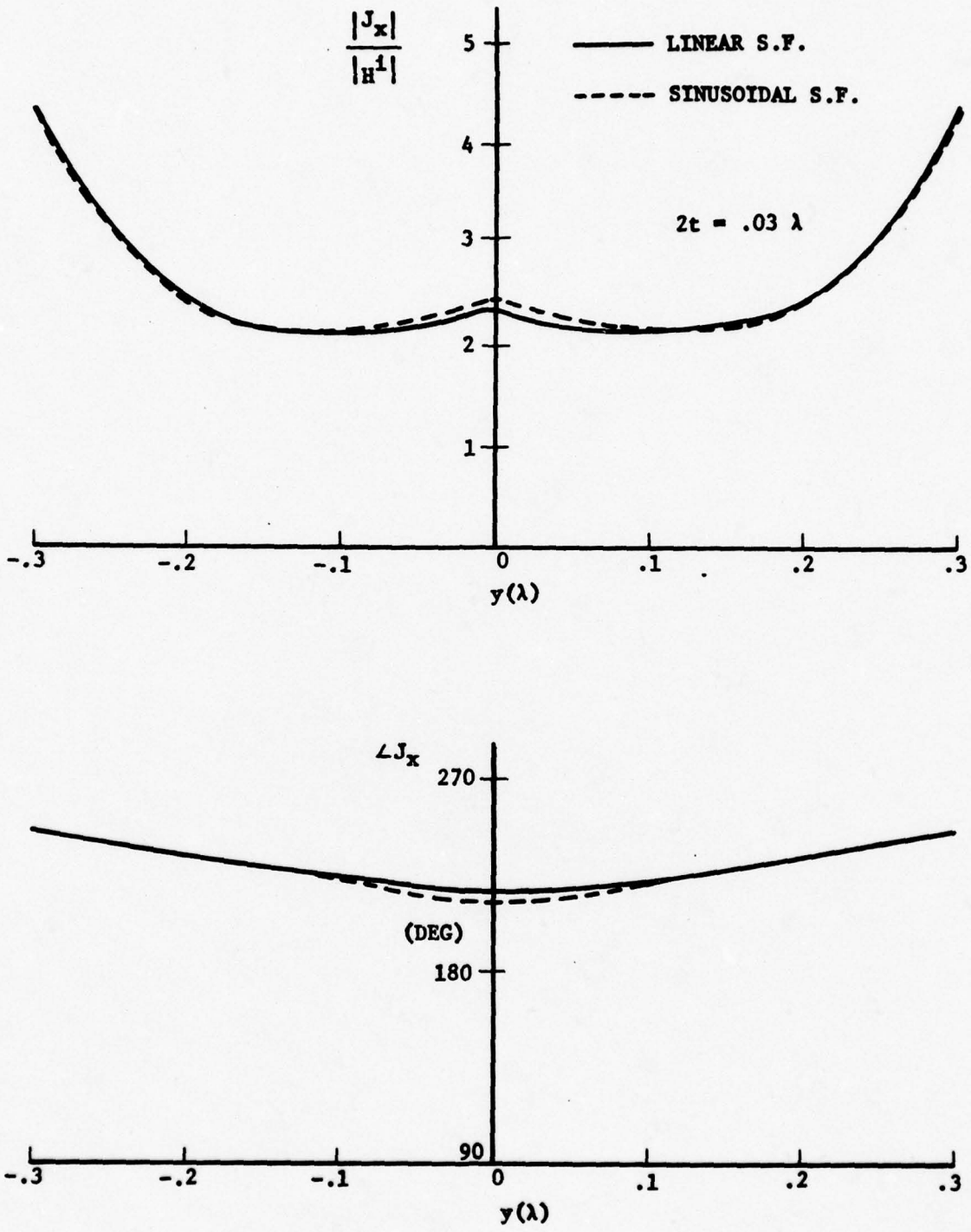

Figure 14. Distributions of J_x Along y-Axis for a Flat-Square Plate with Different Shape Functions, Normal Incidence ($\phi = 90°$) and $\theta=0$.

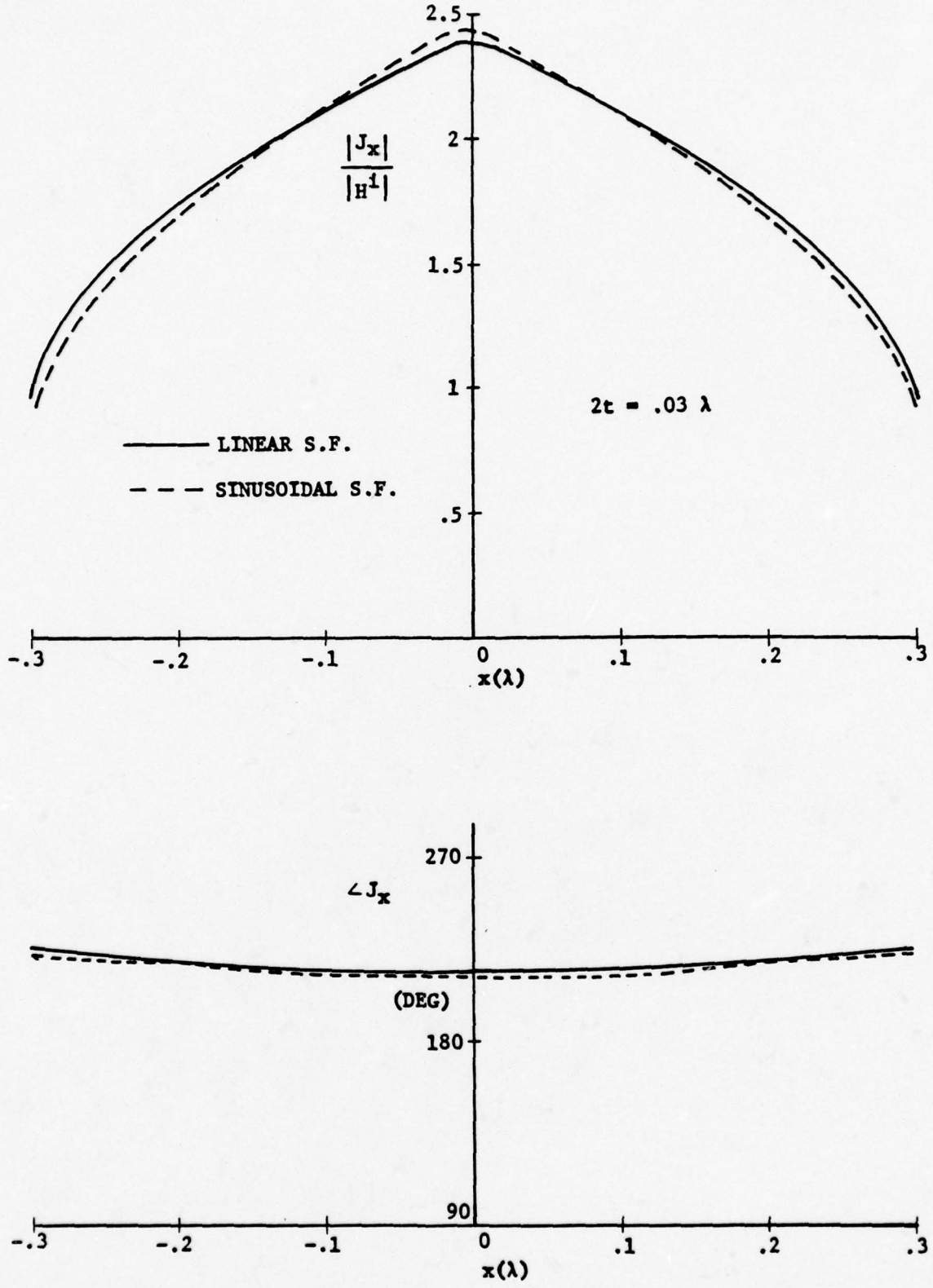

Figure 15. Distributions of J_x Along x-Axis for a Flat-Square Plate with Different Shape Functions, Normal Incidence ($\phi = 90°$) and $\theta = 0$.

(e) Cross-Polarization Current

In most of our computation the polarization of the incident vector was assumed in the x direction ($\theta = 0$); hence the cross polarization current J_y is much smaller than the parallel-polarization component J_x. Because of its smallness, it is difficult to obtain reliable results without using extremely accurate integration scheme. As the angle of polarization increases, the cross-polarization current will likewise increase. This is illustrated in Fig. 16 for square plate of 0.4λ size.

(f) Boundary Conditions

It is known that in solving boundary-value problems, the boundary conditions must be included in order to obtain a unique solution. However, in variational problems, the solution automatically satisfies the natural boundary conditions. In our study here, we have done some investigation about the effect of the edge condition. The edge condition employed here is given by $\hat{n}_e \cdot \underline{J} = 0$, where $\hat{n}_e$ denotes a unit vector normal to the edge. Figure 17 shows $|J_x|$ for a square plate of 0.7λ in length. It is seen that the difference between the two results is negligible in the y direction and significant in the x direction. This discrepancy is primarily caused by the few number of nodes used. The difference will probably be reduced when more nodes are employed instead of only 16 being used here.

(g) Polarization Angle

Figures 18 and 19 show the effect of polarization on the distribution of J_x along x- and y-axes for a square plate of 0.6λ size at normal incidence. As expected the magnitude of J_x is proportional to $\cos\theta$ and the phase is relatively constant. The results have the same kind of behavior as the polarization angle on the cross-polarization current as discussed previously.

(h) Oblique Incidence

The effect due to angle of incidence ϕ on the current distribution is illustrated in Fig. 20. For oblique incidence, we have symmetry

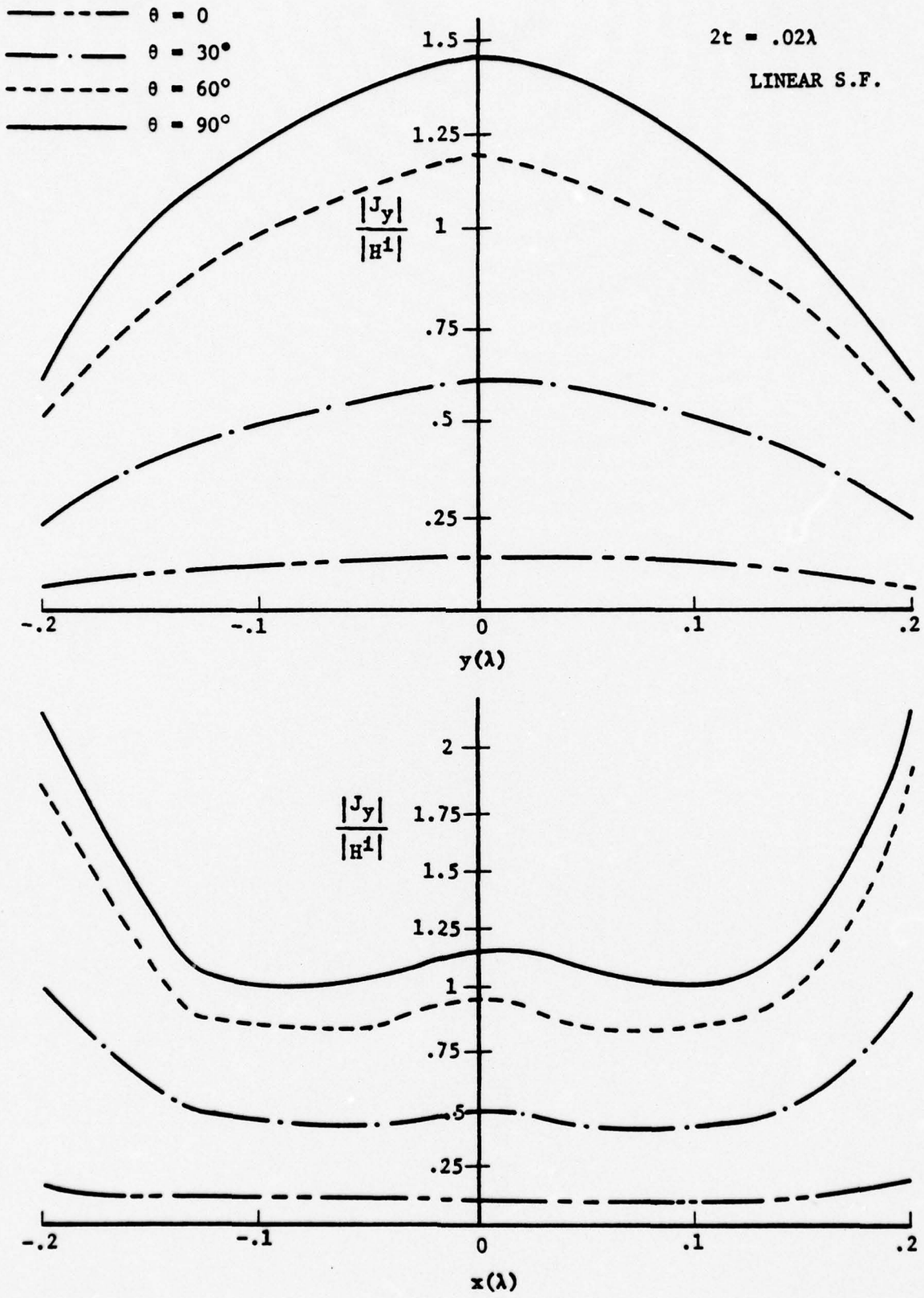

Figure 16. Distributions of $|J_y|$ Along y-Axis and x-Axis for a Flat-Square Plate at Normal Incidence and Various Angles of Polarization.

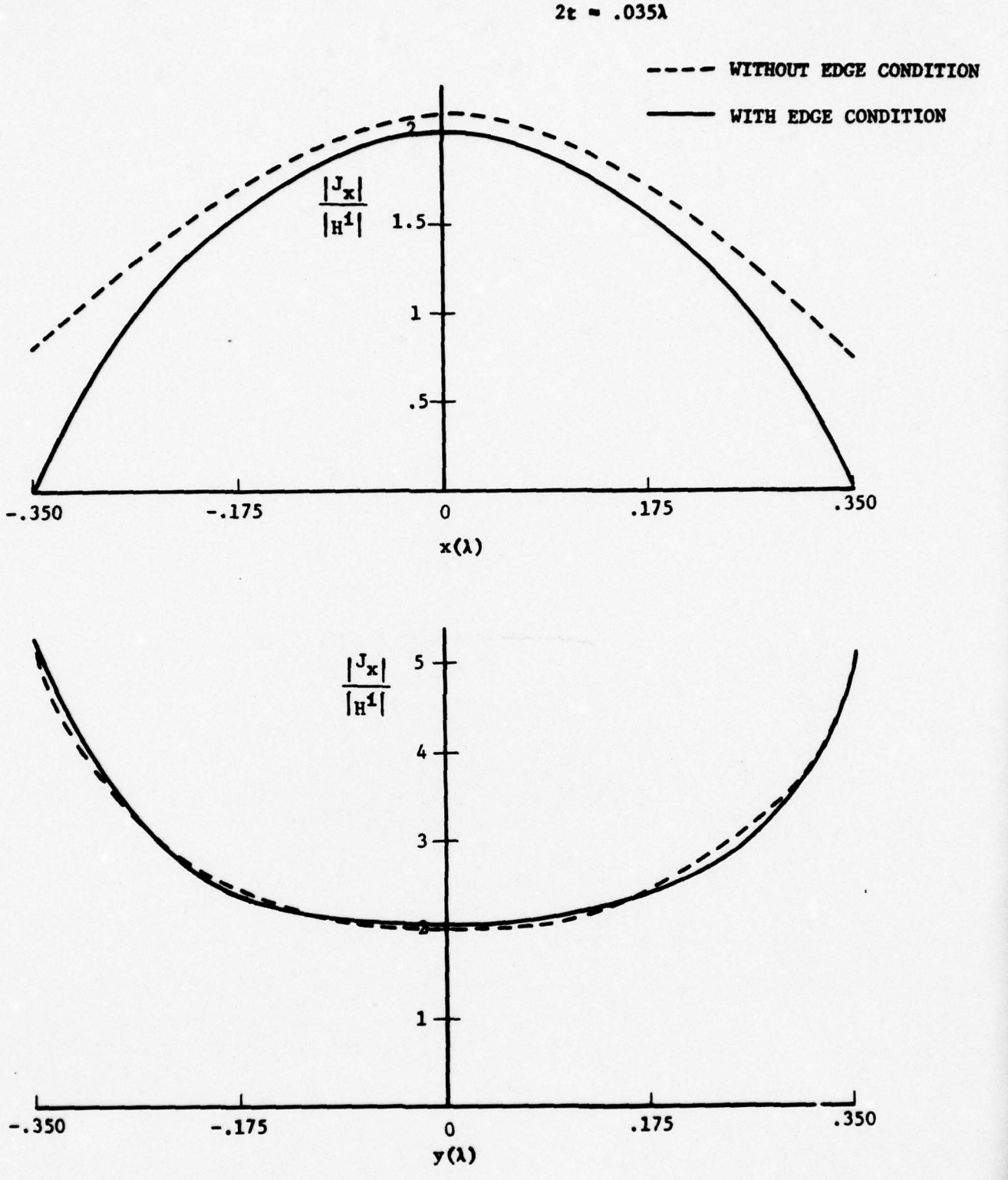

Figure 17. Distributions of $|J_x|$ Along x-Axis and y-Axis for a Flat-Square Plate With and Without Edge Condition, Normal Incidence ($\phi = 90°$) and $\theta = 0$.

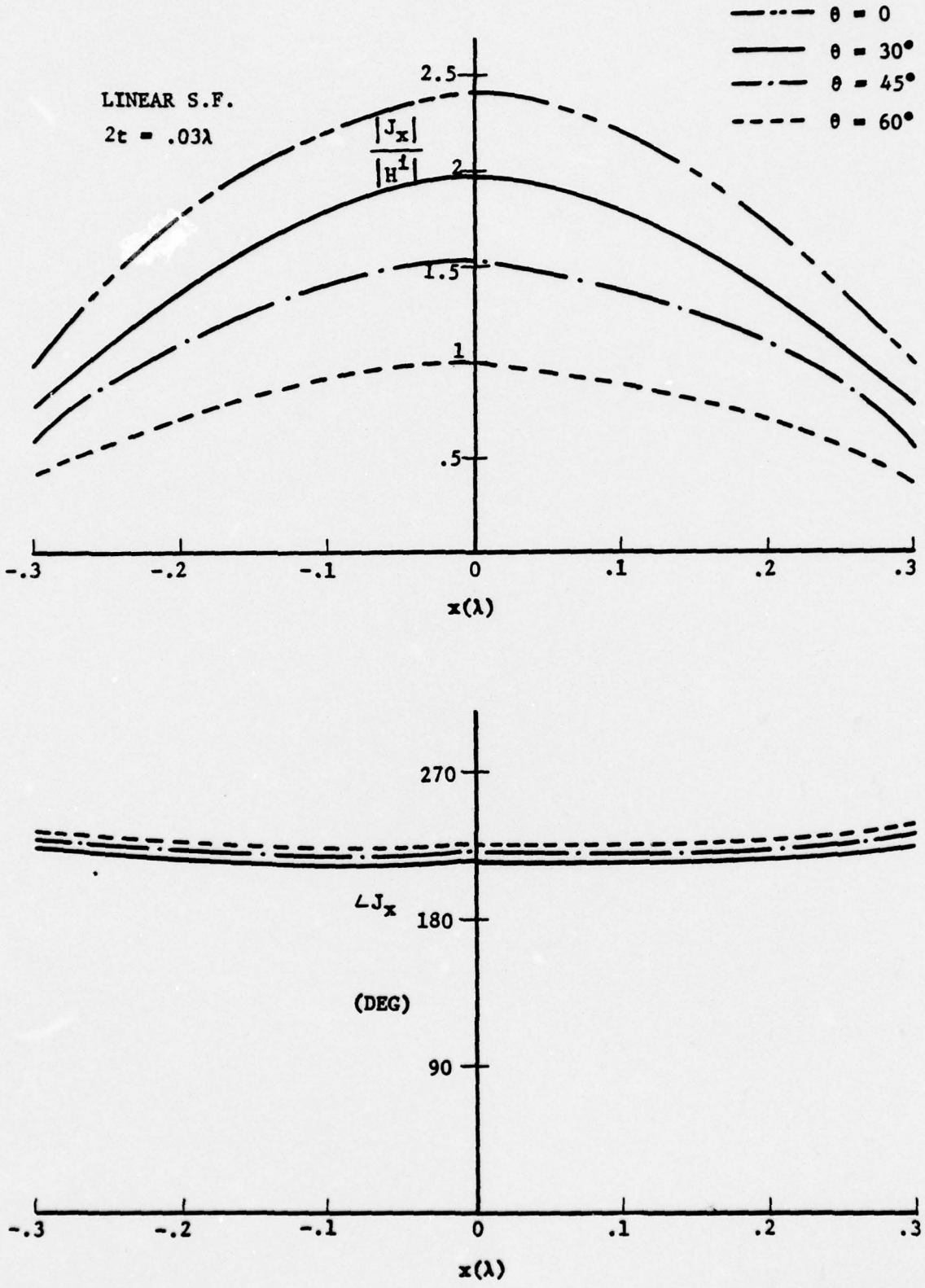

Figure 18. Distributions of $|J_x|$ Along x-Axis for a Flat-Square Plate for Various Polarization Angles and Normal Incidence ($\phi = 90°$).

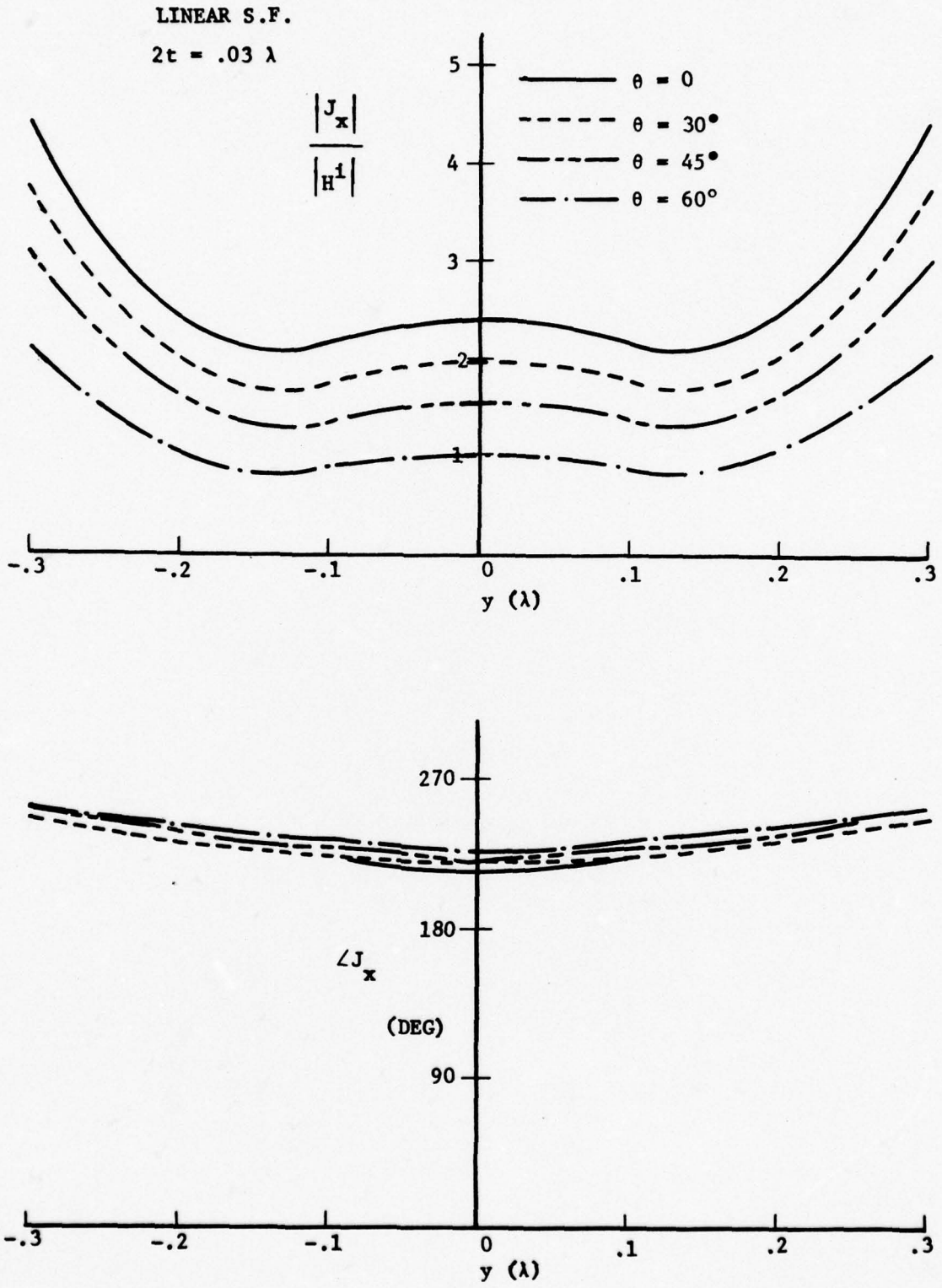

Figure 19. Distributions of $|J_x|$ Along y-Axis for a Flat-Square Plate for Various Polarization Angles and Normal Incidence (ϕ = 90°)

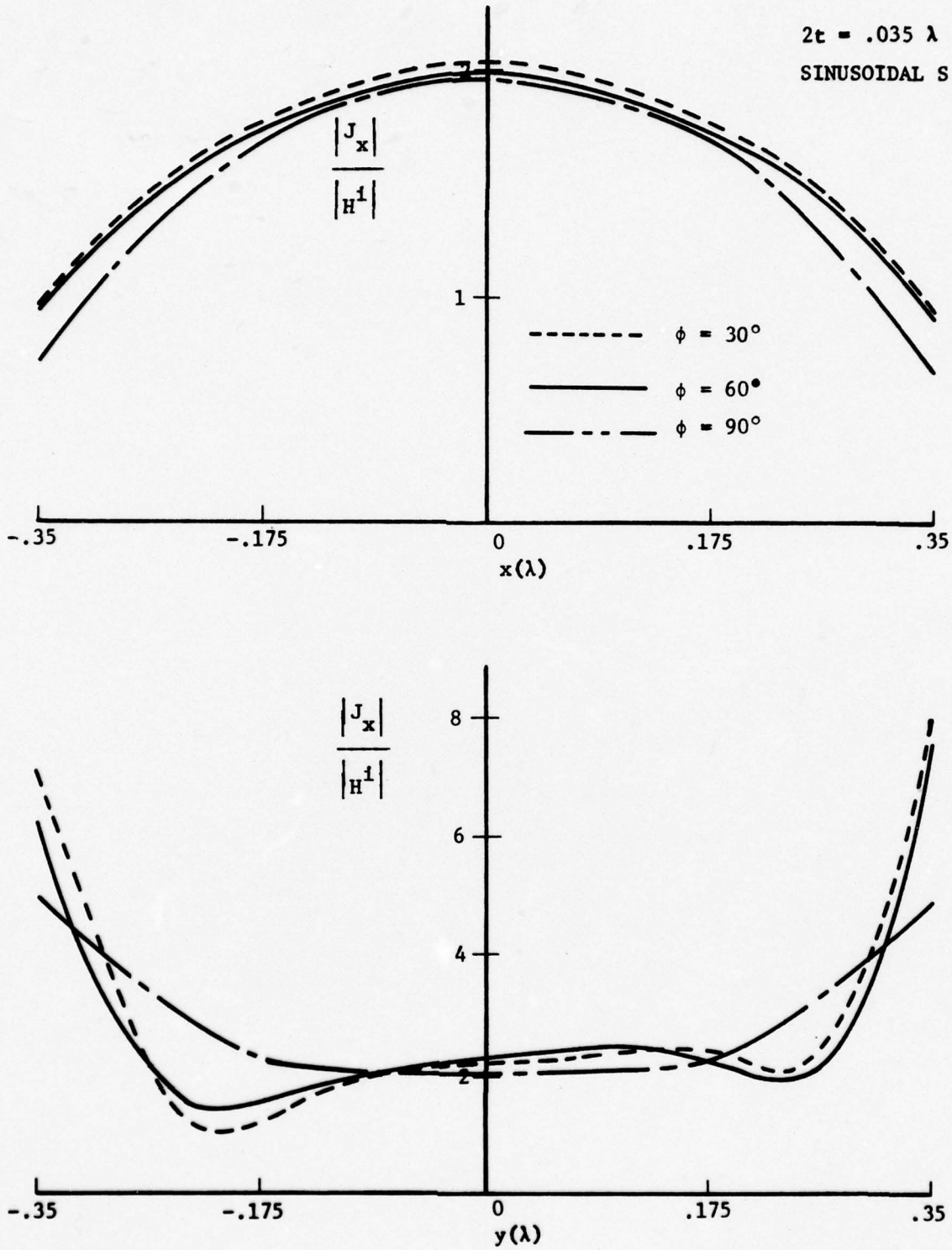

Figure 20. Distributions of $|J_x|$ Along x-Axis and y-Axis for a Flat-Square Plate at Various Angles of Incidence and θ = 0.

only with respect to the y-axis, and therefore we have to use more nodal points in the y direction. In our computation here, 28 nodes were used with 4 in the x direction and 7 in the y direction for each oblique incidence and only 16 for normal incidence. It is seen that $|J_x|$ along x direction increases slightly as ϕ decreases. The results for normal incidence and oblique incidence differ more in the y direction, especially in region close to the edge. The difference between the two oblique incidence cases is small. From the classical solution for the diffraction of a semi-infinite plate [17], we know that the current in the neighborhood of the leading edge is proportional to $\sin\left[\frac{1}{2}(180°-\phi)\right]$. Our numerical results do show this behavior.

(i) Current Distribution for Resonant Size

Figures 21 and 22 show the current distribution of J_x in the x and y directions respectively for a square plate of one wavelength long and various thickness. Even though only 16 nodal points were used, the numerical results are surprisingly good. It is seen that the results here are more stable with respect to change in plate thickness than the cases for small plate sizes. The value of $|J_x|$ at center is very close to the physical optics prediction. Again the phase part is relatively constant over the plate except near the edges. The distribution is found to increase a little bit faster than expected. However, if more nodal points are used, the distribution of $|J_x|$ will improve as shown in Fig. 23.

5.2 Bent-Square Plate

Figure 24 illustrates the current distribution of $|J_x|$ along x_c direction ($y = .3\lambda$) and along y/y_b axis for a bent-square plate of $\phi_b = 130°$ and normal incidence. Again it shows that the results are very close for the two different shape functions used. Comparing these results with those for the flat-square plate, we find that the bent causes changes on the current distribution mainly in the region close to the bent. The current on the inclined side of the plate is larger at $\theta = 45°$. This is understandable since the inclined side is at normal incidence when $\theta = 45°$. The distributions of $|J_x|$ and $|J_y|$ along x_c and y/y_b axes are given in Figures 25 and 26 for the same plate at normal incidence with

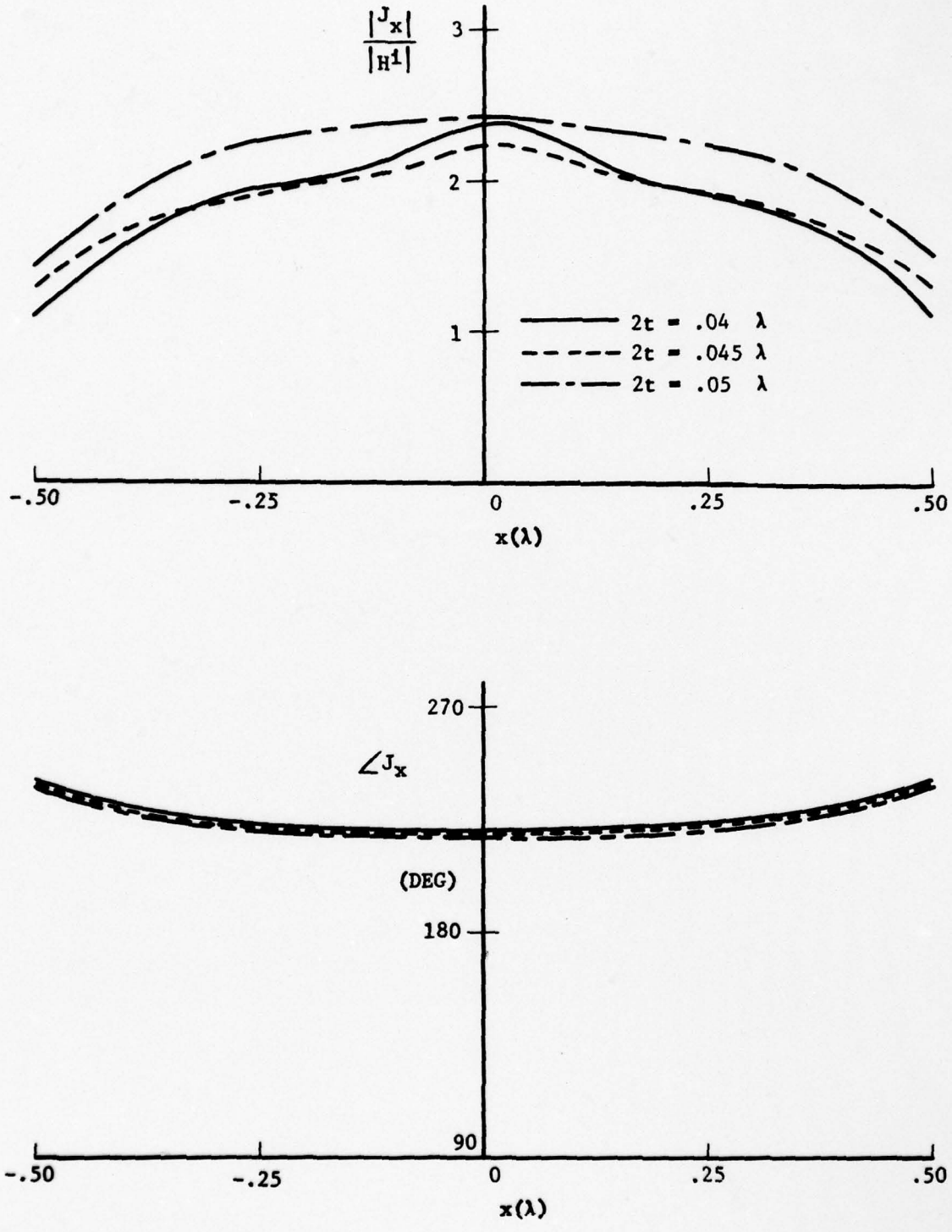

Figure 21. Distributions of J_x Along x-Axis for a Flat-Square Plate for Various Thickness at Normal Incidence ($\phi = 90°$) and $\theta = 0$.

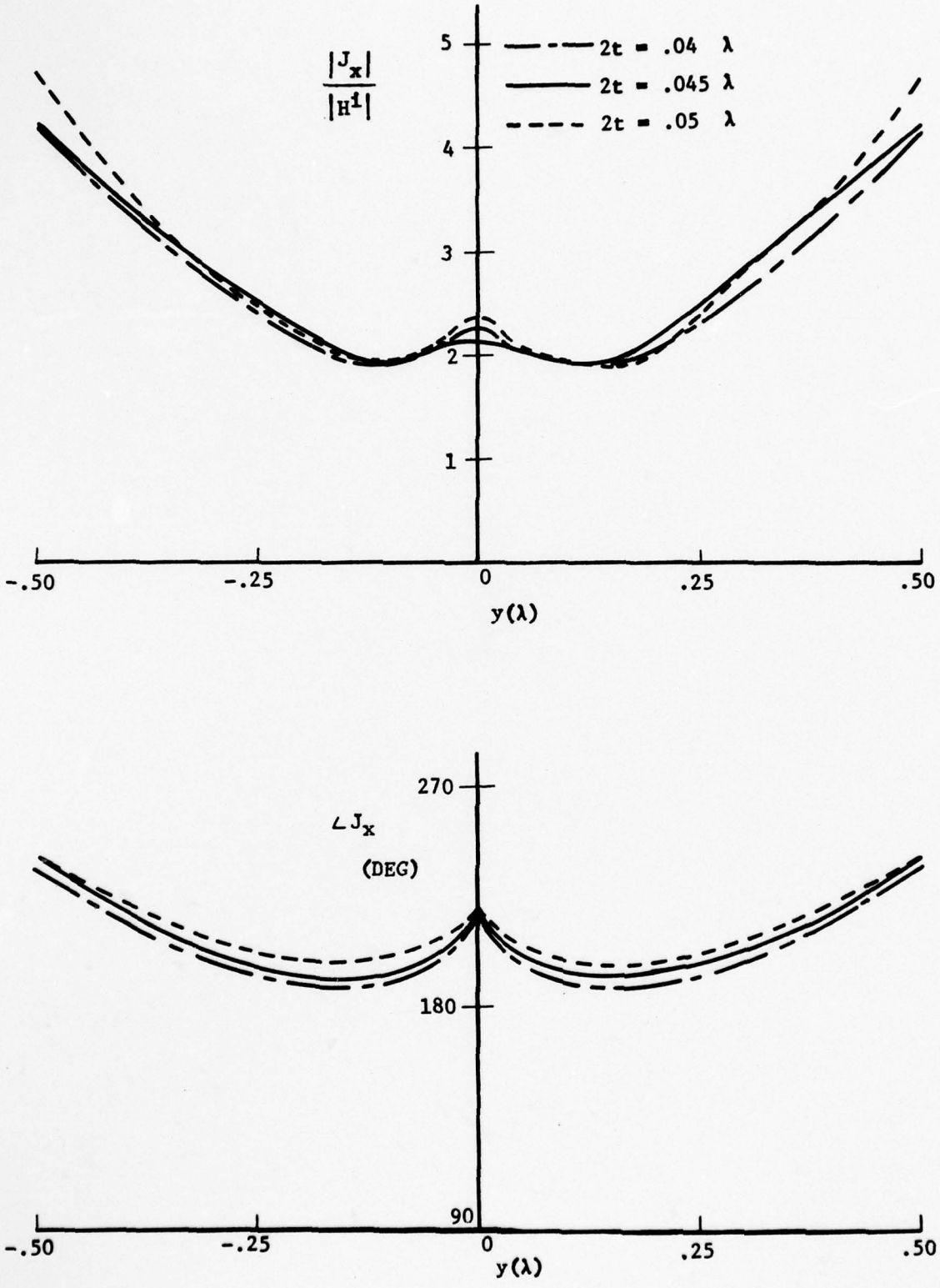

Figure 22. Distributions of J_x Along y-Axis for a Flat-Square Plate for Various Thickness at Normal Incidence ($\phi = 90°$) and $\theta = 0$.

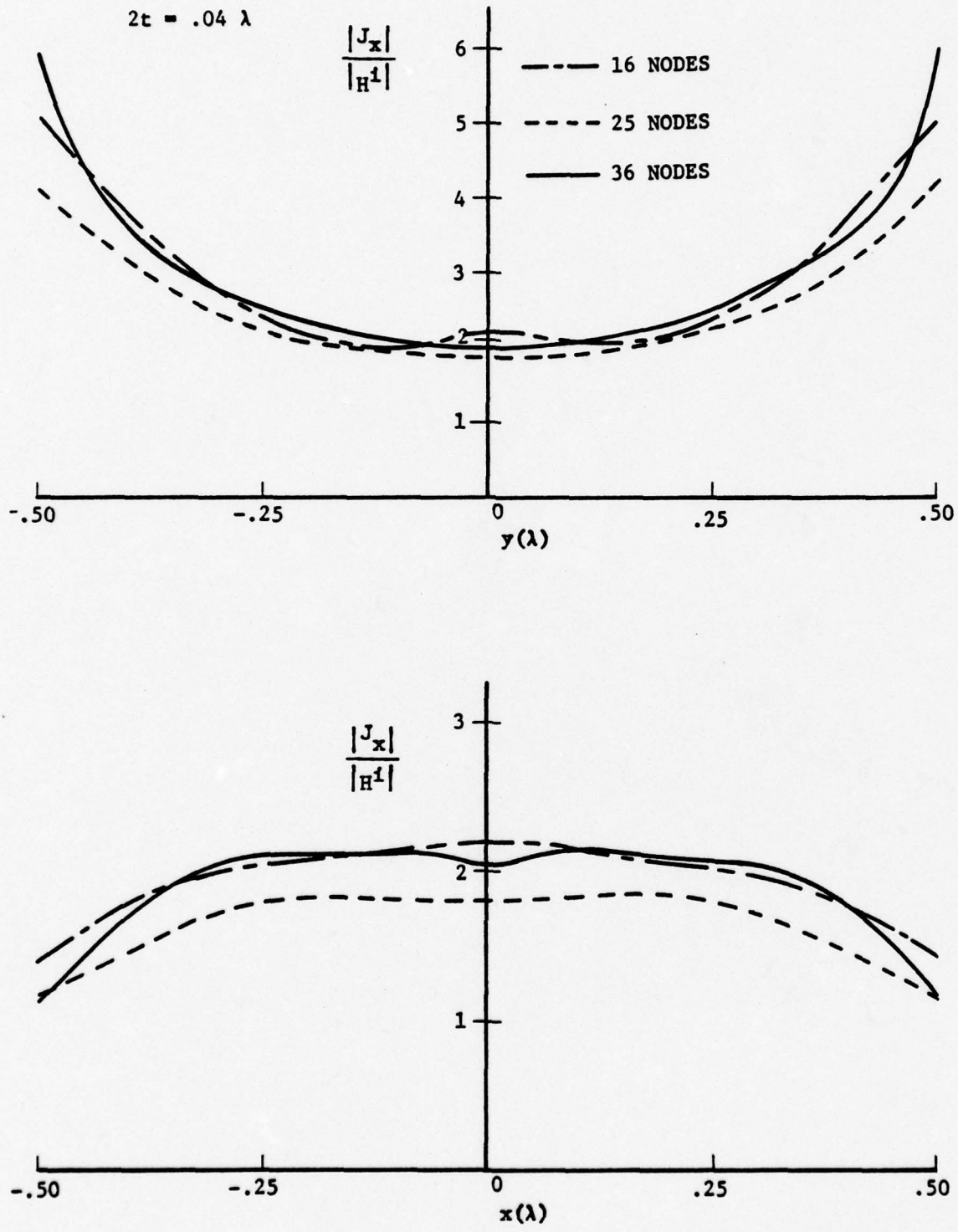

Figure 23. Distributions of $|J_x|$ Along x- and y-Axes for a Flat-Square Plate with More Numbers of Nodes at Normal Incidence ($\phi = 90^\circ$) and $\theta = 0$.

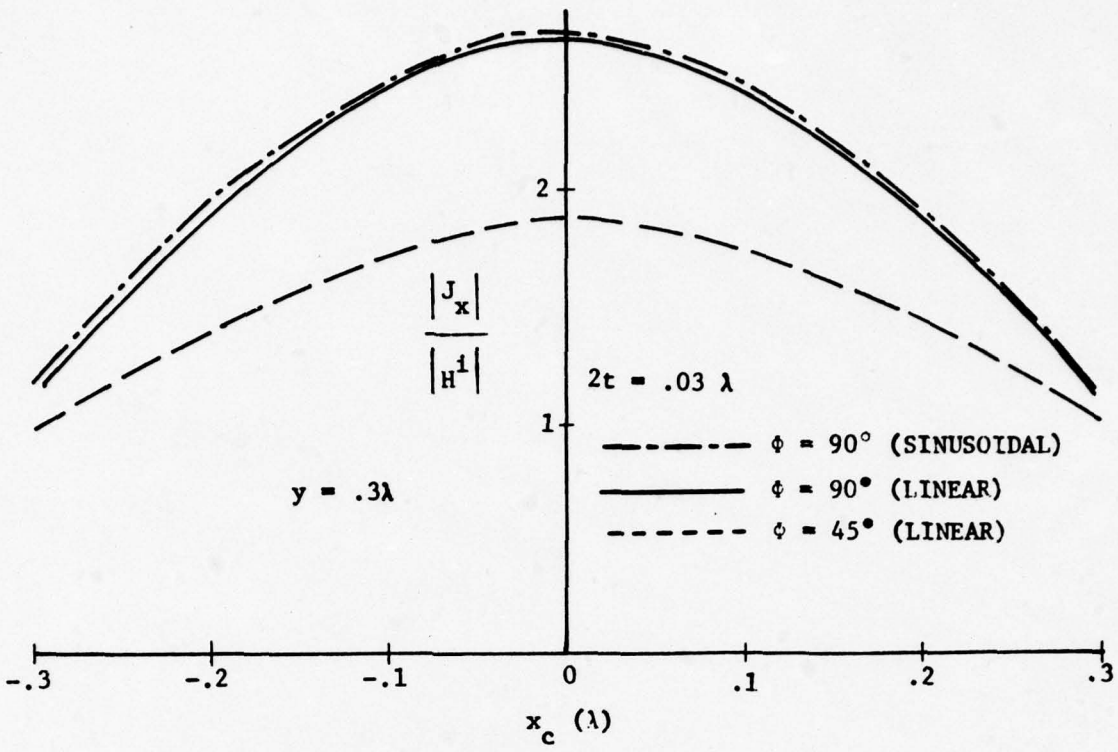

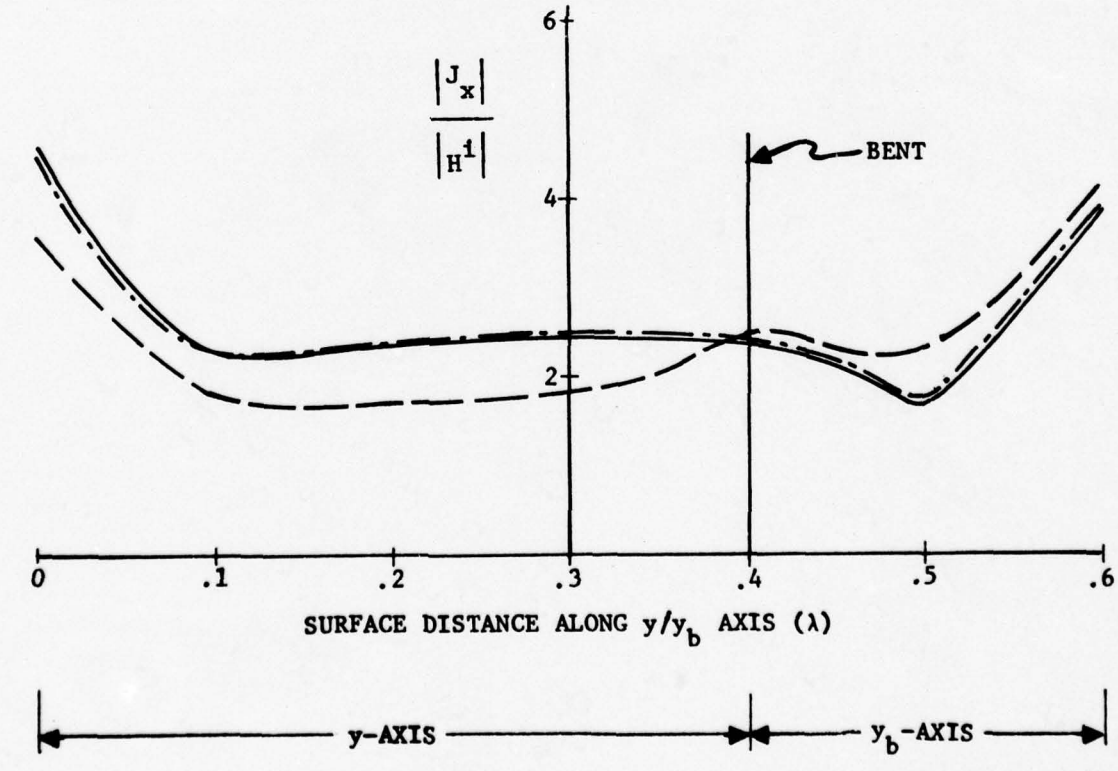

Figure 24. Distributions of $|J_x|$ Along x_c (y = .3 λ) and Along y/y_b Axis for a Bent-Square Plate (ϕ_b = 130°) for Different Angles of Incidence

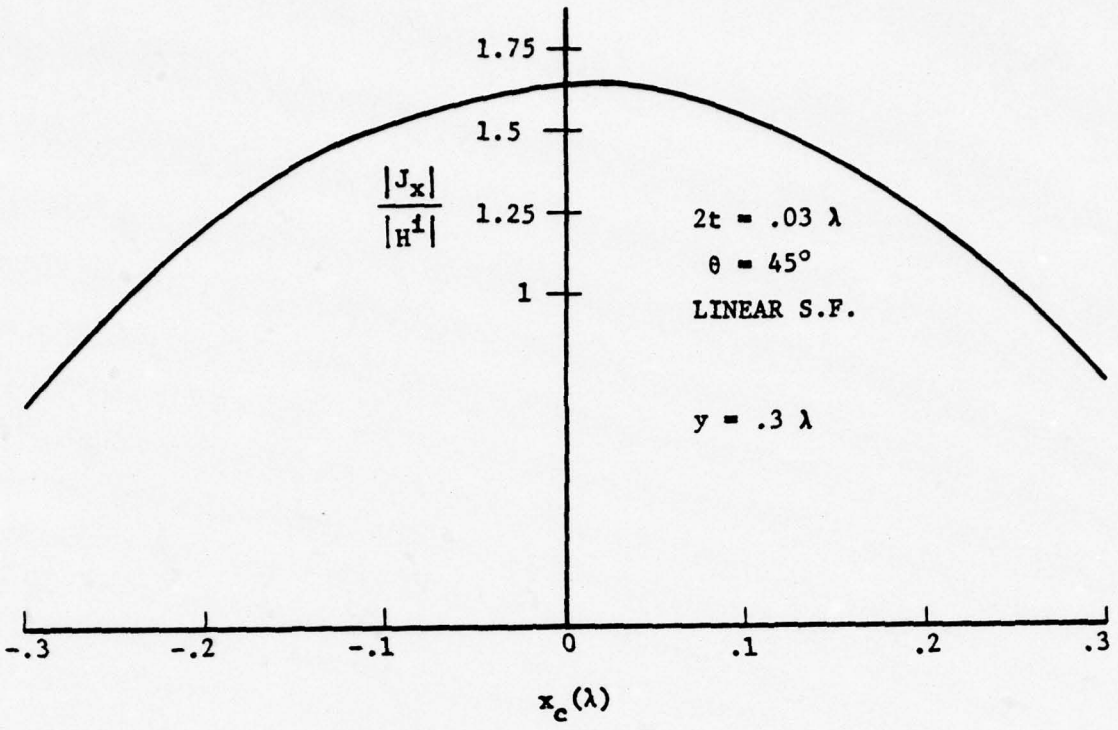

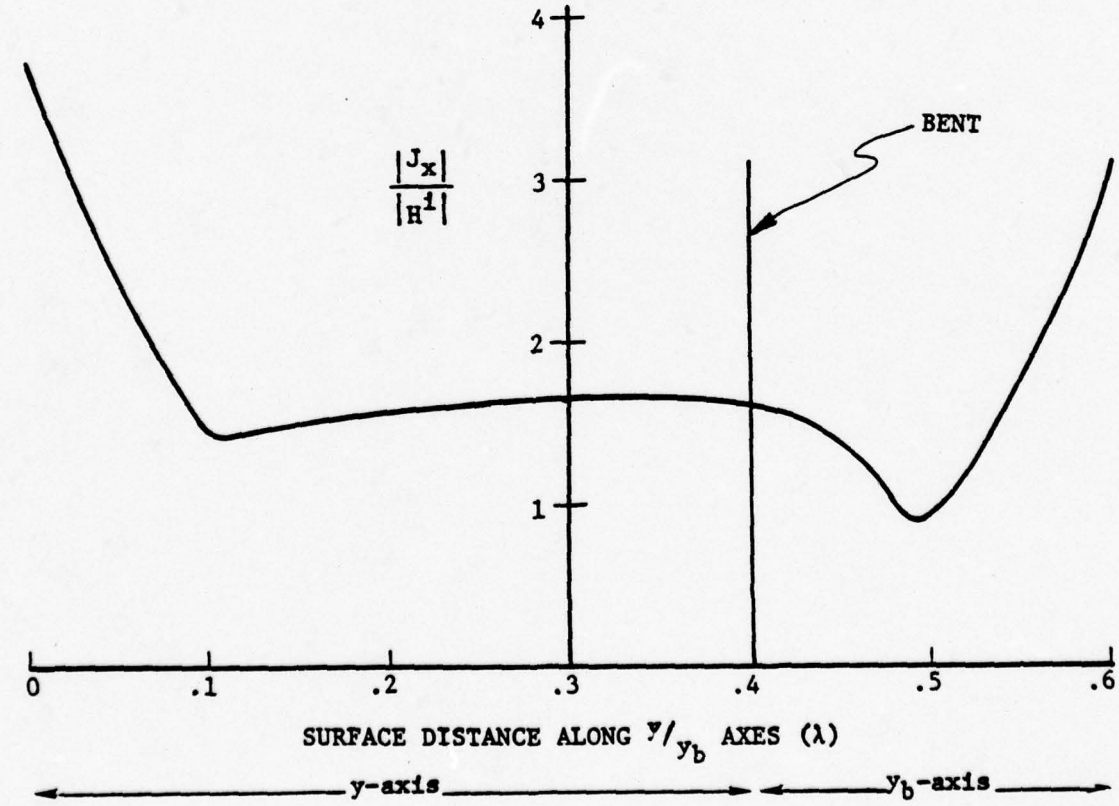

Figure 25. Distributions of $|J_x|$ Along x_c and y/y_b Axes for a Bent-Square Plate (ϕ_b = 130°) at Normal Incidence (ϕ = 90°) and θ = 45°.

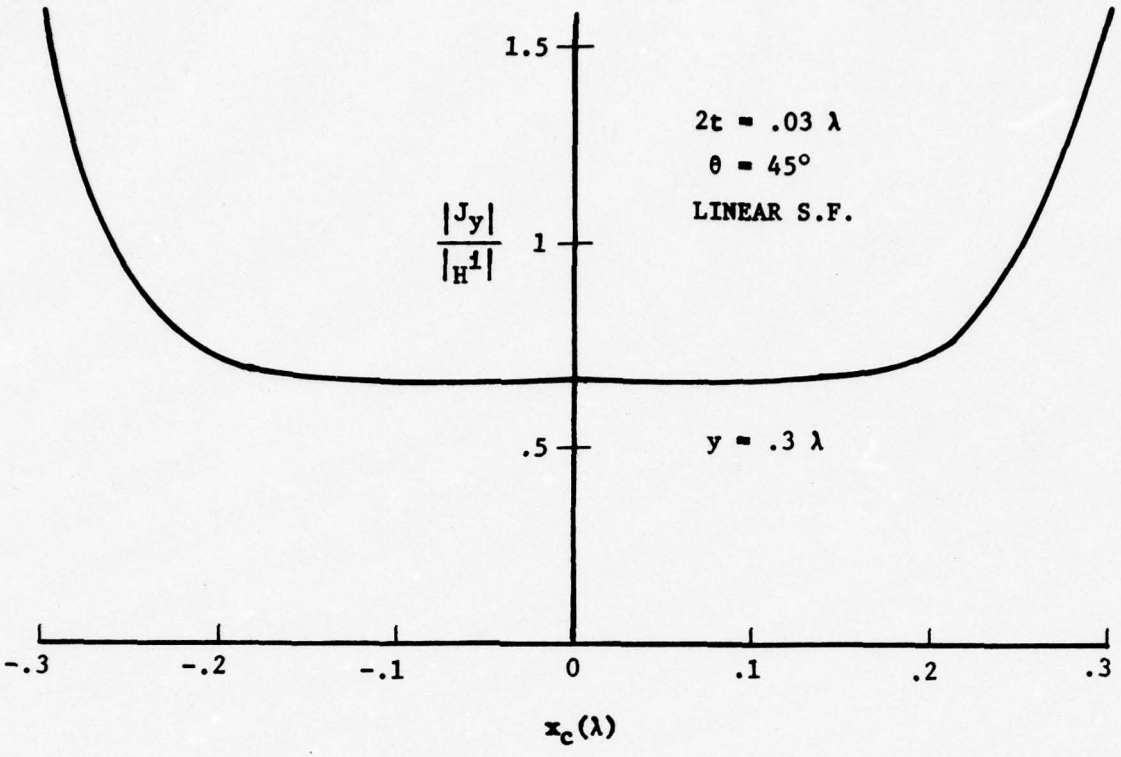

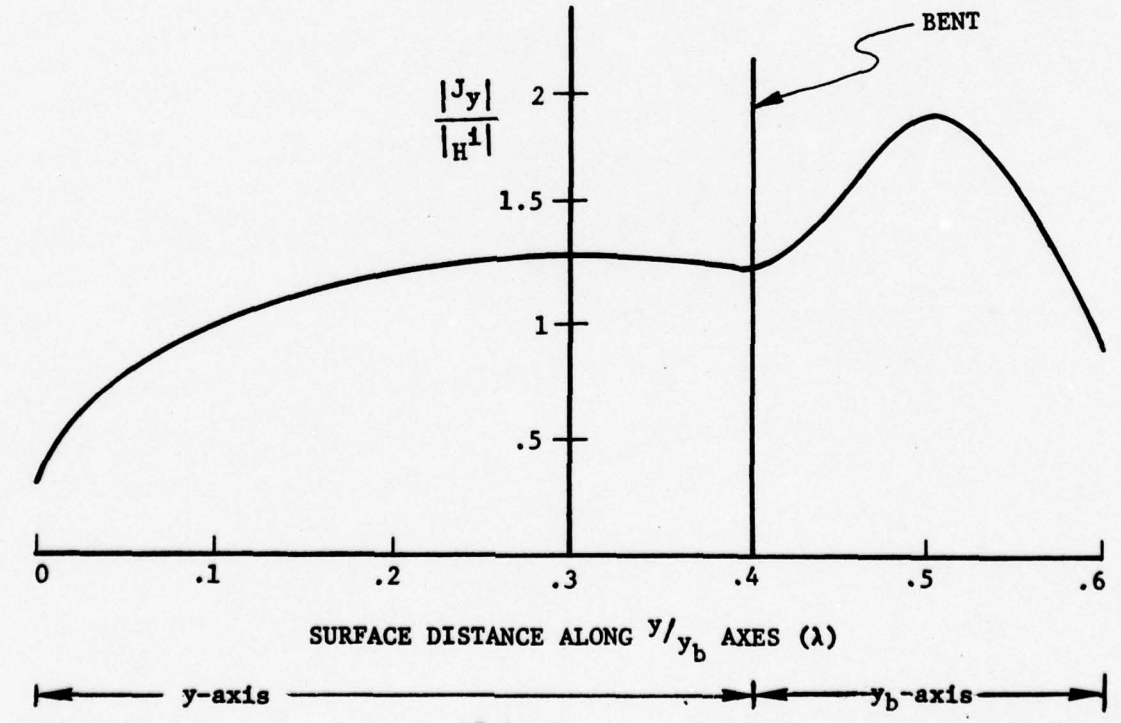

Figure 26. Distributions of $|J_y|$ Along x_c and y/y_b Axes for a Bent-Square Plate ($\phi_b = 130°$) at Normal Incidence ($\phi = 90°$) and $\theta = 0$.

polarization angle of 45°. Unlike the flat-square plate, $|J_x|$ here is larger than $|J_y|$. This indicates that the presence of the bent reduces $|J_y|$. It is also seen that the derivative of $|J_y|$ experiences a discontinuity at the bent. This may be caused by the existence of a line charge there. Figure 27 shows the distribution of $|J_x|$ for plate size of one wavelength. Two angles of incidence are considered: $\phi = 90°$ and 45°. Again as for oblique incidence 28 nodes were used in each computation. To increase matrix stability, a smaller thickness, $\Delta = 0.0375\lambda$, was chosen. It is seen that $|J_x|$ in the x direction is similar to that for a flat-square plate while $|J_x|$ near the inclined surface in the y/y_b direction becomes smaller and shows some multiple diffraction phenomenon. The value of $|J_x|$ at center for $\phi = 90°$ is very close to the physical optics prediction.

5.3 Computational Time and other Factors

The computer time required in each run depends strongly on the number of nodes, the number of subdivisions in each element (three subdivisions were used in most cases here), the integration accuracy as well as the type of shape function used. For a 16 nodal point case, the CPU time for a typical run is about 75 seconds. Most of the time is consumed in matrix fill. Computational time increases rapidly with the number of nodes. In order to reduce the computational time, it is proposed that the entire double surface integral be transformed into a repeated surface integral in the variational integral equation. The transformation is given in Appendix A. Another idea being pursued is to handle the singularity integration analytically rather than numerically with a finite thickness.

Examination of the numerical results shows that the stability and accuracy of the numerical solution depend strongly on many parameters which are characterized by the following ratios: (1) thickness (2t)/ subdivision size (δ), (2) subdivision size (δ)/subdivision size for the singularity integration (δ_s) and the subdivision size (δ) itself. Table 1 shows the dependence of the value of $|J_x|$ at the plate center on these parameters for a plate size of 0.6λ in length.

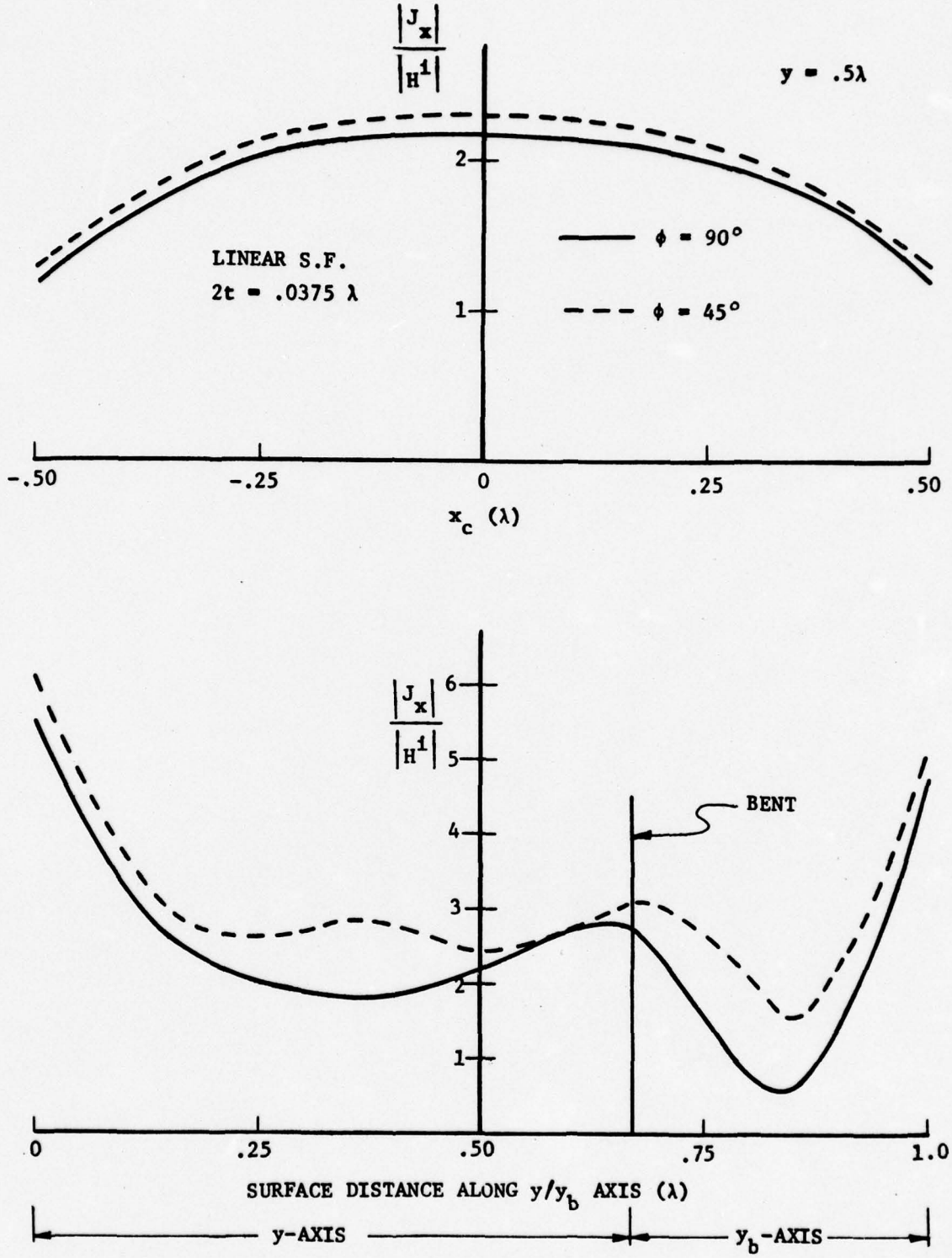

Figure 27. Distributions of $|J_x|$ Along x_c and y/y_b Axes for a Bent-Square Plate (ϕ_b = 130°) at Different Angles of Incidence and θ = 0.

Table 1. Dependence of $|J_x|$ on Plate Thickness, Subdivision Size and Element Size ($\phi = 90°$, $\theta = 0$)

Δ Element Size (λ)	$2t$ Thickness (λ)	δ Subdivision Size (λ)	δ_s Subdivision Size for Self Term (λ)	$\|J_x\|/\|H^i\|$ Plate Center
.06	.03	.02	.0075	1.76
.06	.03	.02	.0075	1.73
.075	.03	.025	.0125	2.61
.075	.03	.025	.009375	1.91
.10	.03	.0333	.0125	2.34
.10	.03	.0333	.00833	1.70
.10	.0225	.0333	.00833	1.61
.10	.03	.0333	.0125	2.34

Experience indicates that to obtain good results we should choose these parameters carefully. Unfortunately there are no exact rules for us to follow in choosing these parameters. However, it is recommended that in our computation we should observe the following guidelines:

- the ratio t/δ should be close to unity
- the subdivision size δ should not be larger than $.03\lambda$
- the ratio δ/δ_s should be about 2.5.

CHAPTER VI

CONCLUSIONS AND RECOMMENDATIONS

The problem concerning scattering of a plane electromagnetic wave from a conducting flat/bent-square plate has been solved numerically using the finite element method. The singularity of the Green's function is treated by assuming a finite thickness. Two computer codes, one for the flat-square plate and the other for the bent-square plate were written. Each computer code can handle different angles of incidence, polarization angles, and plate sizes. Various numerical results for different parameters were presented and discussed. It is found that for plate size less than or equal to 0.8 λ, the numerical results are convergent, stable and good with sixteen nodes. However, when the plate size increases beyond this limit, one has to increase the number of nodal points. Another unsatisfactory feature is the thickness of the plate. To circumvent this, a study is being initiated presently to treat the singularity of the Green's function analytically, and include enough consideration for the current on the back side of the plate. It should be pointed out that all these problems are not due to the FEM but rather it is inherent in the E-field integral equation used. This suggests that all these difficulties may be avoided if other more suitable equations are employed. Investigation is also being carried out in this area of alternate formulation.

Another area which deserves consideration is the reduction of the double surface integral into a repeated integral. The derivation of this has been given in Appendix A. This approach will reduce the computer running times by order of magnitude as has been demonstrated by TRW for one-dimensional problems. Thus, the analytical handling of the singularity and an application of the repeated integral technique will significantly improve the code efficiency.

The FEM method is completely general with respect to geometry and material properties. FEM solutions are formulated by using variational integrals which may often be proportional to the Lagrangian or Hamiltonian of the system — thus bearing close relation to the physically measurable

quantities. The technique can be systematically used to solve such complex and difficult problems as inhomogeneous materials, nonlinear behavior, anisotropic structures, complicated boundary conditions and transient problems. In FEM, the body is discretized without destroying either the structural details or the continuous nature. No separate interpolation process is needed to extend the solution to every point within the continuum. Even though solution is obtained at a finite number of discrete nodal points, the formulation inherently provides a solution at all other locations in the structure. Boundary conditions are very naturally included in this approach and only the geometrical boundary conditions need be specified. The method gives rise to a matrix that is stable, symmetric and often banded.

APPENDIX A

TRANSFORMATION OF THE DOUBLE SURFACE INTEGRAL INTO A REPEATED SURFACE INTEGRAL IN THE VARIATION INTEGRAL EQUATION

As shown in Eq. (34) the variational integral equation involves a double surface integration. From a numerical solution point of view, this is a disadvantage since it requires large computational time. One possible way of reducing the computational time is to transform the double surface integral into a repeated surface integral as given below.

Let

$$I = \int_S \int_{S'} \underline{J}(\underline{r}') \cdot \overline{\overline{G}}(\underline{r}|\underline{r}') \cdot \underline{J}(\underline{r}') dS' \, dS \tag{A-1}$$

$$\underline{J}(\underline{r}) = J_x(x,y)\hat{x} + J_y(x,y)\hat{y} \tag{A-2}$$

From (A-1), (A-2) and using the coordinate system as shown in Fig. A-1, we obtain

$$I = \int_0^{2a}\int_0^{2b}\int_0^{2a}\int_0^{2b} \Big[\lambda_{xx} J_x(x,y) J_x(x',y') + \lambda_{xy} J_x(x,y) J_y(x',y') + \lambda_{xy} J_x(x',y') J_y(x,y) + \lambda_{yy} J_y(x',y') J_y(x,y) \Big] dx'dy'dxdy \tag{A-3}$$

λ_{xx}, λ_{xy} and λ_{yy} are given by (37) to (39).

Let us first consider the first integral and let

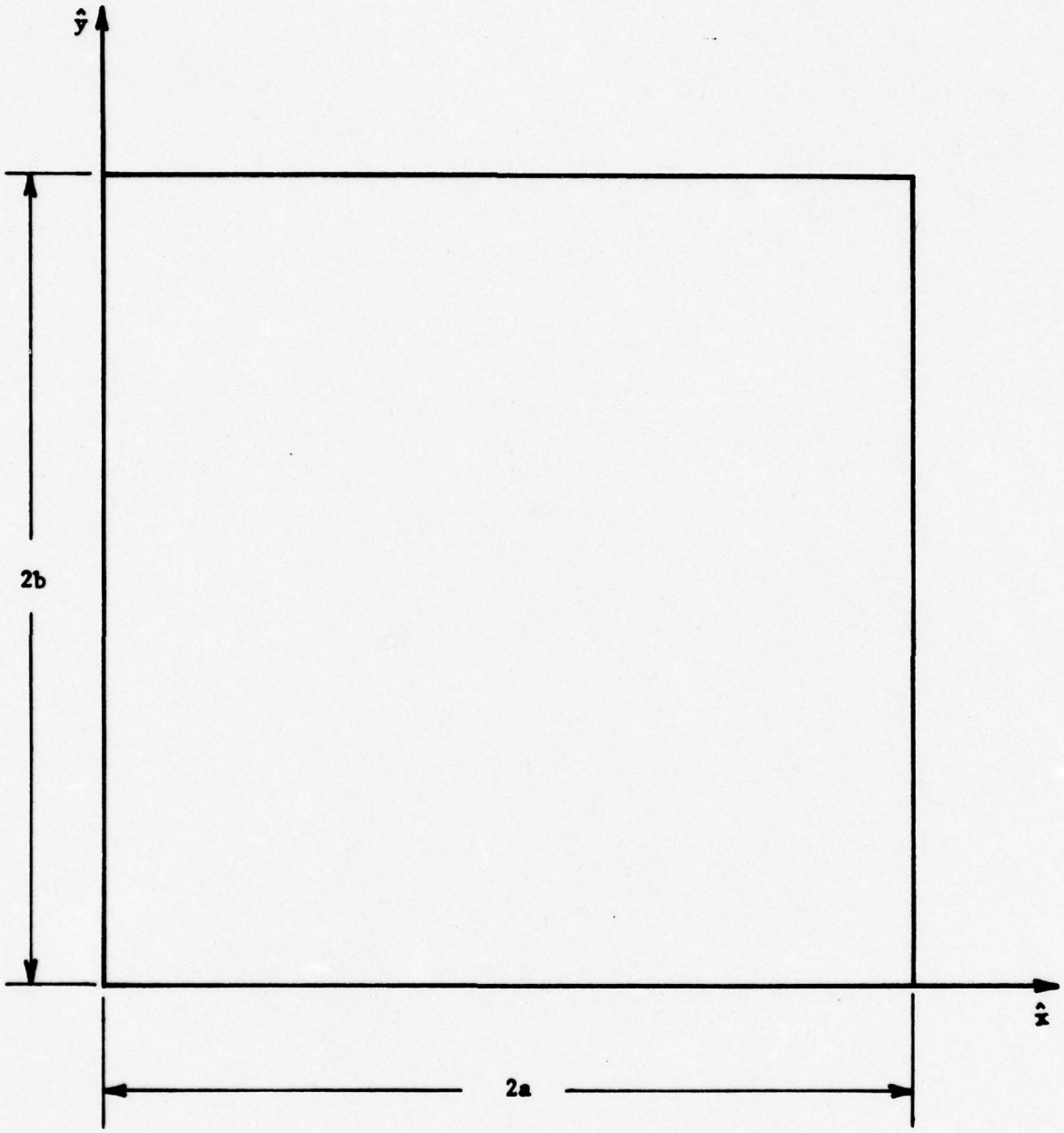

Figure A-1. Coordinate System for Integration

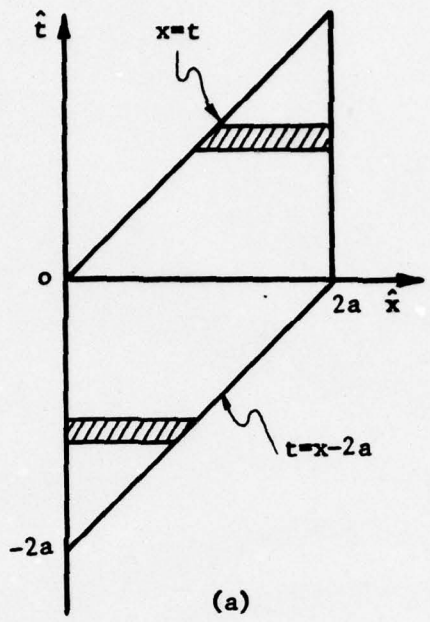

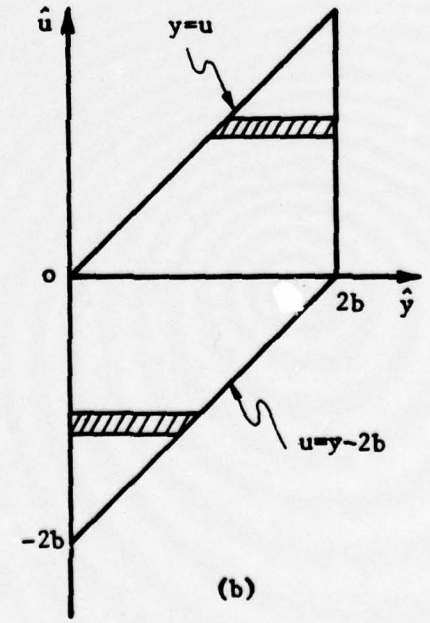

Figure A-2. (a) t-x Diagram and (b) u-y Diagram for Integration

$$I_{xx} = \int_0^{2a}\int_0^{2b}\int_0^{2a}\int_0^{2b} \lambda_{xx}\, J_x(x,y)\, J_x(x',y')\, dx'dy'\, dx\, dy$$

$$= \int_0^{2a}\int_0^{2b} J_x(x,y)\, dx\, dy \int_0^{2a}\int_0^{2b} \lambda_{xx}(x,y,x',y')\, J_x(x',y')\, dx'\, dy' \qquad \text{(A-4)}$$

$$= \int_0^{2a}\int_0^{2b} J_x(x,y) dx\, dy \int_0^{2a}\int_0^{2b} \lambda_{xx}(x-x',y-y')\, J_x(x',y')\, dx'\, dy'$$

Now let us change the variable of integration

$$t = x-x' \qquad \text{(A-5)}$$
$$u = y-y'$$

Substitution of (A-5) into (A-4) yields

$$I_{xx} = \int_0^{2a}\int_0^{2b} J_x(x,y)dxdy \int_x^{x-2a}\int_y^{y-2b} \lambda_{xx}(t,u)J_x(x-t,y-u)dtdu \qquad \text{(A-6)}$$

Let

$$\phi_{xx}(t,u,x,y) = \lambda_{xx}(t,u)J_x(x-t,y-u)J_x(x,y) \qquad \text{(A-7)}$$

By changing the order of integration (Figure A-2) we obtain

$$I_{xx} = \int_{-2a}^{0}dt \int_{-2b}^{0}du \left[\int_0^{2a+t}\int_0^{2b+u} \phi_{xx}(t,u,x,y)\, dx\, dy \right]$$

$$+ \int_0^{2a}dt \int_0^{2b}du \left[\int_t^{2a}\int_u^{2b} \phi_{xx}(t,u,x,y)\, dx\, dy \right] \qquad \text{(A-8)}$$

If we let $t = -t$ and $u = -u$ in the first integral we obtain

$$I_{xx} = \int_0^{2a} dt \int_0^{2b} du \left[\int_t^{2a} \int_u^{2b} \phi_{xx}(t,u,x,y) + \int_0^{2a-b} \int_0^{2b-u} \phi_{xx}(-t,-u,x,y) \right] dxdy \qquad \text{(A-9)}$$

Considering the integration inside the bracket, since t and u are merely parameters there, we can let

$x = x + t$, $t = t$ for the first integral

$y = y + u$, $u = u$ for the second integral

We get from (A-9)

$$I_{xx} = \int_0^{2a} dt \int_0^{2b} du \left[\int_0^{2a-t} \int_0^{2b-u} \phi_{xx}(t,u,x+t,y+u) + \int_0^{2a-t} \int_0^{2b-u} \phi_{xx}(-t,-u,x,y) \right] dx\, dy \qquad \text{(A-10)}$$

Since from (A-7) we have

$$\begin{aligned} \phi_{xx}(-t,-u,x,y) &= \lambda_{xx}(-t,-u) J_x(x+t,y+u) J_x(x,y) \\ \phi_{xx}(t,u,x+t,y+u) &= \lambda_{xx}(t,u) J_x(x,y) J_x(x+t,y+u) \end{aligned} \qquad \text{(A-11)}$$

and from (37) we have

$$\begin{aligned} \lambda_{xx}(t,u) &= \lambda_{xx}(-t,-u) \\ &= g(t,u) + \frac{g(t,u)}{R} \left\{ \frac{t^2}{R} \left[\left(\Omega + \frac{1}{R} \right)^2 - \frac{\Omega}{R} \right] - \Omega \right\} \end{aligned} \qquad \text{(A-12)}$$

with $g(t,u) = -\frac{1}{4\pi} \frac{e^{-jkr}}{R}$

and $R = \sqrt{t^2 + u^2 + t_k^2}$ t_k stands for the half thickness now

therefore we have

$$\phi_{xx}(t,u,x+t,y+u) = \phi_{xx}(-t,-u,x,y) \text{ and (A-9)}$$

becomes

$$I_{xx} = 2\int_0^{2a}\int_0^{2b} \lambda_{xx}(t,u)\, dt\, du \int_0^{2a-t}\int_0^{2b-u} J_x(x+t,y+u)\, J_x(x,y)\, dx\, dy \qquad \text{(A-13)}$$

In a similar manner we obtain

$$I_{yy} = \int_0^{2a}\int_0^{2b}\int_0^{2a}\int_0^{2b} \lambda_{yy}\, J_y(x,y)\, J_y(x',y')\, dx'\, dy'\, dx\, dy$$

$$I_{yy} = 2\int_0^{2a}\int_0^{2b} \lambda_{yy}(t,u)\, dt\, du \int_0^{2a-t}\int_0^{2b-u} J_y(x+t,y+u)\, J_x(x,y)\, dx\, dy \qquad \text{(A-14)}$$

Next let us consider the cross product terms

Let

$$I_{xy} = \int_0^{2a}\int_0^{2b}\int_0^{2a}\int_0^{2b} \lambda_{xy}\, J_x(x,y)\, J_y(x',y')\, dx'\, dy'\, dx\, dy \qquad \text{(A-15)}$$

Following the same procedure as before we obtain

$$I_{xy} = \int_0^{2a} dt \int_0^{2b} du \left[\int_0^{2a-t}\int_0^{2b-u} \phi_{xy}(t,u,x+u) + \int_0^{2a-t}\int_0^{2b-u} \phi_{xy}(-t,-u,x,y) \right] dx\, dy \qquad \text{(A-16)}$$

However, in this case we cannot combine the two integrals inside the bracket together because

$$\phi_{xy}(t,u,x+t,y+u) = \lambda_{xy}(t,u)\, J_y(x,y)\, J_x(x+t,y+u)$$

$$\phi_{xy}(-t,-u,x,y) = \lambda_{xy}(-t,-u)\, J_x(x,y)\, J_y(x+t,y+u) \qquad \text{(A-17)}$$

Since $\lambda_{xy}(t,u) = \frac{g(t,u)}{R^2}\, tu \left[\left(\Omega + \frac{1}{R} \right)^2 - \frac{\Omega}{R} \right]$

So $\phi_{xy}(-t,-u,x,y) = \lambda_{xy}(t,u)\, J_x(x,y)\, J_y(x+t,y+u)$ (A-18)

Substitution of (A-17) and (A-18) into (A-16) we get

$$I_{xy} = \int_0^{2a}\int_0^{2b} dt\, du \left\{ \int_0^{2a-t}\int_0^{2b-u} \lambda_{xy}(t,u) \left[J_x(x+t,y+u)\, J_y(x,y) + J_x(x,y)\, J_y(x+t,y+u) \right] dx\, dy \right\} \quad \text{(A-19)}$$

Similarly we have

$$I_{yx} = \int_0^{2a}\int_0^{2b} dt\, du \left\{ \int_0^{2a-t}\int_0^{2b-u} \lambda_{xy}(t,u) \left[J_x(x+t,y+u)\, J_y(x,y) + J_x(x,y)\, J_y(x+t,y+u) \right] dx\, dy \right\} = I_{xy} \quad \text{(A-20)}$$

Combining (A-13), (A-14), (A-19) and (A-20) we have

$$I = 2\int_0^{2a}\int_0^{2b} \lambda_{xx}(t,u)\, dt\, du \int_0^{2a-t}\int_0^{2b-u} J_x(x,y)\, J_x(x+t,y+u)\, dx\, dy$$

$$+ 2\int_0^{2a}\int_0^{2b} \lambda_{yy}(t,u)\, dt\, du \int_0^{2a-t}\int_0^{2b-u} J_y(x,y)\, J_y(x+t,y+u)\, dx\, dy$$

$$+ 2\int_0^{2a}\int_0^{2b} \lambda_{xy}(t,u)\, dt\, du \int_0^{2a-t}\int_0^{2b-u} \left[J_x(x+t,y+u)\, J_y(x,y) + J_y(x+t,y+u)\, J_x(x,y) \right] dx\, dy \quad \text{(A-21)}$$

which is the repeated surface integral form.

From a numerical point of view Eq. (A-21) is superior to (A-3) since.

1. The limit of integration of one of the surface integrals is reduced.
2. The singularity appears only in one of the integrals.
3. Since in the repeated surface integral, the integrand involves simple functions, such as polynomials for the linear shape function and sinusoidal functions for the sinusoidal shape function, the integration may be integrated out analytically.

APPENDIX B

A BRIEF DESCRIPTION OF COMPUTER PROGRAMS

Since a system operators' and users' manual will be written later, only a brief description of the two computer programs will be given here.

1.0 Names of Programs

Finite (Bent-Square Plate) and Element (Flat-Square Plate)

2.0 Language

FORTRAN IV

3.0 Inputs

The following are the inputs to be supplied and their meaning:

(a) For the Flat-Plate (PROGRAM "ELEMENT")

DELT — thickness of plate (λ)

AL2 — half length of plate (λ) (y-axis)

BL2 — half width of plate (λ) (x-axis)

KAX — number of the divisions for the width, if value is less than 2, program will abort

KAY — number of divisions for the length, if value is less than 2, program will abort

JX — number of divisions in the self-term integration in the x direction

JY — number of divisions in the self-term integration in the y direction

Typical value for JX and JY is 8 or 10.

NKAX — number of subdivisions for the singular cell integration of the self-term in the x direction

NKAY — number of subdivisions for the singular cell integration of the self-term in the y direction

Typical value for NKAX and NKAY is 10.

JBC — a control parameter for boundary condition. If JBC = 0, no edge boundary condition is imposed; if JBC = 1, the edge boundary condition $\underline{J} \cdot \hat{n} = 0$ is used.

KSIN — a control parameter for choosing shape function. KSIN = 0 for linear shape function, KSIN = 1 for sinusoidal shape function.

KMORE — a control parameter for integration. KMORE = 0 for normal accuracy; KMORE = 1 for additional accuracy.

ZETA — angle of polarization of the E vector with the positive x-axis, $0 \leq$ ZETA $\leq 90°$.

THETA — angle of incidence made with the negative y-axis. $0 \leq$ THETA $\leq 90°$

JCF — a control parameter. JCF = 0 for normal incidence, JCF = 1 for oblique incidence, i.e., THETA $\neq 90°$.

NPRINT — a control parameter for printing out output. If NPRINT = 0, normal output is given; NPRINT = 1, more output such as the matrix is dumped. More output is needed only for diagnostic purpose.

NDX — number of subdivisions for each nonsingular element in the x direction.

NDY — number of subdivisions for each nonsingular element in the y direction.

Typical value for NDX and NDY is 3.

XPOJ — a control parameter for integration

Typical value is 2.0.

XDEL — a control parameter for integration

Typical value is .3λ.

(b) <u>For the Bent-Plate (PROGRAM "FINITE")</u>

DELT — thickness of plate (λ)

YL1 — length of the unbent portion of plate (λ) (y-axis)

YL2 — length of the bent portion of plate (λ)

XL — half width of plate (λ) (x-axis)

PHI — the obtuse angle for the bent $90° \leq \phi \leq 180°$, (deg)

KAX — number of divisions for the width, if value is less 2, program will abort

KAY1 — number of divisions for the length of the unbent portion, if value is less than 2, program will abort

— JX, JY, NKAX, NKAY, JBC, NPRINT, NDX, NDY, XPOJ, KSIN, KMORE, ZETA, JCF, THETA and XDEL are the same as described in the flat-plate case.

4.0 Dimensions Statement

In using the programs, all the arrays should be dimensioned consistently according to the following guidelines

Let L = number of elements for one quadrant of plate

M = total number unknown quantities, counting both the Jx and the Jy components.

N = total number of nodes

J = total number of subdivisions for nonsingular elements.

We have for the flat-plate case —

L = 2(KAX) (KAY)

M = 2(KAX+1) (KAY+1)

N = (KAX+1) (KAY+1) = M/2

J = [(NDX) (NDY) + NDX] /2 (assuming NDX = NDY)
for the bent-plate case —

L = 2(KAX) (KAY1 + KAY2)

M = 2(KAX+1) (KAY1 + KAY2 + 1)

N = (KAX+1) (KAY1 + KAY2 + 1) = M/2

J = [(NDX) (NDY) + NDX] /2

and the dimensions of the arrays are —

A(M,M), B(M), W(M), IZW(M), CMAG(M), PHS(M), ST(M,M), BS(M), MLL(L), MML(L), MNL(L), X(N), Y(N), Z(N), SUX(J,L), SUY(J,L), SUZ(J,L), FSA(J,L), FXY(NDX,NDY), PMNE(N,L)

(same for all other arrays grouped under common block C3), CXX(L), CYY(L), CZZ(L), TEX(NDX,NDY), TEY(NDX,NDY), and TEZ(NDX,NDY).

5.0 Print Out

The program will abort if the value of KAX or KAY in PROGRAM ELEMENT is zero. The same applies to Program Finite for the values of KAX, KAY1, KAY2. The normal print outs are: the supplier input values, the node numbers and nodal current densities for Jx and Jy in $a|m^2$. The current densities are given as real part, imaginary part, magnitude and phase.

6.0 Program Flow

The main program performs the following items in order —

a. Read the input data.

b. Select the shape functions.

c. Decide whether it is normal or oblique incidence.

d. Calculate the x and y coordinates of each node and other essential parameters and constants.

e. Call in subroutines to label each element and calculate the area coordinates. All these values are stored in common blocks for later uses.

f. Construct the linear system by calling in subroutines to compute the singular and nonsingular matrix elements. To save computational time, the singular matrix element is computed only once.

g. Impose the edge boundary conditions if needed.

h. Invert the matrix.

i. Print out the results. A flow diagram is shown in Figure B-1.

7.0 Brief Description of Subroutines

XABEL — This subroutine labels the triangular elements from one to N^t, N^t being the total number of elements. Another function of this subroutine is to identify the correct node numbers for each element. Their values are stored in the arrays MLL, MML and MNL of the common block TLAB. It is called only once in the main program.

TRAN — This subroutine computes the area coordinate parameters, namely P_{mn}^{e}, Y_{mn}^{e} and X_{mn}^{e} and the centroids for each element. These values are stored in two common blocks, C3 and C18. The first integer in an array of the common block C3, such as PMNE represents the node number while the second integer denotes the element number. The index in the array in the common block C18, such as CXX represents the element number. Another function of TRAN is to divide each element

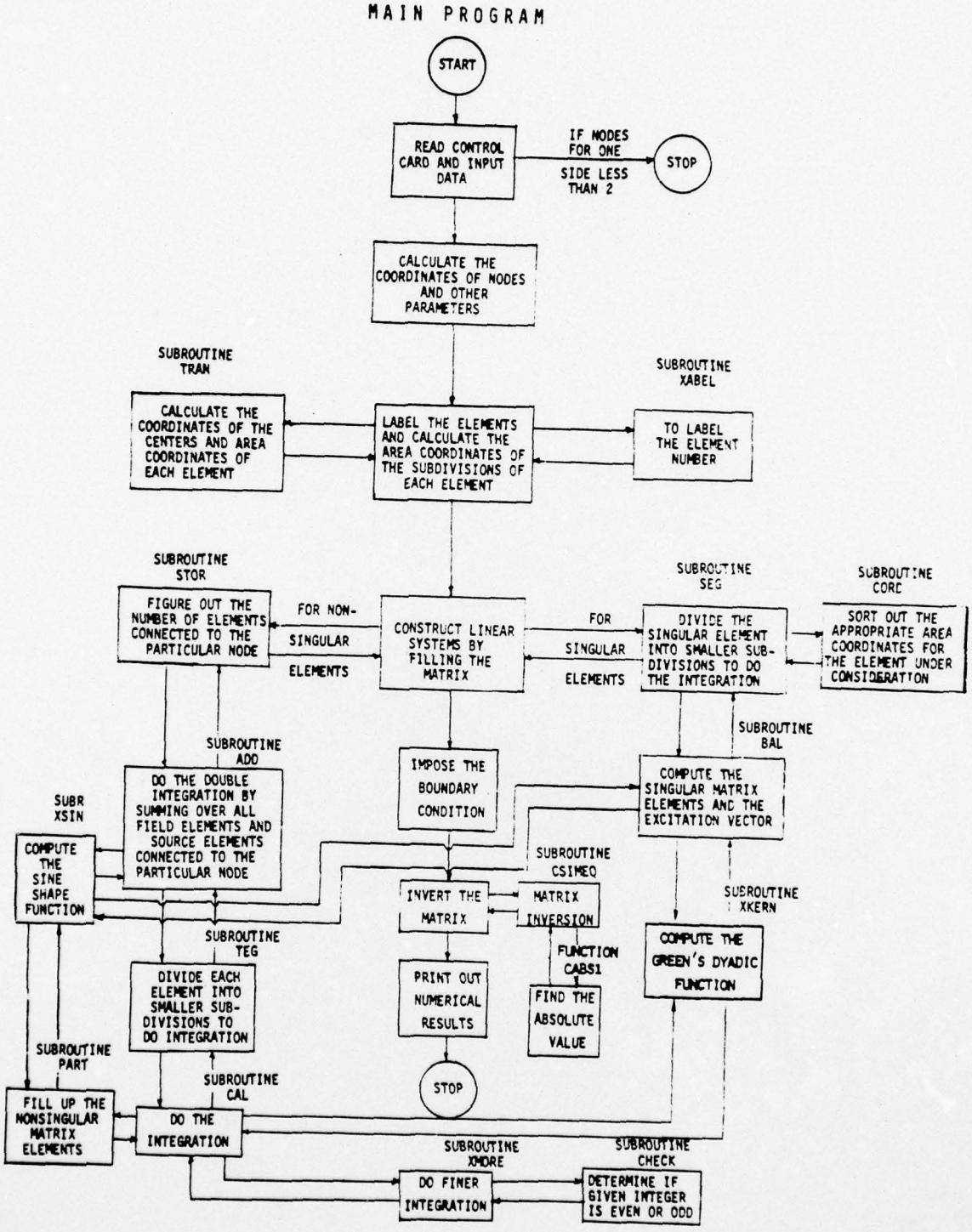

Figure B-1. Flow Diagram of Programs

into smaller subdivisions, either rectangular or triangular in shape. The number of the subdivisions is controlled by NDX and NDY which are part of the input data. TRAN then computes the centroids and areas of the subdivisions and store them in the common block TT. TRAN is called only once in the main program.

SEG — This subroutine is for the singular element. Because of higher accuracy requirement for the self-term integration (the self-term is the element where the field and the source points coincide), SEG divides the singular element into JX and JY subdivisions along the x and y directions. Then it calls in subroutine BAL to do the computation. To save computational time, the self-term integration is only performed once and the data are stored in the arrays ST and BS of common block SORT. To sort out the correct area coordinate parameters for doing the computation, SEG calls in CORD. The last part of SEG is just to fill up the singular matrix element for each node. SEG is called only once in the main program.

BAL — This subroutine computes the singular matrix element and the source excitation. The source excitation is stored in the vector B. To calculate the dyadic Green's function, BAL calls subroutine XKERN. The results from XKERN are stored in the common block AAA. BAL then uses these values and the appropriate area coordinates as represented by XCV, XCW and XCQ, etc. The last parameter, KGO, controls computation. If KGO = 0, computation will be done but if KGO = 1, computation will be excluded and previously stored information in ST and BS will be used instead. BAL is called only in SEG.

CORD — This subroutine has a unique simple function which is to sort out the correct area coordinate parameters

when it is called by giving the node and the element numbers for the field and source elements. The resulting information is stored in the common block C15. This common block has eighteen parameters; nine for the field element (the ones with P as their last alphabet) and nine for the source element. CORD is called both in SEG and TEG.

STOR — This subroutine is called in the main program when it is desired to compute the nonsingular matrix elements. The primary function of this subroutine is to figure out the number of elements connected to each node. From Fig. 1, it is understood that the number of elements connected to a particular node can be 1, 2, 3 and 6 after taking symmetry into account (considering only one quadrant of the plate). STOR then calls in ADD to perform the other functions.

ADD — The primary function of this subroutine is to figure out how the field element and the source element are combined as far as a particular node is concerned. Three cases can arise: (a) both the field and the source elements are connected to that node; (b) only the field element is connected to that node; in this case, the control parameters are set by letting MSON = 1 and MDUB = 0; (c) only the source element is connected to that node; here we have MSON = 0 and MDUB = 1. For each combination of the source and the field elements, ADD then calls in TEG to do the integration. ADD is called only in STOR.

TEG — This is a very simple subroutine. Its function is to divide each source element into NDIM subdivisions and call in CAL to do the integration.

CAL — For the nonsingular matrix elements, this subroutine does the most important job. It is called TEG. The subroutine makes use of the symmetry of the problem by dividing the area of the plate into four quadrants. To save computational time, accuracy of integration is controlled by several input parameters such as XPOJ, XDEL, NDX and NDY. To do the computation, CAL calls in XKERN to do the dyadic Green's function computation and PART to do the area coordinates computation and filling in the matrix elements. The resulting information from PART is stored in the common block SAD which is then used to fill in the main matrix A.

XKERN — The primary function of this subroutine is to handle the dyadic Green's function. It is called in BAL and CAL. The computed values are stored in the common block AAA.

PART — This subroutine is called only in CAL and its function is to calculate the area coordinate parameters and their combinations with the dyadic Green's function as computed in XKERN. The resulting computed values are stored in the common block SAD. In computing the area coordinate parameters, attention is given to the way the source element and the field element are combined. This is controlled by the control parameters MSON and MDUB of the common block TCH.

XMORE — This subroutine is sometimes needed to do more accurate integration by subdividing each subdivision again into smaller subdivisions. Because of the computational time involved, this subroutine is not used most of the time for smaller plate sizes. It is called only in CAL.

CHECK — This subroutine determines whether a given integer is even or odd. It is called in XMORE.

CSIMEQ — This is a matrix inversion subroutine. It simply performs the inversion of a given complex matrix by Gaussian elimination alogrithm. In calling the subroutine, the first integer number must be equal to the dimension of the matrix A; the second integer represents the number of unknowns of the linear system; the third parameter is the matrix to be inverted; the fourth parameter is a vector to store the solution after inversion; the fifth parameter is the excitation vector and the last parameter is a dummy vector for storage purpose.

CABS1 — Its function is to determine the absolute value of a complex number. It is called by CSIMEQ.

XSIN — This subroutine is to compute the sinusoidal shape function. In computing the sinusoidal coordinates, the subroutine makes use of the area coordinates stored in common block C15. It is called in ADD, BAL and PART. In calling, the cartesian coordinates of the observation and field points are supplied and the resulting values are returned through arguments.

8.0 System Requirement

A FORTRAN compiler w/standard input/output and mathematical macros is all that is needed to run this job. The storage requirement for running a particular job depends on the dimension size set by the programmer. For a particular problem run here at TRW, it took 90 cpu seconds and 50 k of core to run and execute on a CDC 174 computer.

REFERENCES

[1] Raimat-Samii and Mittra, R., Integral Equation Solution and RCS Computation of a Thin Rectangular Plate," IEEE Trans. Antennas and Propagat., Vol. AP-22 pp 608-610, July 1974.

[2] Wang, N. N. Richmond, J. H. and Gilreath, M. C., "Sinusoidal Reaction Formulation for Radiation and Scattering from Conducting Surfaces," IEEE Trans. Antennas and Propagat., Vol AP-23, pp 376-382, May 1975.

[3] Zienkiewicz, O. C., "The Finite Element Method in Engineering Science," McGraw-Hill Book Co., London, 1971.

[4] Brebbia, C. A. and Connor, J. J., "Fundamentals of Finite Element Techniques - for Structural Engineers," John Wiley & Sons Book Co., New York, 1974.

[5] McDonald, B. H., Friedman, M., and Wexler, A., "Variational Solution of Integral Equations," IEEE Trans. Microwave Theory Tech., Vol. MTT-22, pp 237-248, March 1974.

[6] Kinsner, W. and Torre, D. E., "An Iterative Approach to the Finite Element Method in Field Problems," IEEE Trans. Microwave Theory Tech., Vol. MTT-22, pp 221-228, March 1974.

[7] Silvester, P., "A General High-Order Finite Element Waveguide Analysis Program, IEEE Trans. Microwave Theory Tech., Vol. MTT-17, pp 204-210, April, 1969.

[8] Ahmed, S. and Daly, P., "Waveguide Solutions by the Finite Element Method," Radio Electron. Eng., Vol. 38, pp 217-223, Oct. 1969.

[9] Strang, G. and Fix, G. J., "Analysis of the Finite Element Method," Prentice-Hall, Inc., N. J., 1973.

[10] Melosh, R. J., "Basis of Derivatives of Matrices for Direct Stiffness Method," AIAA J., Vol. 1, pp 1631-1637, 1963.

[11] Zienkiewicz, O. C., "The Finite Element Method in Structural and Continuum Mechanics," McGraw Hill Book Co., New York, 1967.

[12] Irons, B, Zienkiewicz, O. C., et al, "Comments on the Paper: Theoretical Foundations of the Finite Element Method," Int. J. Solids Structures, Vol. 6, pp 695-697, 1970.

[13] Kouyoumjian, R. G., "The Calculation of the Echo Area of Perfectly Conducting Objects by the Variational Method," Ph.D. Dissertation, Ohio State University, Columbus, 1953.

AD-A035 223 TRW DEFENSE AND SPACE SYSTEMS GROUP REDONDO BEACH CALIF F/G 20/3
CURRENT COMPUTATION BY THE FINITE ELEMENT METHOD.(U)
NOV 76 A SANKAR, T C TONG N00123-76-C-0729
UNCLASSIFIED NL

2 OF 2
ADA035223

END

DATE
FILMED
3-77

REFERENCES (Continued)

[14] Van Bladel, J., "Some Remarks on Green's Dyadic for Infinite Space," IEEE Trans. Antennas and Propagat., Vol. AP-9, pp 563-566, Nov. 1961.

[15] Waterman, P. C., "Matrix Formulation of Electromagnetic Scattering," Proc. IEEE, Vol. 53, pp 805-811, August 1965.

[16] Jones, D. S., "The Theory of Electromagnetism," McMillan Book Co., New York, 1964.

[17] Mentzer, J. R., "Scattering and Diffraction of Radio Waves," Pergamon Press, Oxford, 1955.